UNIVERSITAT POLITÈCNICA DE CATALUNYA
BARCELONATECH
Escola Tècnica Superior d'Enginyeries
Industrial i Aeronàutica de Terrassa

Master's Degree in Aeronautical Engineering

David Veiga Fernández

Numerical Resolution of Fluid Dynamics and Heat and Mass Transfer problems
Application to Combustion Processes

Director: Carles-David Pérez-Segarra

Spring Semester, Course 2019 – 2020

Delivery Date: June 30, 2020

Report

UNIVERSITAT POLITÈCNICA DE CATALUNYA
BARCELONATECH
Escola Tècnica Superior d'Enginyeries
Industrial i Aeronàutica de Terrassa

Abstract

The study and optimization of Combustion processes has transcended the engineering necessity to become an environmental concern. Recent regulations implement growing restrictions on emissions produced in industries that somehow are connected to this way of obtaining energy, such as power generation, transport (land, sea and air) or even in domestic use. In this phenomenon, equations of Fluid Dynamics, Heat and Mass Transfer and Chemical Kinetics are related, and this makes it a complex issue to tackle with accuracy.

In the line of this rising interest, this study is intended to deepen in the field of Computational Fluid Dynamics applied to Combustion, by way of the development, verification and testing of an algorithm to solve this type of problems.

Acknowledgements

Firstly, I would like to manifest my special thanks to the professor Carles-David Pérez-Segarra, for giving me the opportunity of developing this fascinating project under such conditions that have allowed me to take profit of the experience of studying abroad at the same time. His invaluable guidance and feedback have been fundamental for taking the right decisions and working on the correct direction.

I would also like to express my gratitude to my friend Albert Canyelles for his advices on programming from an expert point of view, as well as all the people who, at any point, contributed to the success of this project, either directly or indirectly.

Last but not least, to my parents, for their continuous patience and support, even in the distance due to the abnormal times in which the project was developed. It would not have been possible to reach this point on my career without them. Thank you for giving me courage and strength to carry on from the very beginning until the end.

UNIVERSITAT POLITÈCNICA DE CATALUNYA
BARCELONATECH
Escola Tècnica Superior d'Enginyeries
Industrial i Aeronàutica de Terrassa

I declare that,

the work in this Master Thesis is completely my own work,

no part of this Master Thesis is taken from other people's work without giving them credit,

all references have been clearly cited,

I understand that an infringement of this declaration leaves me subject to the foreseen disciplinary actions by *The Universitat Politècnica de Catalunya – BarcelonaTECH*.

Student name	**Signature**	**Date**
David Veiga Fernández		June 26, 2020

Title of the Thesis: Numerical Resolution of Fluid Dynamics and Heat and Mass Transfer problems. Application to Combustion Processes

Table of contents

Figures and tables

List of Figures

List of Tables

Nomenclature

In this section a summary of the variables used along the whole study is provided, with its correspondent symbol, meaning and units. If any variable used along the report is missing in this section, its description is done at the same point of its appearance.

Variable	Description	Units (S.I.)
$\hat{E}_a$	Activation energy of the reaction l	J/mol
AR	Aspect ratio	-
k_l^b	Backward kinetic constant of the reaction l	-
β	Compressibility coefficient	1/K
ρ	Density	kg/m^3
d	Distance between two nodes	m
μ	Dynamic viscosity	Pa·s
K_{C_l}	Equilibrium constant (in terms of molar concentrations) of the reaction l	-
K_{p_l}	Equilibrium constant (in terms of pressure) of the reaction l	-
k_l^f	Forward kinetic constant of the reaction l	-
$\dot{\omega}_k$	Generation/destruction term of the species k	-
Γ_ϕ	Generic diffusion coefficient	-
ϕ	Generic variable, equivalence ratio	-
$\vec{g}$	Gravity acceleration	m/s^2
c_p	Heat capacity at constant pressure	J/kg·K
c_v	Heat capacity at constant volume	J/kg·K
$\dot{q}$	Heat flux	W/m^2
x	Horizontal coordinate	m
b_P	Independent term	-
u	Internal Energy	J
a_I	Linear coefficient corresponding to the node I (see subscripts)	-
m	Mass	kg
D_{km}	Mass diffusivity coefficient of the species k in the mixture	m^2/s
$\dot{m}$	Mass flow rate	kg/s
$\vec{j}_k$	Mass flux of the species k	kg/m^{2}s
Y_k	Mass fraction of the species k	-
C	Molar concentration (moist air)	mol/m^3
$[X_k]$	Molar concentration of the species k	mol/m^3
$\hat{h}_k^0$	Molar standard enthalpy of the species k	J/mol
$\hat{s}_k^0$	Molar standard entropy of the species k	J/mol·K
$\hat{g}_k^0$	Molars standard Gibbs energy of the species k	J/mol
W_k	Molecular weight of the species k	kg/kmol
∇	Nabla operator	-
Nu	Nusselt number	-
Pe	Péclet number	-
$\vec{v}^p$	Predictor velocity vector	m/s
p	Pressure	Pa
Ra	Rayleigh number	-
Re	Reynolds number	-

Variable	Description	Units (S.I.)
Sh	Sherwood number	-
S_ϕ	Source term	-
ν''_{kl}	Stoichiometric coefficient of the product k in the reaction l	-
ν'_{kl}	Stoichiometric coefficient of the reactant k in the reaction l	-
ψ	Stream function	-
$\vec{\tau}$	Stress tensor	Pa
S	Surface	m^2
T	Temperature	ºC, K
λ	Thermal conductivity	W/m·K
t	Time	s
$\hat{R}$	Universal gas constant	J/mol·K
$\vec{n}$	Vector normal to the surface	-
$\vec{v}$	Velocity vector	m/s
y	Vertical coordinate	m
V	Volume	m^3
$\vec{\omega}$	Vorticity vector	-

Subscript	Description
av	Average value
k	Designation of a particular species
max	Local maximum value
min	Local minimum value
ϕ	Parameter of the property ϕ
E	Property evaluated at the east control volume
e	Property evaluated at the east face of the main control volume
P	Property evaluated at the main control volume
N	Property evaluated at the north control volume
n	Property evaluated at the north face of the main control volume
S	Property evaluated at the south control volume
s	Property evaluated at the south face of the main control volume
W	Property evaluated at the west control volume
w	Property evaluated at the west face of the main control volume
x	Property field in the x-direction
y	Property field in the y-direction
$0, ref$	Reference value

Superscript	Description
$n+1$	Property evaluated at the current timestep
n	Property evaluated at the previous timestep
$n-1$	Property evaluated two timesteps before
HRS	Property evaluated using a High-order Resolution Scheme
UDS	Property evaluated using an Upwind Difference Scheme
0	Thermodynamic property evaluated at the reference state (25ºC)

1. Introduction

1.1. Aim and scope

This report is intended to summarize the development of a Computational Fluid Dynamics study involving the implementation of a computer algorithm for studying combustion phenomena.

The point of departure of this project consists of a research and review on numerical methods applied to Fluid Dynamics and Heat and Mass transfer problems in the literature. All the acquired knowledge will be applied to construct a self-developed C++ code that aims to solve simple problems in the field of application chosen.

The elaboration of the algorithm has been progressive and verified with existing studies in the literature at each stage. The following phases have been used:

1. Implementation of an algorithm to solve transient Conduction Heat Transfer problems and Potential Flow problems.
2. Implementation of an algorithm to solve steady Convection and Diffusion problems with a prescribed velocity field.
3. Implementation and verification of an algorithm to solve transient problems involving the resolution of Navier-Stokes equations of momentum and energy.
4. Incorporation of Mass Transfer phenomenon to code developed in phase 3, leading to a combined mass, momentum and energy transfer resulting algorithm.
5. Incorporation of Chemical Kinetics of reactive species to the code developed in phase 4.

As the reader may appreciate, this step-by-step implementation and verification ensures the acquisition and understanding of all required knowledge before reaching the next stage, which involves a higher degree of complexity. On the other hand, the correctness of the results obtained is verified continuously, which facilitates the debugging process and improves the programming efficiency.

In the end, the result consists of a complete CFD code capable of solving different types of Fluid Dynamics and Heat and Mass transfer transient problems of different degrees of complexity for simple geometries, coupled with the chemistry mechanisms involved in a fuel-oxidizer reaction. This will be used to study the particular case of laminar flames in simple combustion processes.

It is important to remark that this study only concerns two-dimensional incompressible Fluid Dynamics, limiting the results obtained to problems in which this hypothesis can be applied. It is thus out of the scope the study of compressible flows. Added to this, turbulence models and radiative heat transfer have neither been considered, as well as a complete optimization of the computational cost of the simulations. Priority has been given to clarity of the code instead of efficiency. All the points mentioned in this paragraph are out of the scope of the project.

Further comments about future improvements beyond the above-mentioned defined scope are detailed at the end of the report in chapter *10. Future lines of work*.

1.2. Requirements

The development of this study was subject to certain restrictions and specifications beforehand. These constraints are listed below:

- The programming language used for the development of the CFD algorithms shall be C++. This obeys to the speed of this particular language according to its purpose for this project.
- The code shall be verified at each one of the above-mentioned steps, either with analytical solutions of simple cases or reference solutions provided by the literature.
- Discrepancies between reference and simulated solutions shall always be explained and argued.

Additionally, some other issues have to be mentioned since, although not being strict requirements, the project was also developed according to the following concerns:

- The post-processing and results treatment will be developed using MATLAB programming language since it provides easier and more intuitive plot displaying tools.
- The programming structure will be modular and well-detailed, rather than fully-optimized, to ensure that a third user is perfectly capable of using and modifying the algorithm in the future if needed.
- The code will be enhanced by allowing the user to choose some parameters to optimize the solution, i.e. through the implementation different solvers, convective evaluation schemes or optimized mesh distributions. Analyses will be done along the report regarding these improvements.
- Other additional features, such as output displays and loading-saving options, will be added to the code. This is due to the computation time required for some simulations and the necessity of tracking their progress.

1.3. Justification and utility

Fluid Dynamics, Heat and Mass transfer and Combustion problems are present in a wide range of aspects of our ordinary lives. Especially in industrial and aerospace engineering, all these issues are the theoretical basis of many fields of application, such as the aerodynamic design of a car, the behaviour of flow through a gas turbine, the development of heating and cooling devices for buildings or the combustion of a mixture of gases in a rocket nozzle, to put few examples.

Thus, being capable of reproducing correctly and accurately the behaviour of fluids is a mirror of enhancing performance and improving the efficiency of current engineering designs. On the other hand, this also raises the possibility of considering environmental impacts on the designs and, hence, to propose improvements in terms of sustainability, i.e. by reducing the quantity of toxic gases produced during the combustion process. Further comments on this particular line of work are made in the following section.

However, due to the complex nature of the physics behind Fluid Dynamics, Heat and Mass transfer and Combustion phenomena, analytical solutions of their governing equations can only be found for few cases and under a wide amount of assumptions. This make differ the problem conditions with the real conditions, especially when also combustion chemistry is involved in the processes. Further details on this issue are given in section *1.5. Background: Introduction to Numerical Methods*.

This leads to the conclusion that the way to accurately find the real fluid behaviour of this kind of problems is through experimental techniques. Nevertheless, experiments are limited by other factors apart from the complexity that is the economic resources, since normally tests under different conditions are required and developing a single test is expensive.

Yet, the use of computers for solving this type of problems has broadly improved this situation thanks to their calculation capacity, but even in those cases, it is impossible to perform precise large-scale simulations in manageable amounts of time. This is even more critical when turbulence is also involved. Reducing the computational cost of a simulation at the same time that refining the precision of the solution obtained is, therefore, one of the most significant challenges of current Computational Engineering.

In any case, a CFD simulation is more precise than a simplified analytical solution and cheaper than an experiment, and this makes evident the utility of deepening in the field of Computational Fluid Dynamics applied to the resolution of real problems.

Following this principle, the presented study allows to gain theoretical knowledge in the physics behind this matter as well as to analyse current approaches and methodologies used in CFD. With this, the nature of Fluid Dynamics, Heat and Mass transfer and Combustion will be better understood, and at the same time, the main principles of elaborating a simulation from scratch until reaching accurate enough converged results in feasible amounts of time will be reviewed and put in practice.

1.4. State of the art

The study of Combustion phenomena using a CFD approach dates back to the early 70s. According to the computational power available at that time, the first models developed aimed to solve laminar flame propagation, since it required a simple geometry and allowed the understanding of reaction mechanisms involved in simple combustion processes. On the following years, many authors studied this particular case of combustion, focusing the attention on the flammability limits of the fuel-oxidizer mixture [1].

On the other hand, many models have been developed for tackling combustion in CFD analysis, that are described in [2]. The different existing models account for different approaches to tackle aspects such as turbulent combustion or the velocity of the reaction concerning the transport of species, and its use is strongly conditioned by the problem to be solved.

There are also some studies regarding the prediction of chemical kinetics for the combustion of generalized hydrocarbons [3]. In this line, there is particular interest on the combustion of methane (CH_4), which obeys to its widespread use as a fuel (it is the main component of the natural gas mixture), but also due to the large amount of energy it releases per unit mass as well as per unit of carbon dioxide [4].

For this particular fuel, several reaction mechanisms have been proposed and used in a wide range of simulations, being the most detailed one the Gri-Mech 3.0, which considers 325 chemical reactions where 53 different species are involved [5]. However, due to the enormous complexity of this approach, many reduced mechanisms, involving one to ten reactions are typically used in simulations [3] [6] [7] [8] [9]. Even some studies have recently proposed new simplified mechanisms [10].

Investigations and simulations in the line of sustainability are also being developed, and they are gaining more relevance in the last years [10] [11]. These aim to develop strategies in order to optimize the combustion processes and decrease the generation of potentially hazard products to the environment. Some proposals consider pure oxygen combustions (oxy-fuel conditions) by removing the nitrogen from the air, which would allow, first, to decrease the production of NO_x substances and to separate the CO_2 generated for its later storage [6]. Simulations of dual fuel and gas combustion engines as well as gas turbines have also been developed and compared to experimental results, due to the rising role of gas in future power generation [2] [12]. Finally, some proposals of the use of catalysts for decreasing the nitrogen oxide emissions have also been developed [4].

All in all, it can be confirmed that there is an increasing interest on the study of combustion processes especially in recent years, mainly due to the awareness of the environmental problems derived by this mechanism of obtaining energy.

1.5. Background: Introduction to Numerical Methods

1.5.1. Introduction

This section is intended to present the resolution procedure with numerical methods used to tackle the problem stated.

Fluid Mechanics and Heat Transfer governing equations, that will be described in detail along with this report, have a degree of complexity that allows them to be solved analytically only for particular cases with simple geometries, simplifications to one-dimensional or two-dimensional cases, cylindrical or spherical symmetry, specific BC's, etc. Nevertheless, the physical problems that need to be solved generally do not fulfil the previous conditions, meaning that no analytical methods are known to solve the equations.

Hence, the use of numerical methods and iterative processes is required to develop a resolution procedure for more sophisticated problems, consisting of being capable of finding the solution under some particular conditions. In the case of this project, the Finite Volume Method (FVM from now on) will be applied, to finally solve a linear system of equations that represent the field of the property to be analysed. This procedure is one of the most used for Computational Fluid Dynamics, although other alternatives exist, such as the Finite Element Method (FEM) [13], yet it uses a different formulation that is out of the scope of this project.

On the following sections, the discretization procedures of the FVM applied to Fluid Dynamics and Heat Transfer problems are explained, from a general overview of space and time discretization to detailing how to discretize each one of the terms seen in the governing equations of this field.

1.5.2. Space discretization

The FVM consists on subdividing the whole resolution domain into a mesh (or grid) made of smaller domains, named control volumes (CV from now on), inside of which the function that is going to be solved is integrated with some kind of approximation [14], as displayed in Figure 1 below.

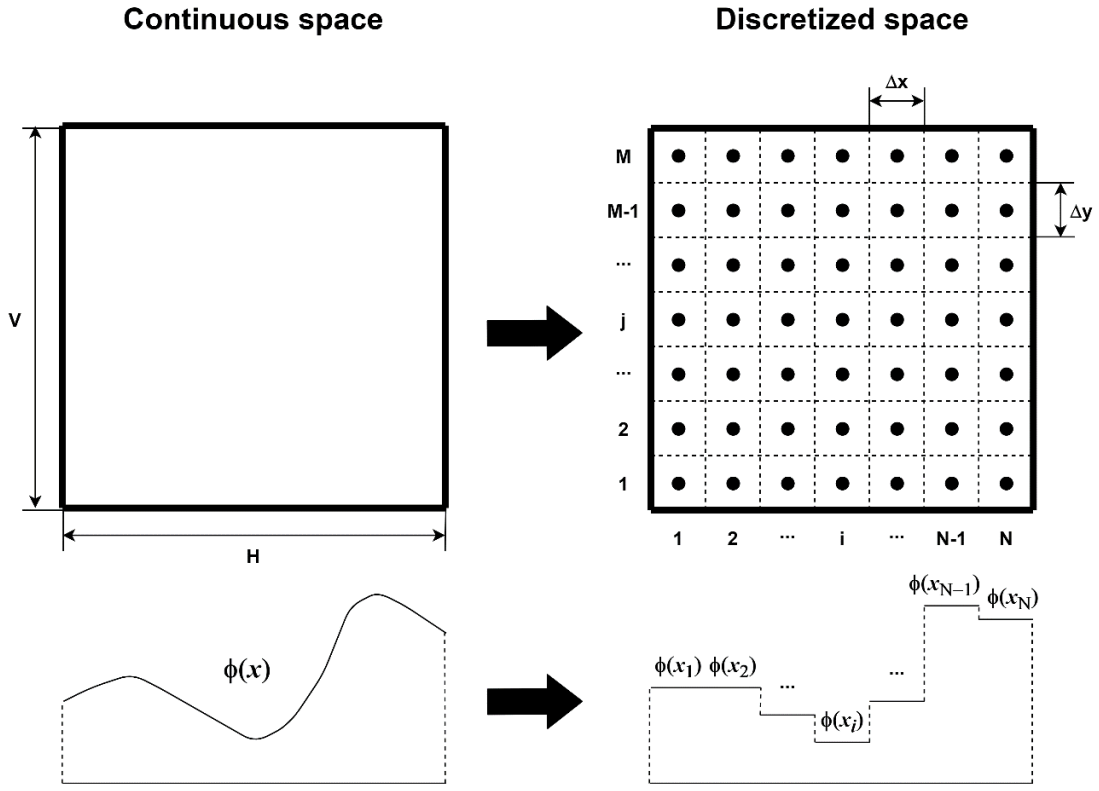

Figure 1. Space discretization used in the FVM.

Typically, and also for the case of this project, the value of the function at the CV coincides with the value at a particular point of the CV (named node). This value and is assumed to be constant in the whole CV, that is to say

$$\int_{V_P} \phi dV \approx \phi_P V_P \tag{1.1}$$

where V_P refers to the CV evaluated and ϕ_P to the value of the property ϕ at the reference grid point of the CV evaluated. This discretization methodology allows obtaining an approximation to the real solution, with an error that is expected to decrease with the square of the element size. This means that the smaller the elements (this is the greater number of elements), the more accurate the solution will be.

It is also important to highlight that, depending on the discretization procedure followed, it is possible to obtain structured meshes (such as the one of Figure 1), which are regular, or unstructured meshes, that have irregular shapes and elements of different sizes. This project is limited to dealing with structured meshes, since they allow to be easily implemented, define direct relationships between nodes as well as be stored computationally speaking.

However, it must be remarked that this is possible due to the fact that simple geometries (i.e. square domains) are analysed in the proposed problems. For more complex geometries the use of unstructured meshes is imperative.

For the structured meshes, it is possible to define a particular arrangement according to the node that is being studied and its immediate neighbours, as displayed in Figure 2 (for a bidimensional domain) [15].

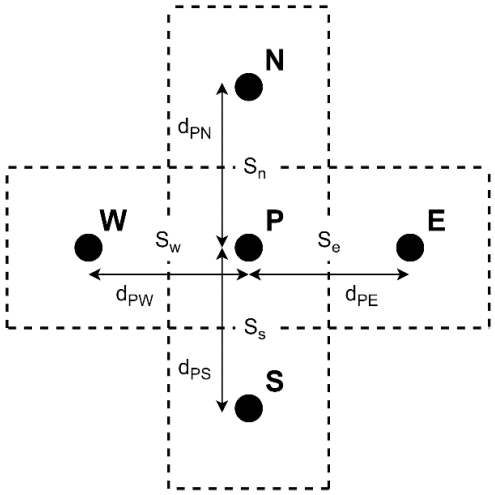

Figure 2. Discretization basic molecule.

From the figure, P stands for the Principal node, which is the one that is being studied, and its neighbours are defined as W, E, S and N, that stands for west, east, south and north respectively, according to its position respect to the principal node. For some cases, it is necessary to define an extended molecule that also takes into account further nodes respect to the node P. These cases will be treated in more depth later on in chapter *3. Convection-diffusion equation*.

Taking all these issues into consideration, the final aim of the discretization is to obtain an equation that linearly relates the value of any property at any node and its respective immediate neighbours. This leads to an equation of the form

$$a_P\phi_P = a_W\phi_W + a_E\phi_E + a_S\phi_S + a_N\phi_N + b_P \tag{1.2}$$

Thus, by applying the previous equation to each node of the domain, the continuous problem that was unsolvable has become a discrete problem consisting of the resolution of a linear system of equations. Now the problem can be solved by using any possible method available in the literature. Due to the size of the resultant matrices and thus the difficulty to invert it directly, iterative solvers are proposed [15].

For the case of this project, three different solvers have been implemented:

- **Point-by-point or Gauss-Seidel:** solver in which equation (1.2) is solved directly for each node P, assuming that the values of the neighbour nodes are known and have been calculated in a previous iteration, such as:

$$\phi_P = \frac{a_W\phi_W + a_E\phi_E + a_S\phi_S + a_N\phi_N + b_P}{a_P} \tag{1.3}$$

  Hence, as iterations advance, the values computed get closer to the real solution.
  The simplicity of this solver makes it easy to implement, but it does not provide the exact solution and its convergence is relatively slow. The way of ending the iterative process is by means of a convergence criterion that must be satisfied for all nodes in the domain, which consists of establishing a maximum difference for two values of a node computed between two consecutive iterations.
- **Line-by-line:** evolution of the Gauss-Seidel that can be applied when the matrix of the linear system of equations is tri-diagonal. For those cases, this algorithm provides the exact solution in the case of one-dimensional problems (i.e. a single row or column of nodes). In order to extend it to two-dimensional domains, computations are iteratively done for all rows and columns, assuming that contribution of the other dimension's nodes is part of the independent term, such as:

$$a_P\phi_P - a_W\phi_W - a_E\phi_E = b'_P \text{ with } b'_P = a_S\phi_S + a_N\phi_N + b_P \tag{1.4}$$

  for the case of a row, and

$$a_P\phi_P - a_S\phi_S - a_N\phi_N = b'_P \text{ with } b'_P = a_W\phi_W + a_E\phi_E + b_P \tag{1.5}$$

  for the case of a column.
  This implies that, for two-dimensional domains, the exact solution is neither achieved and thus some iterations are required. Hence, the same convergence criterion that for the case of Gauss-Seidel is used. However, this solver allows a faster convergence than the Gauss-Seidel one, meaning that the convergence criterion is satisfied with a shorter number of iterations.
- **Conjugate gradient:** method developed especially for sparse systems of linear equations, which consists of, in rough words, finding the closest path to the solution of the system, under the condition that the matrix of the system is symmetric and positive-definite. If this is satisfied, by means of the gradient and an iterative process the procedure rapidly converges in the solution of the system [16].

The convergence of the previous methods is subject to the Scarborough criterion as a sufficient condition, which establishes that the sum of the coefficients of neighbour nodes divided by the coefficient of the main node must be smaller or equal to one for all equations [15].

1.5.3. Time discretization

It is remarkable to notice that equation (1.2) only spatial discretization is considered. However, for unsteady problems it is also required to discretize the temporal domain in discrete timesteps as well likewise that has been done with space, as shown below.

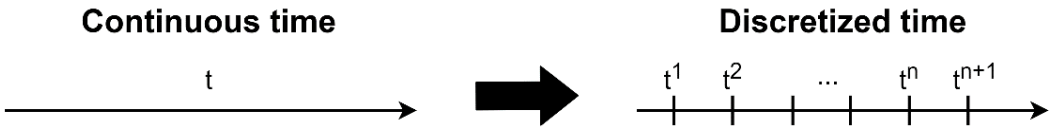

Figure 3. Time discretization used in the FVM.

The procedure to compute the general variable ϕ at a particular timestep will be following the time direction. This means that from the previous timestep t^n, where the field of ϕ^n is known, the field of ϕ^{n+1} at current timestep t^{n+1} will be computed.

In order to establish the relationship between ϕ^n and ϕ^{n+1}, a weight factor β is introduced when integrating versus time as follows [15]

$$\int_{t^n}^{t^{n+1}} \phi_P dt \approx [\beta\phi_P^{n+1} + (1-\beta)\phi_P^n]\Delta t \tag{1.6}$$

Taking this discretization into account, equation (1.2) can be rewritten in the following way:

$$\beta a_P \phi_P^{n+1} = \beta[a_W\phi_W^{n+1} + a_E\phi_E^{n+1} + a_S\phi_S^{n+1} + a_N\phi_N^{n+1}] + b'_P \tag{1.7}$$

where $b'_P = (1-\beta)[a_W\phi_W^n + a_E\phi_E^n + a_S\phi_S^n + a_N\phi_N^n - a_P\phi_P^n] + b_P$.

Depending on the value of β, more weight is going to be given to the current field ϕ^{n+1} or the previous field ϕ^n. There are three particular values of β that are worthwhile to mention:

- $\beta = 0$, which accounts for the **fully explicit scheme**. This approximation considers that the value of ϕ_P along the interval from t^n to t^{n+1} corresponds to ϕ_P^n. Calculations of the explicit scheme are easier, but it may show convergence problems for large values of Δt, as commented later on in chapter *6. Combustion*.
- $\beta = 1$, which accounts for the **fully implicit scheme**. This approximation considers that the value of ϕ_P along the interval from t^n to t^{n+1} corresponds to ϕ_P^{n+1}, and it is more stable computationally speaking, but implies the full resolution of the system of equations at the current timestep, thus meaning that an iterative solver may have to be used.
- $\beta = \frac{1}{2}$, which accounts for the **Crank-Nicolson scheme**. This a hybrid between implicit and explicit schemes, which considers that the weight of the previous and the current timesteps is equal.

2. Diffusion phenomena

2.1. Introduction

The concept of diffusion applied to Fluid Dynamics and Heat Transfer refers to how a property is "spread out" into an either solid or fluid domain when there is a difference of magnitude of this property in different regions of a domain. Two cases of diffusion phenomena will be treated in this chapter: heat conduction and potential flow. The first one is developed in section *2.2. Heat conduction*, whilst the latter is explained in section *2.3. Potential flow*. Both of them are governed by similar mathematical equations, since the underlying concept is the Poisson's equation $\Delta\varphi = f$, where $\Delta = \frac{\partial^2}{\partial x^2} + \frac{\partial^2}{\partial y^2}$, f is a given function and φ is the unknown function.

2.2. Heat conduction

2.2.1. Mathematical formulation

This phenomenon consists of the transference of internal energy by the contact of molecules that are at different internal energy states. This gradient generates a propagation of energy along the studied domain, which is described by the so-called Fourier's Law, displayed below in differential form for a two-dimensional transient case [15].

$$\rho c_p \frac{\partial T}{\partial t} = \frac{\partial}{\partial x}\left(\lambda \frac{\partial T}{\partial x}\right) + \frac{\partial}{\partial y}\left(\lambda \frac{\partial T}{\partial y}\right) + S \qquad (2.1)$$

where S refers to the source term (i.e. amount of heat generation inside the domain). In this case, the variable propagated (this is "diffused") through the domain is, as mentioned above, the internal energy, which gives a temperature distribution on the control volume studied. Thus, from the previous equation three different terms can be appreciated:

- **Unsteady (or transient) term** $\rho c_p \frac{\partial T}{\partial t}$, which provides how the temperature field changes versus time.
- **Diffusive term** $\frac{\partial}{\partial x}\left(\lambda \frac{\partial T}{\partial x}\right) + \frac{\partial}{\partial y}\left(\lambda \frac{\partial T}{\partial y}\right)$, which defines the propagation of temperature along the domain at a particular time instant.
- **Source term** S, which introduces or extracts heat from the domain.

Heat Conduction is the first phenomenon tackled since there is no presence of convective forces because no the transport of energy due to the movement of particles is involved. This simplifies the discretization of the domain and the resolution of the equation for each control volume. Mathematical formulation of the convective term will be introduced in chapter *3. Convection-diffusion equation*. In this phase, the particular case studied is heat conduction in solids (see section *2.2.4. Test case: Four-Material Conduction* for the problem analysed).

2.2.2. Discretization of the equations

In order to discretize the two-dimensional heat conduction equation (2.1) displayed above, it is required to integrate it along the timestep of analysis and over a CV:

$$\int_{t^n}^{t^{n+1}} \int_{V_P} \rho c_p \frac{\partial T}{\partial t} dV\, dt = \int_{t^n}^{t^{n+1}} \int_{V_P} \left(\frac{\partial}{\partial x}\left(\lambda \frac{\partial T}{\partial x}\right) + \frac{\partial}{\partial y}\left(\lambda \frac{\partial T}{\partial y}\right) + S \right) dV\, dt \tag{2.2}$$

According to this, each term will be discretized as follows

- **Unsteady term:** discretized by converting the derivative to a finite difference.

$$\int_{t^n}^{t^{n+1}} \int_{V_P} \rho c_p \frac{\partial T}{\partial t} dV\, dt \approx \rho c_p (T^{n+1} - T^n) V_P \tag{2.3}$$

  Note that the timestep size is cancelled as it is multiplying and dividing.

- **Diffusive term:** discretized by converting the volume integral to a surface integral with the divergence theorem, and approximating the derivative with a finite difference.

$$\begin{aligned} \int_{t^n}^{t^{n+1}} \int_{V_P} \left(\frac{\partial}{\partial x}\left(\lambda \frac{\partial T}{\partial x}\right) + \frac{\partial}{\partial y}\left(\lambda \frac{\partial T}{\partial y}\right) \right) dV\, dt &= \int_{t^n}^{t^{n+1}} \int_{S_f} \lambda \frac{\partial T}{\partial \vec{n}} \vec{n} dS\, dt \\ &\approx \lambda \left[\beta \left(\frac{T_P^{n+1} - T_W^{n+1}}{d_{PW}} S_w + \frac{T_E^{n+1} - T_P^{n+1}}{d_{PE}} S_e + \frac{T_P^{n+1} - T_S^{n+1}}{d_{PS}} S_s + \frac{T_N^{n+1} - T_P^{n+1}}{d_{PN}} S_n \right) \right. \\ &\left. + (1-\beta) \left(\frac{T_P^n - T_W^n}{d_{PW}} S_w + \frac{T_E^n - T_P^n}{d_{PE}} S_e + \frac{T_P^{n+1} - T_S^n}{d_{PS}} S_s + \frac{T_N^n - T_P^n}{d_{PN}} S_n \right) \right] \Delta t \end{aligned} \tag{2.4}$$

  Note that here the β factor denotes the use of implicit, explicit or Crank-Nicolson temporal discretization scheme.

- **Source term:** discretized by simply integrating the average value over the CV and along the timestep.

$$\int_{t^n}^{t^{n+1}} \int_{V_P} S\, dV\, dt \approx [\beta S_P^{n+1} + (1-\beta) S_P^n] V_P \Delta t \tag{2.5}$$

Taking all this into consideration, a linear system of equations that relates the nodes of the main molecule for each CV is obtained.

$$a_P T_P^{n+1} = a_W T_W^{n+1} + a_E T_E^{n+1} + a_S T_S^{n+1} + a_N T_N^{n+1} + b_P \tag{2.6}$$

where the numerical coefficients have the following expressions:

$$a_W = \beta\lambda \frac{S_w}{d_{PW}} \tag{2.7}$$

$$a_E = \beta\lambda \frac{S_e}{d_{PE}} \tag{2.8}$$

$$a_S = \beta\lambda \frac{S_s}{d_{PS}} \tag{2.9}$$

$$a_N = \beta\lambda \frac{S_n}{d_{PN}} \tag{2.10}$$

$$a_P = a_W + a_E + a_S + a_N + \rho c_p \frac{V_P}{\Delta t} \tag{2.11}$$

$$b_P = (1-\beta)\left(\frac{T_P^n - T_W^n}{d_{PW}} S_w + \frac{T_E^n - T_P^n}{d_{PE}} S_e + \frac{T_P^{n+1} - T_S^n}{d_{PS}} S_s + \frac{T_N^n - T_P^n}{d_{PN}} S_n\right) + \rho c_p \frac{V_P}{\Delta t} T_P^n \tag{2.12}$$

Thus, equation (2.6) will have to be solved iteratively in the computer algorithm developed.

Note that, in the previous equations, the thermal conductivity λ has been evaluated as constant. However, in some cases (i.e. if different materials are involved) the value of this parameter changes along the domain, meaning that it will have to be computed for the particular position of each face. This is done according to the harmonic mean, as

$$\lambda_i = \frac{d_{PI}}{\frac{d_{Pi}}{\lambda_P} + \frac{d_{iI}}{\lambda_I}} \tag{2.13}$$

This approach is used since it provides more accurate results than the evaluation through the arithmetic mean.

2.2.3. Global resolution algorithm

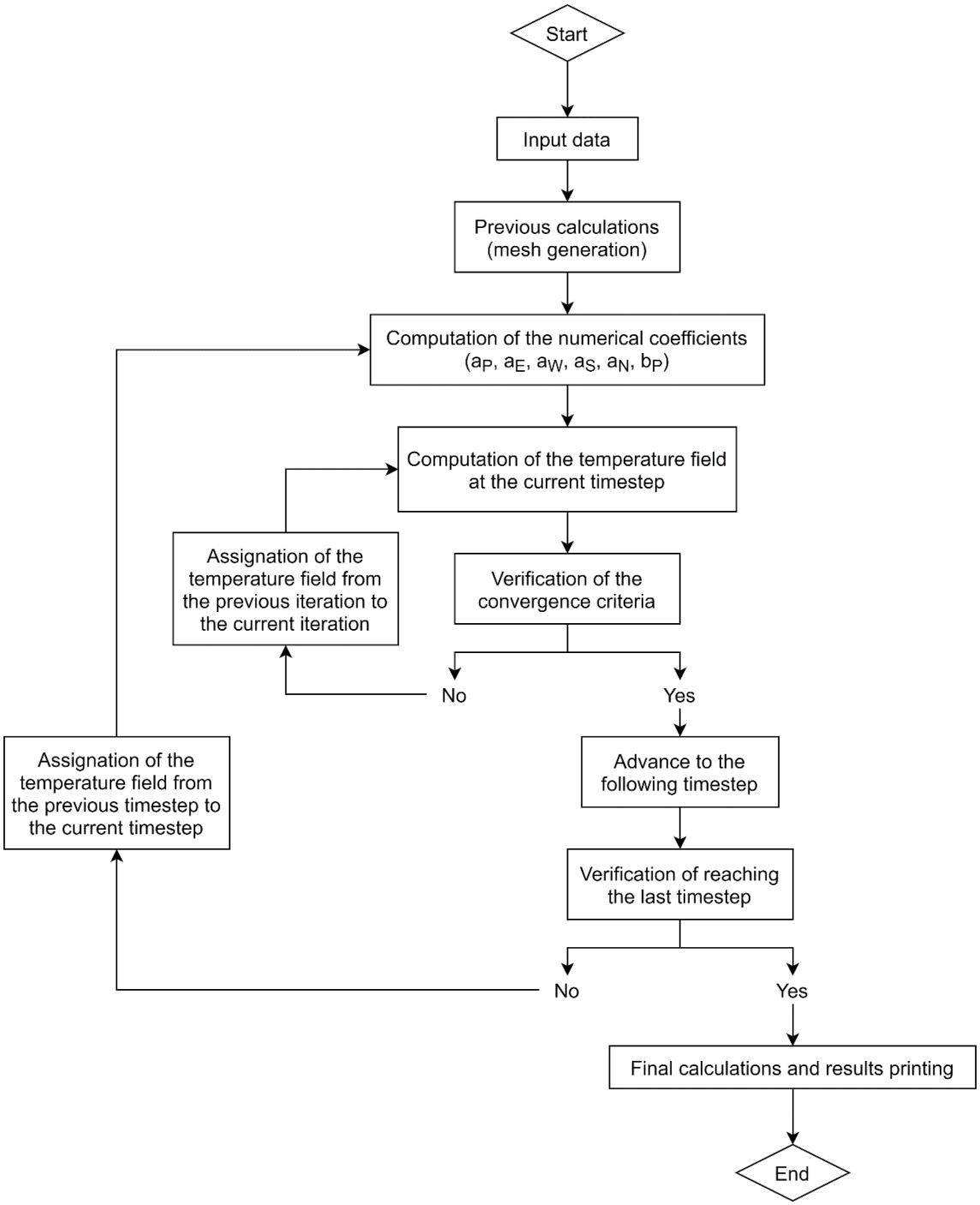

Figure 4. Transient Conduction global resolution algorithm.

2.2.4. Test case: Four-Material Conduction

Consider a two-dimensional domain composed of four different materials, as displayed in Figure 5 below, with $p_1(0.50,0.40)$, $p_2(0.50,0.70)$ and $p_3(1.10,0.80)$, and the material properties displayed in Table 1.

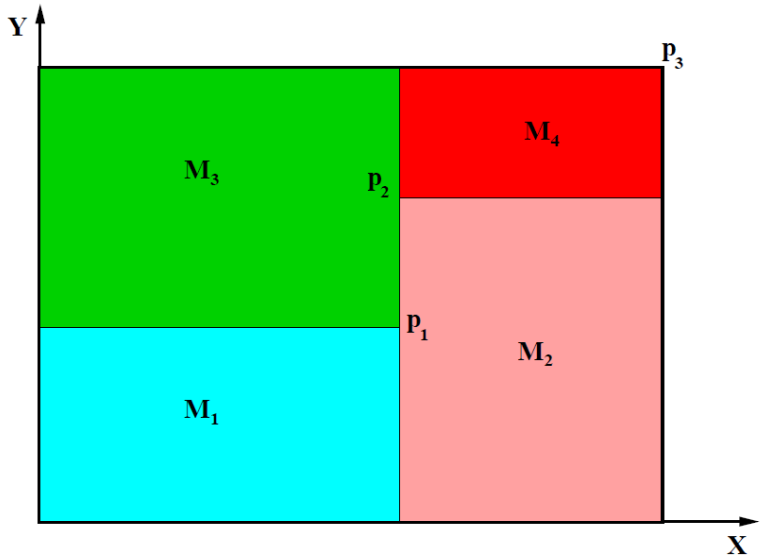

Figure 5. Four-material problem geometry. [17]

	$\rho\ [kg/m^3]$	$c_p\ [J/kgK]$	$\lambda\ [W/mK]$
M_1	1500	750	170
M_2	1600	770	140
M_3	1900	810	200
M_4	2500	930	140

Table 1. Four-material problem physical properties. [17]

The aim is to find the temperature field versus time at the defined domain according to the following boundary conditions:

BOUNDARY	BC TYPE	BC DESCRIPTION
BOTTOM	Dirichlet	Isotherm at $T = 23\ ºC$
TOP	Neumann	Uniform $Q_{flow} = 60\ W/m$
LEFT	Dirichlet	In contact with a fluid at $T_g = 33\ ºC$ and heat transfer coefficient $\alpha_g = 9\ W/m^2K$
RIGHT	Dirichlet	Uniform temperature $T = 8 + 0.005t\ ºC$ (where t is the time in seconds)

Table 2. Four-material problem boundary conditions. [17]

The interesting part of this particular case is the fact that different materials are applied, and the same for the BC's applied, which also depend on time.

2.2.5. Verification

The reference solutions provided by CTTC [17] consisted of the temperature field at $t = 5000\ s$ and the temporal evolution of the temperature at points $p_{ref1}(0.65,0.56)$ and $p_{ref2}(0.74,0.74)$. On a first instance, in Figure 6 are presented the isotherms of the temperature field at $t = 5000\ s$.

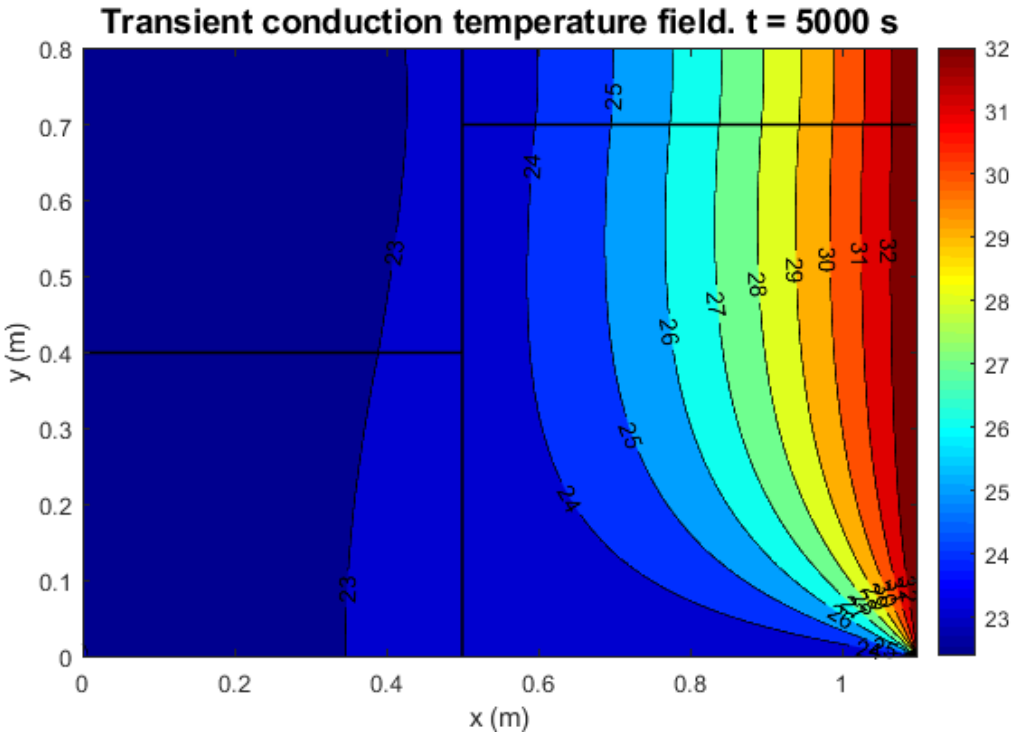

Figure 6. Four-material problem temperature field at t = 5000 s.

As it can be seen, the isobars coincide in shape with the ones displayed in [17], which is a first indicator for validating the algorithm. On the other, hand, from the previous figure it is important to highlight how bottom and right boundaries remain at a uniform temperature of $T = 23\ ºC$ and $T = 33\ ºC$ respectively, according to the BC set established.

Having discussed this issue, a more quantitative analysis is done to validate the algorithm. The following plot depicts the solutions obtained with the implemented code compared to reference solutions at points p_{ref1} and p_{ref2} with a timestep of $t = 1\ s$ and a resolution of 0.002 m, which is equivalent to a mesh of 550x400 elements. The solver used for obtaining the solutions was the Line-by-line, since it was observed to perform faster than the Gauss-Seidel.

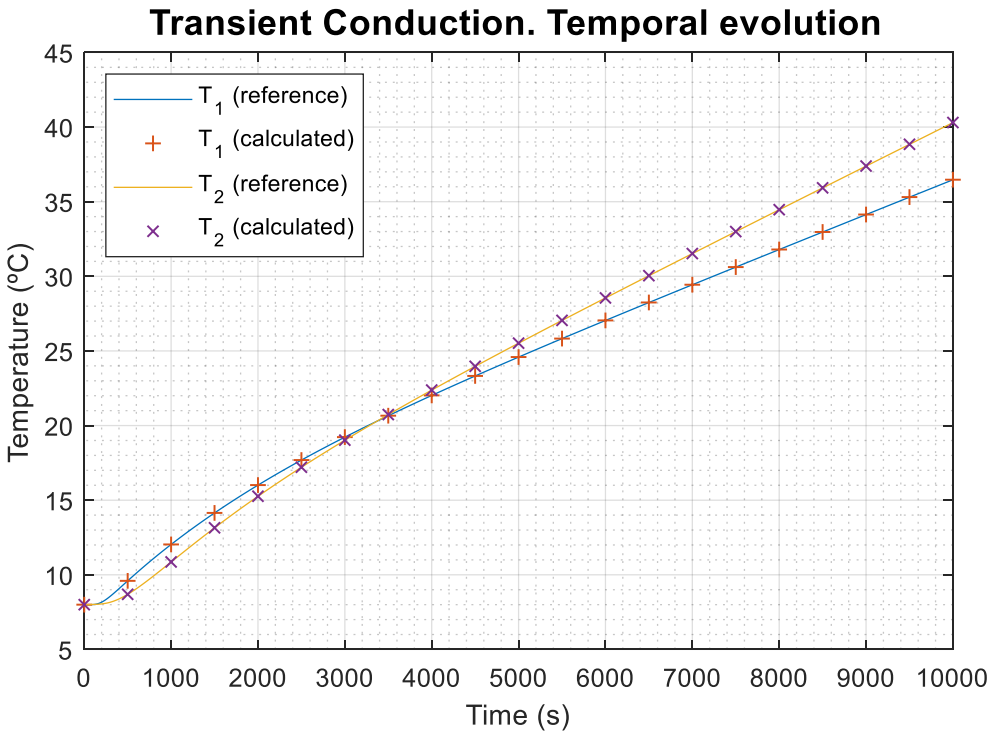

Figure 7. Four-material problem temperature evolution at reference points.

It is corroborated that numerical results coincide with a high degree of accuracy with the reference solution versus time. However, since this can be due to the fact that a fine mesh with a small timestep has been chosen to display the final results, further analyses are developed on the following section.

2.2.6. Numerical studies

Additional studies varying the mesh resolution for a constant timestep size and vice versa have been developed. Results of this error studies are depicted in Figure 8 on the following page.

The study on the effect of the mesh resolution the results (see Figure 8 top) on ranges from an element size of 0.1 m (correspondent to a mesh of 11x8 elements) to 0.001 m (correspondent to a mesh of 1100x800 elements), with a constant timestep size of 0.5 s.

The study on the effect of the timestep size on the results (see Figure 8 bottom) on includes timesteps from 1000 s to 0.1 s, tested with a resolution of 0.005 m (correspondent to a mesh of 220x160 elements).

Data obtained was contrasted with the reference solutions at points p_{ref1} and p_{ref2}.

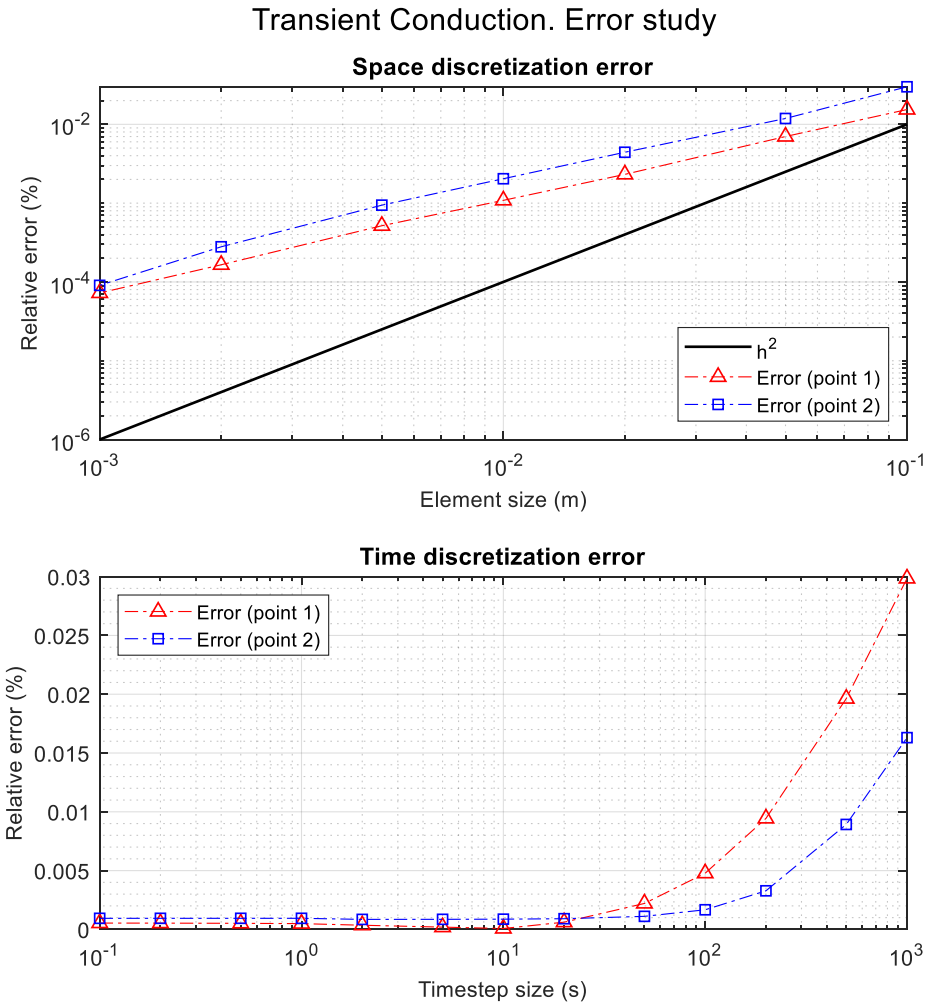

Figure 8. Four-material problem error study.

The first issue that has to be noted from the above displayed study concerns the decrease of the error with the mesh resolution: since a second-order problem is being dealt, the error should decrease quadratically with the number of elements. It can be observed that this tendency is almost accomplished for the smaller elements. For ensuring that this is true, tests with larger number of elements should be conducted, but due to lack of computational resources, this was not possible.

On the other hand, it can also be observed that error decreases with the timestep, until reaching a stabilization point. According to the observations, error is stabilized for timesteps smaller than 10 seconds. This data is important for choosing appropriate number of timesteps without increasing pointlessly computational resources.

It is also important to remark that results obtained are subject to the convergence criteria established (10^{-6}) and the precision of the reference solution (10^{-5}). Again, further studies could be done with denser meshes, smaller timesteps and more precise convergence criteria. Nevertheless, more computational power is required, and thus it was decided to leave it out of the scope of the project, giving as verified the current solvers.

2.3. Potential flow

2.3.1. Mathematical formulation

The concept of potential flow applies to regions of the fluid domain where effects of friction and heat transfer can be neglected, this is out of the boundary layer [18]. A flow under these conditions is called external flow, and it is possible to define the velocity components of the fluid by differentiating the so-called stream function as follows (for a two-dimensional steady case)

$$v_x = \frac{\rho_0}{\rho}\frac{\partial \psi}{\partial y} \tag{2.14}$$

$$v_y = -\frac{\rho_0}{\rho}\frac{\partial \psi}{\partial x} \tag{2.15}$$

Note that equations (2.14) and (2.15) are defined in a bidimensional domain. This, together with the steady state, are two conditions that must be satisfied when dealing with this approach of potential flows, with the mathematical formulation based on the stream function.

Besides, the vorticity of the fluid is defined as

$$\vec{\omega} = \nabla \times \vec{v} \tag{2.16}$$

and the previous expression can be rewritten in terms of the stream function defined above. If also the flow is assumed to be irrotational, equation (2.16) rewritten in terms of ψ results as

$$\frac{\partial}{\partial x}\left(\frac{\rho_0}{\rho}\frac{\partial \psi}{\partial x}\right) + \frac{\partial}{\partial y}\left(\frac{\rho_0}{\rho}\frac{\partial \psi}{\partial y}\right) = 0 \tag{2.17}$$

Notice that the previous expression has a similar form to equation (2.1) of heat conduction, without the unsteady term according to initial assumptions of the formulation.

The previous equation is the one that will be solved for the potential flow problem developed in section *2.3.4. Test case: Flow along a Cylinder*. However, as seen in equation (2.17), this approach can be also applied to non-irrotational flows.

Since stream function equation is defined in a differential form, it will be required to integrate it over a control volume in order to solve the problem, and here the Stokes' theorem must be applied

$$\Gamma = \int_S (\nabla \times \vec{v}) dS = \oint_C \vec{v} d\vec{l} \tag{2.18}$$

which relates the circulation Γ of a vector field (in this case, the velocity field $\vec{v}$) along a closed curve C with the rotational of the same vector field in the surface S enclosed by C [19].

An additional approach, based on the velocity potential function instead of the stream function can be alternatively used, obtaining a similar equation that can be solved using the same methodology. This alternative approach allows to deal with unsteady 3D flows, but the condition of irrotationality is a must [18]. From the point of view of this project, the potential function approach has not been considered since only 2D problems will be tackled in this project, and the stream function equation is thus enough to reach the final objectives.

2.3.2. Discretization of the equations

It can be appreciated that equation (2.17) does not have either transient term or source term. Thus, the only term to be discretized is the diffusive-like term, and since only steady state is considered, only the integration in the CV has to be performed. Divergence theorem will as well used.

$$\int_{V_P}\left[\frac{\partial}{\partial x}\left(\frac{\rho_0}{\rho}\frac{\partial\psi}{\partial x}\right)+\frac{\partial}{\partial y}\left(\frac{\rho_0}{\rho}\frac{\partial\psi}{\partial y}\right)\right]dV=\int_{S_f}\frac{\rho_0}{\rho}\frac{\partial\psi}{\partial\vec{n}}\vec{n}dS$$
$$\approx\frac{\rho_0}{\rho}\left(\frac{\psi_P-\psi_W}{d_{PW}}S_w+\frac{\psi_E-\psi_P}{d_{PE}}S_e+\frac{\psi_P-\psi_S}{d_{PS}}S_s+\frac{\psi_N-\psi_P}{d_{PN}}S_n\right) \quad (2.19)$$

Thus, the linear system of equations to be solved has the form

$$a_P\psi_P=a_W\psi_W+a_E\psi_E+a_S\psi_S+a_N\psi_N+b_P \quad (2.20)$$

where the numerical coefficients have the following expressions:

$$a_W=\frac{\rho_0}{\rho}\frac{S_w}{d_{PW}} \quad (2.21)$$

$$a_E=\frac{\rho_0}{\rho}\frac{S_e}{d_{PE}} \quad (2.22)$$

$$a_S=\frac{\rho_0}{\rho}\frac{S_s}{d_{PS}} \quad (2.23)$$

$$a_N=\frac{\rho_0}{\rho}\frac{S_n}{d_{PN}} \quad (2.24)$$

$$a_P=a_W+a_E+a_S+a_N \quad (2.25)$$

$$b_P=0 \quad (2.26)$$

Thus, equation (2.20) will have to be solved iteratively in the computer algorithm developed.

2.3.3. Global resolution algorithm

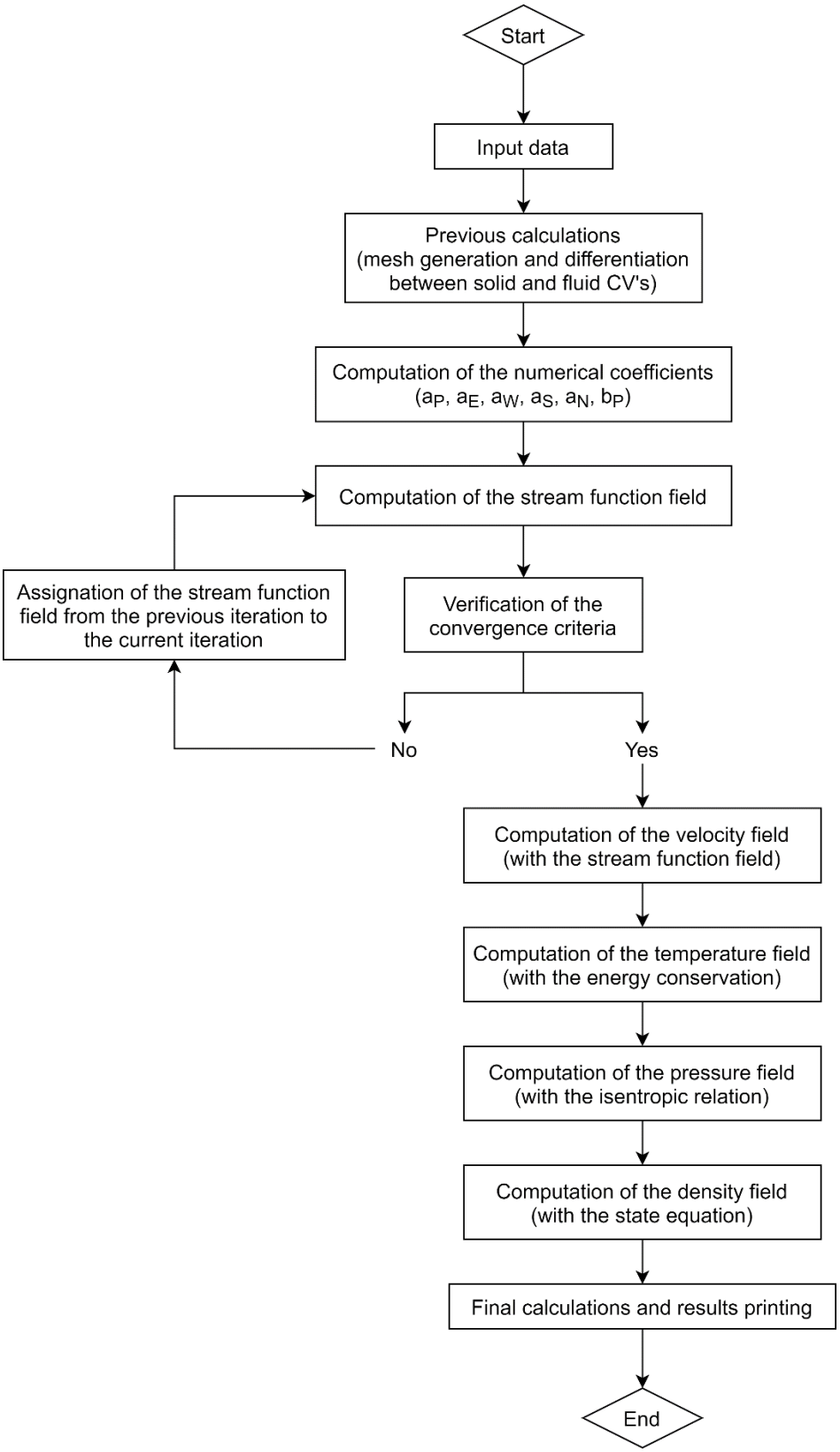

Figure 9. Potential flow global resolution algorithm.

2.3.4. Test case: Flow along a Cylinder

Consider a two-dimensional domain consisting of a channel of length H and height V, with an inlet at the left side and an outlet at the right side, as displayed in Figure 10. A fluid enters parallel to the channel at the inlet (with null vertical velocity) and at particular fluid properties u_{in}, T_{in}, p_{in} and ρ_{in}. Inside the channel, the presence of a solid object, in this case a circular cylinder of diameter D, interferes with the flow altering the velocity field.

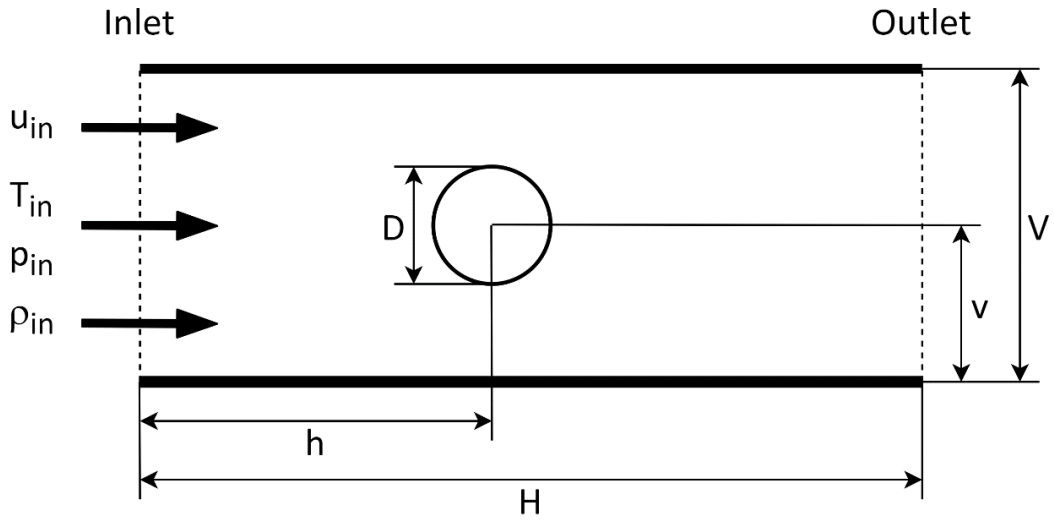

Figure 10. Potential flow problem geometry.

For the test case, the geometrical and physical properties used are summarized in the following table. Note that gas properties used coincide with air at ambient conditions.

VARIABLE	$H\ [m]$	$V\ [m]$	$h\ [m]$	$v\ [m]$	$D\ [m]$	M_{in}	$T_{in}\ [K]$	$p_{in}\ [bar]$	$c_p\ [J/kg \cdot K]$	γ
VALUE	1	1	0.5	0.5	0.02	0.1	288.15	1	1004	1.4

Table 3. Potential flow problem geometrical and physical properties.

Hence, the aim is to find the velocity field in the channel, as well as the fluid properties at each point of the domain according to the following boundary conditions:

BOUNDARY	BC TYPE	BC DESCRIPTION
BOTTOM	Dirichlet	Uniform stream function value $\psi = \psi_A$
TOP	Dirichlet	Uniform stream function value $\psi = \psi_B = \psi_A + v_{in}H$
INLET	Dirichlet	Uniform velocity, which corresponds to linear variation of the stream function value $\psi = \psi_B = \psi_A + v_{in}y$
OUTLET	Neumann	Parallel flow condition $\frac{\partial \psi}{\partial n} = 0$

Table 4. Potential flow problem boundary conditions.

2.3.5. Verification

Results can be contrasted with the known analytical solution of the problem, consisting of the stream function for a doublet superposed with uniform flow, that has the form

$$\psi_d = v_{in}\left[\frac{V}{2} + y\left(1 - \left(\frac{D/2}{\sqrt{x^2+y^2}}\right)^2\right)\right] \tag{2.27}$$

Some problems were encountered in this stage since, at the end, the analytical solution only coincides with the boundary conditions imposed if the cylinder is small enough to consider that, in the analytical case, streamlines are parallel far from the object.

For this reason, a cylinder of diameter 0.02 m was tested in front of a domain of size 1-by-1 m. Plotting the error versus different mesh resolutions, the following result is obtained.

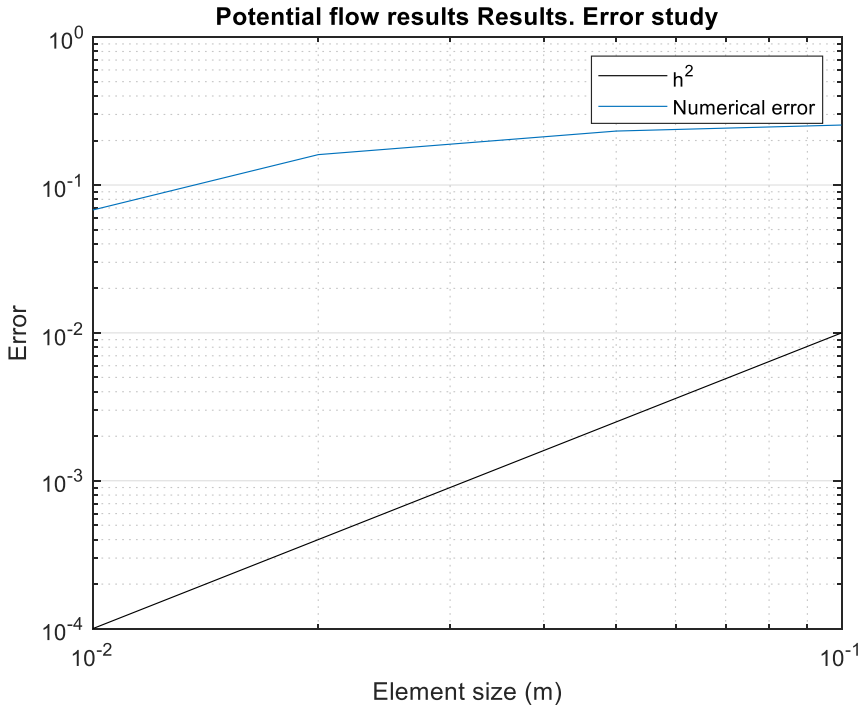

Figure 11. Potential flow problem convergence study.

It is appreciated that the tendency of the error is to decrease with the square of the element size. Higher number of elements was not tested due to computational resources limitations. As it was mentioned before, the smaller the cylinder, the better the match between analytical and numerical results, but small cylinder means higher number of elements to properly discretize it, thus meaning more computational time. This was the main difficulty found with these simulations.

2.3.6. Discussion of the results

Due to the presence of an object inside the channel, in this case a mesh hyperbolically concentrated towards the cylinder of 101x101 elements was used and a concentration factor of 2 (see Figure 12 below).

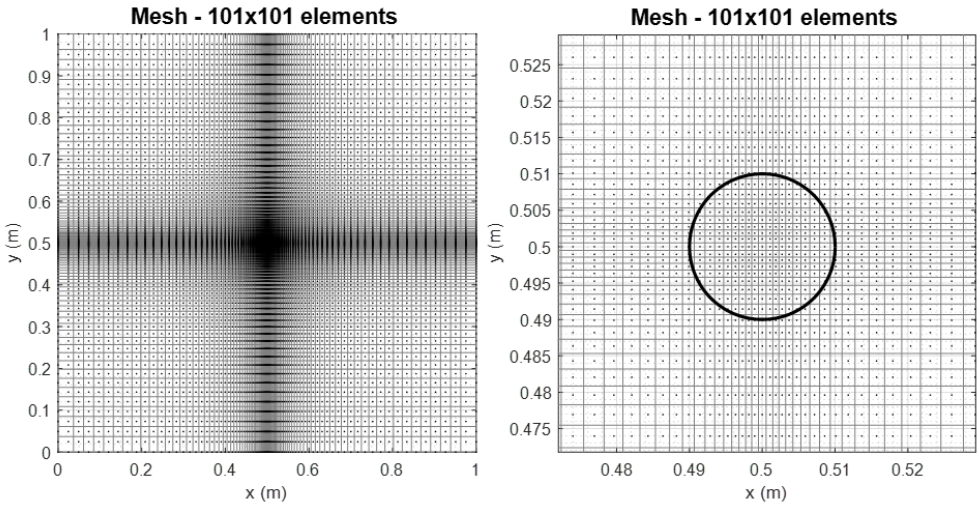

Figure 12. Potential flow problem mesh (left), with a zoom on the cylinder (right).

On the following figure is presented the stream function field.

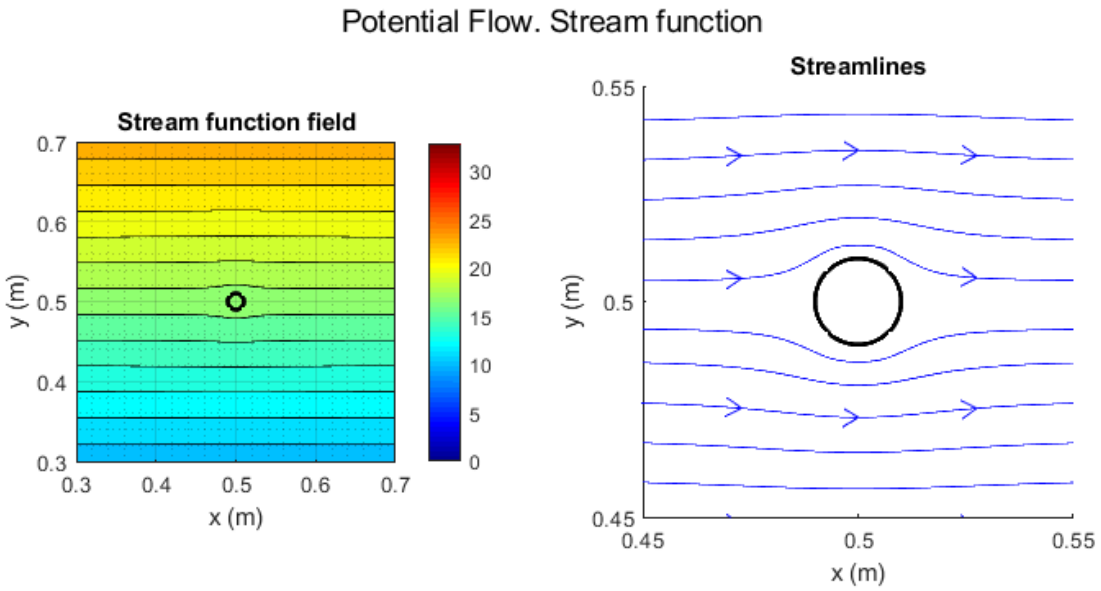

Figure 13. Potential flow problem stream function field (left) and streamlines (right).

It can be appreciated that effect of the cylinder inside the flow consists of a squeezing of the streamlines above and below the object, which is translated to an increase of velocity and a decrease of pressure and temperature (see Figure 14 below). However, far from the cylinder, the stream function field is not perturbed and streamlines remain parallel, according to the BC's set at top and bottom boundaries.

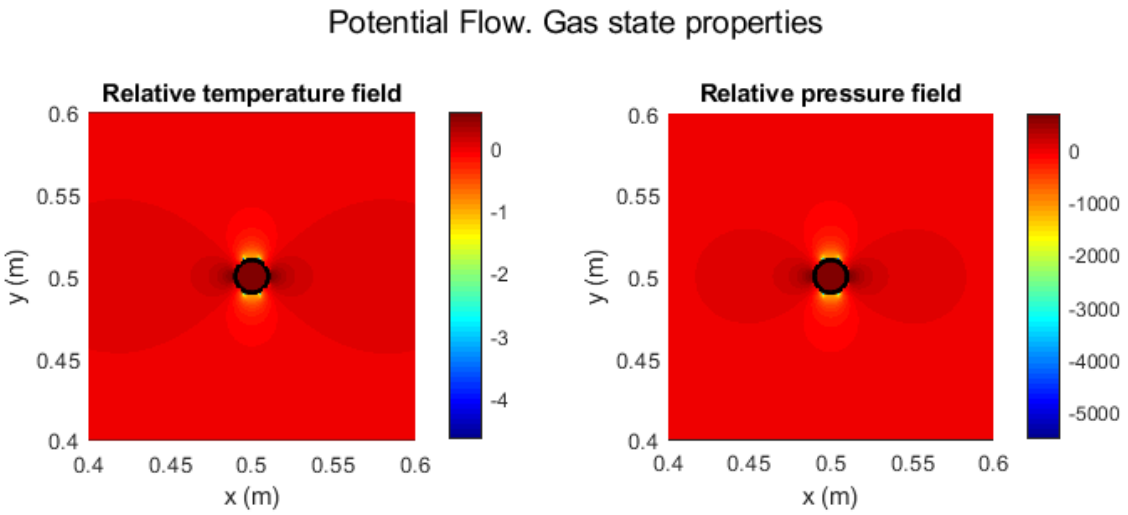

Figure 14. Potential flow problem temperature field (left) and pressure (right).

Regarding the pressure and temperature fields, it can be observed that energy conservation is verified, as high velocity regions account for low temperature regions and vice versa. The same happens with the pressure.

Nevertheless, it is important to highlight that the discretization of the cylinder was based on the location of the nodes, considering solid nodes the ones whose coordinates are inside the circle and external if the coordinates fall outside. Since the shape of the control volumes is still rectangular, this gives a sharp and low-precision discretization of the curved surface of the cylinder, which may easily induce to peaks of pressure and temperature (four of those can be observed in Figure 14) or some imprecisions in the result.

Despite that, the expectations according to the aims of this project are fulfilled, and for this reason no further studies of the problem are developed.

2.4. Conclusions

In this chapter, the underlying physics of simple diffusion phenomena, such as heat conduction and the behaviour of external flows, has been studied and discussed, as well as with dealing with both steady and transient problems. Additionally, first encounters with the numerical methods and finite volume analysis have been achieved, studying the effect of basic discretization parameters as mesh size, nodal distribution or timestep size on the final problem solution.

Several problems had to be tackled in this initial stage. As a matter of example, one of these difficulties was the computational time required to perform calculations with fine meshes and small timesteps. For the development of further (and more complex) problems, which are explained later on in this report, this issue becomes even more critical, thus meaning that some improvements are going to be done, with the implementation of more powerful solvers such as the Conjugate Gradient.

Moreover, it has been observed that computational resources can be optimized by modifying the nodal distribution for the same number of control volumes, as done in the potential flow problem with an object. Despite this, it has to be remarked that the discretization used for the circular cylinder is poor, even with hyperbolic concentration, with a structured mesh. Here is highlighted the fact that, for complex geometries, other types of meshes, i.e. unstructured meshes, would fit better the shape of the bodies. However, this is out of the scope of this project, and it has been considered that the depth with which diffusion problems has been treated is enough.

In summary, the most basic concepts and formulation have been reviewed and understood, leading to a new stage on the development of this project.

3. Convection-diffusion equation

3.1. Introduction

Up to this point, the terms of Fluid Dynamics and Heat Transfer equations that have been mathematically reviewed are the unsteady term, the diffusive term and the source term in different types of Fluid Dynamics and Heat Transfer physical problems. In this chapter, the convective term will be analysed and brought together with the other terms studied.

3.2. Mathematical formulation

The concept of convection (also called advection) refers to how a property is transported along a fluid domain due to the movement of the particles conforming the fluid. This is the reason why it only makes sense to talk about convection with fluids (either liquids or gases), as there is no movement of particles in solids.

The convective term is characterised by coupling the movement of the fluid (through its density and velocity) with the property that is being transported, which gives the form $\frac{\partial}{\partial x}(\rho u \phi)$ [15]. If one incorporates the convective term to the abovementioned terms in a single equation, the following expression is obtained for a generic variable ϕ in a multidimensional domain:

$$\frac{\partial(\rho\phi)}{\partial t} + \nabla \cdot (\rho \vec{v} \phi) = \nabla \cdot \left(\Gamma_\phi \nabla \phi\right) + S_\phi \tag{3.1}$$

This equation is known as the generic convection-diffusion transport equation, and here the four terms can be clearly distinguished:

- Unsteady term $\frac{\partial(\rho\phi)}{\partial t}$
- Convective term $\nabla \cdot (\rho \vec{v} \phi)$
- Diffusive term $\nabla \cdot \left(\Gamma_\phi \nabla \phi\right)$
- Source term S_ϕ

It is relevant to remark that equation (3.1) is called "generic" because it is possible to obtain all the conservation laws by setting the values of the generic property ϕ, the diffusion coefficient Γ_ϕ and the source term S_ϕ. On the following table are summarized the different well-known conservation equations according to the values of ϕ, Γ_ϕ and S_ϕ [20].

Conservation law	ϕ	Γ_ϕ	S_ϕ	*Equation*
Mass	1	0	0	$\frac{\partial \rho}{\partial t} + \nabla \cdot (\rho \vec{v}) = 0$
Momentum	$\vec{v}$	μ	$-\nabla p + \nabla \cdot (\vec{\tau} - \mu \nabla \vec{v}) + \rho g$	$\frac{\partial(\rho \vec{v})}{\partial t} + \nabla \cdot (\rho \vec{v} \vec{v}) = \nabla \cdot (\mu \nabla \vec{v}) - \nabla p + \nabla \cdot (\vec{\tau} - \mu \nabla \vec{v}) + \rho g$
Energy	u	$\frac{\lambda}{c_v}$	$\frac{1}{c_v}(-\nabla \cdot \dot{q}^R - p \nabla \cdot \vec{v} + \vec{\tau} : \nabla \vec{v})$	$\frac{\partial(\rho u)}{\partial t} + \nabla \cdot (\rho \vec{v} u) = \nabla \cdot \left(\frac{\lambda}{c_v} \nabla u\right) + \frac{1}{c_v}(-\nabla \cdot \dot{q}^R - p \nabla \vec{v} + \vec{\tau} : \nabla \vec{v})$
Species	Y_k	ρD_k	$\dot{\omega}_k$	$\frac{\partial(\rho Y_k)}{\partial t} + \nabla \cdot (\rho \vec{v} Y_k) = \nabla \cdot (\rho D_k \nabla Y_k) + \dot{\omega}_k$

Table 5. Deduction of NS and mass transport equations from generic convection-diffusion equation.

The set of the first three equations are known as the Navier-Stokes equations, whilst the last one corresponds to the mass transport equation of species.

For the particular case of this stage of the project, the problem treating the convection-diffusion equation will be limited to incompressible steady regime and with $S_\phi = 0$ in a two-dimensional domain, which leads to the following simplified equation:

$$\nabla \cdot (\rho \vec{v} \phi) = \nabla \cdot \left(\Gamma_\phi \nabla \phi\right) \tag{3.2}$$

The previous simplification is done due to the fact that the important part of this step is to understand the convective term and its numerical discretization, which requires a slightly different treatment than the diffusive or unsteady terms. Further information about this issue can be found in the following section.

Another important issue to remark is that, for the convection-diffusion problem tackled in this chapter of the report, the transport velocity field is assumed to be known beforehand.

3.3. Discretization of the equations

In order to integrate the diffusive term of equation (3.1), which is in differential form, it is first required to do a mathematical manipulation first in order to reduce the order of the derivative. Hence, the divergence theorem can be applied and the volume integrals become surface integrals, as follows:

$$\int_{V_P} \nabla \cdot \left(\Gamma_\phi \nabla \phi\right) dV = \int_{S_f} \left(\Gamma_\phi \nabla \phi\right) \cdot \vec{n} dS \tag{3.3}$$

Now the diffusive term has only a gradient that is no more than a first order derivative. Thus, integrating the right-hand term of equation (3.3) also versus time, for a bidimensional domain the discretized diffusive term has the form

$$\begin{gathered} \int_{S_f} \left(\Gamma_\phi \nabla \phi\right) \cdot \vec{n} dS \approx \\ \approx \left(\Gamma_e \frac{\phi_E - \phi_P}{d_{PE}} S_e - \Gamma_w \frac{\phi_P - \phi_W}{d_{PW}} S_e + \Gamma_n \frac{\phi_N - \phi_P}{d_{PN}} S_n - \Gamma_s \frac{\phi_P - \phi_S}{d_{PS}} S_s \right) \end{gathered} \tag{3.4}$$

Notice that, in this case, the temporal integration is fully implicit since unsteady term was eliminated from equation (3.1) according to the above explained simplifications. Additionally, it can be seen that the discretization shown in equation (3.4) is analogous to the ones in equations (2.4) and (2.19).

Similar to the diffusive term, divergence theorem can be applied to the convective term in order to reduce the order of the derivatives, as displayed below.

$$\int_V \nabla \cdot (\rho \vec{v} \phi) dV = \int_{S_f} (\rho \vec{v} \phi) \cdot \vec{n} dS \tag{3.5}$$

with this manipulation, the derivatives disappear from the convective term. Additionally, the definition of mass flow can be applied:

$$d\dot{m} = \rho \vec{v} \cdot \vec{n} dS \tag{3.6}$$

and this leads to the following expression of the convective term:

$$\int_{S_f} (\rho \vec{v} \phi) \cdot \vec{n} dS \approx \dot{m}_e \, \phi_e \, - \dot{m}_w \phi_w \, + \dot{m}_n \, \phi_n \, - \dot{m}_s \, \phi_s \tag{3.7}$$

Note that it is required to estimate the values of ϕ at the control volume faces. It is this issue what generates the main difficulty of the calculation of the convective term. Several schemes have been developed to provide an estimated value of the property at the face [21]. Each one of them has its advantages and drawbacks regarding convergence, accuracy and complexity. Below are detailed the ones that have been considered in this project:

- **Upwind Difference Scheme (UDS):** assumes that the property value at the face coincides with the value of the upstream node, taking into account the direction of the flow.
  This is the simplest scheme and one of the most stable ones. However, its use must be carefully selected, since it amplifies the phenomenon of false diffusion. It is for this reason why higher-order schemes have been developed.
- **Central Difference Scheme (CDS):** assumes that the property value changes linearly between two consecutive nodes. It is more accurate than UDS, but also more unstable under certain conditions.
- **Quadratic Upwind Interpolation for Convective Kinematics (QUICK):** scheme that parabolically interpolates the property value at the face using three nodes: two upstream and one downstream with respect to the face.
- **Sharp and Monotonic Algorithm for Realistic Transport (SMART):** high-order scheme that fits the interpolation region inside a particular domain for convergence and stability reasons (bounded scheme).

An analysis of the accuracy of each scheme is developed later on in the report.

Finally, arranging and manipulating conveniently the discretized convective and diffusive term in order to introduce the evaluation through high-order resolution schemes, the following linear equation is obtained

$$a_P\phi_P = a_W\phi_W + a_E\phi_E + a_S\phi_S + a_N\phi_N + b_P \tag{3.8}$$

where the numerical coefficients have the following expressions:

$$a_W = \Gamma_w \frac{S_w}{d_{PW}} + \frac{\dot{m}_w + |\dot{m}_w|}{2} \tag{3.9}$$

$$a_E = \Gamma_e \frac{S_e}{d_{PE}} - \frac{\dot{m}_e - |\dot{m}_e|}{2} \tag{3.10}$$

$$a_S = \Gamma_s \frac{S_s}{d_{PS}} + \frac{\dot{m}_s + |\dot{m}_s|}{2} \tag{3.11}$$

$$a_N = \Gamma_n \frac{S_n}{d_{PN}} - \frac{\dot{m}_n - |\dot{m}_n|}{2} \tag{3.12}$$

$$a_P = a_W + a_E + a_S + a_N \tag{3.13}$$

$$b_P = \dot{m}_w(\phi_w^{HRS} - \phi_w^{UDS}) - \dot{m}_e(\phi_e^{HRS} - \phi_e^{UDS}) + \dot{m}_s(\phi_s^{HRS} - \phi_s^{UDS}) - \dot{m}_n(\phi_n^{HRS} - \phi_n^{UDS}) \tag{3.14}$$

Thus, equation (3.8) will have to be solved iteratively in the computer algorithm developed.

3.4. Global resolution algorithm

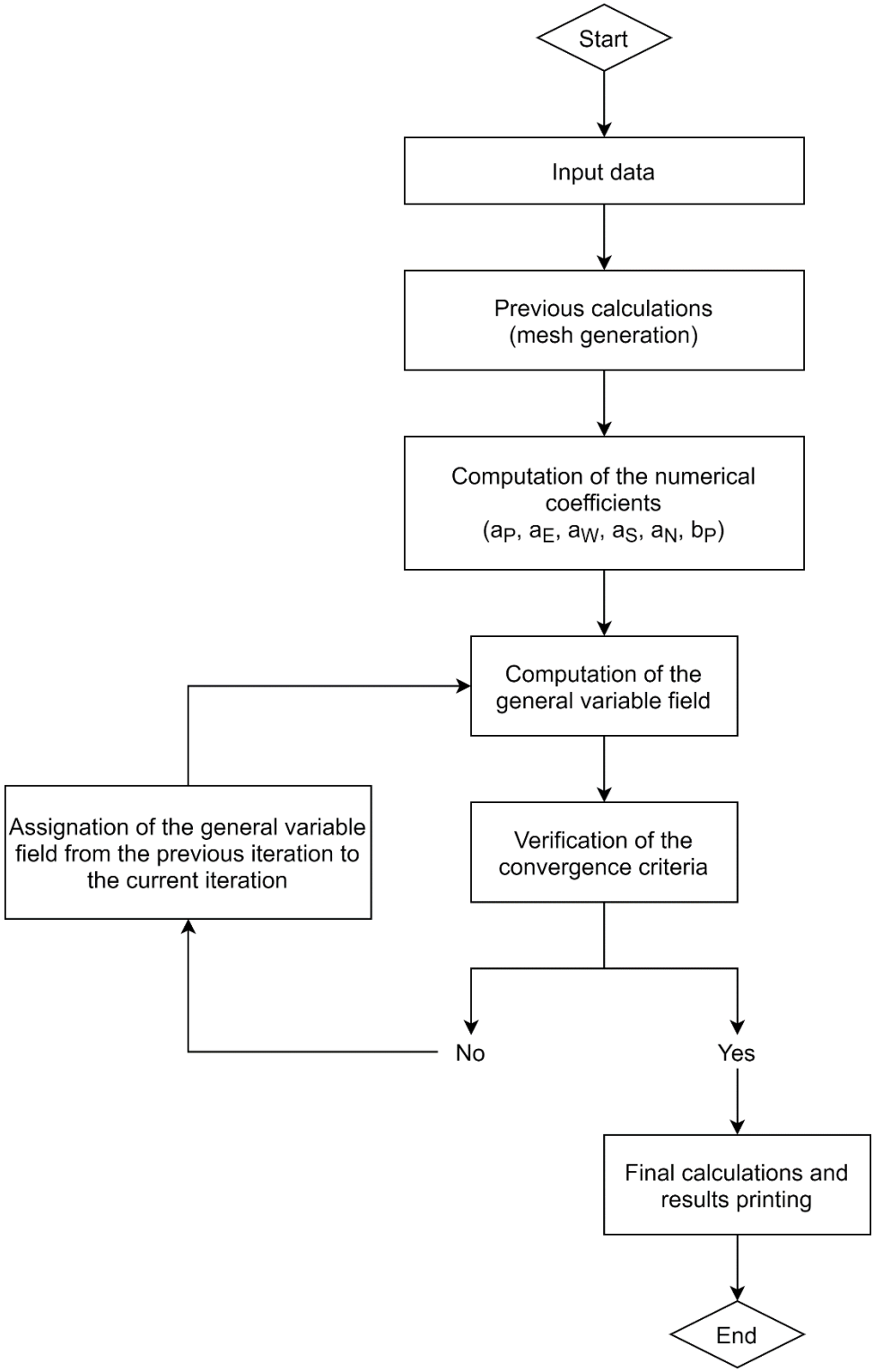

Figure 15. Steady Convection-Diffusion global resolution algorithm.

3.5. Test cases description

This section provides the explanation of the two problems used as verification for convection-diffusion algorithm implemented. Unlike the previous chapter, verification and discussion of the results is done for both cases together in sections *3.6. Verification* and *3.7. Discussion of results*, respectively.

3.5.1. Test case 1: Diagonal Flow

Consider a two-dimensional squared domain of length and height L, where a fluid flows with a prescribed uniform steady velocity v_0 in a direction α respect to the horizontal (see Figure 16).

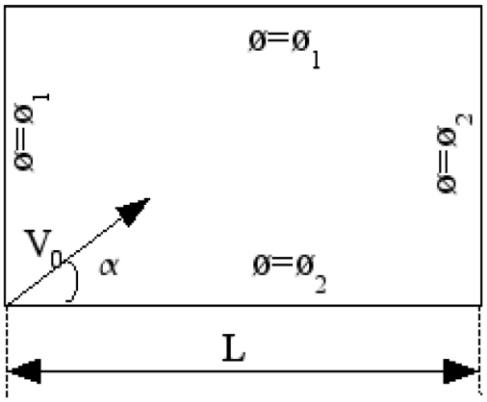

Figure 16. Diagonal flow problem geometry and velocity field. [22]

Velocity is considered to be unitary and $\alpha = 45º$. The aim of this problem is to find the general property distribution along the domain for different convection-to-diffusivity ratios, or in other words, for different Péclet numbers, non-dimensional group defined as

$$Pe = \frac{\rho v L}{\Gamma} \tag{3.15}$$

The boundary conditions set for this problem are summarized on the table below.

BOUNDARY	BC TYPE	BC DESCRIPTION
BOTTOM	Dirichlet	Uniform general property value $\phi = \phi_2$
TOP	Dirichlet	Uniform general property value $\phi = \phi_1$
LEFT	Dirichlet	Uniform general property value $\phi = \phi_1$
RIGHT	Dirichlet	Uniform general property value $\phi = \phi_2$

Table 6. Diagonal flow problem boundary conditions. [22]

This problem is of special interest in order to qualitatively observe the dominance of convection or diffusion varying the main non-dimensional parameter of the problem. Additionally, special attention has to be paid to the evaluation scheme of the convective term used, so as to deal with the false diffusion phenomenon.

3.5.2. Test case 2: Smith-Hutton Problem

Consider a two-dimensional rectangular domain, where a fluid flows with a prescribed steady solenoidal velocity field that has the form

$$v_x = 2y(1 - x^2) \tag{3.16}$$

$$v_y = -2x(1 - y^2) \tag{3.17}$$

The domain has an inlet at the bottom left and an outlet at the bottom right, as depicted in Figure 17.

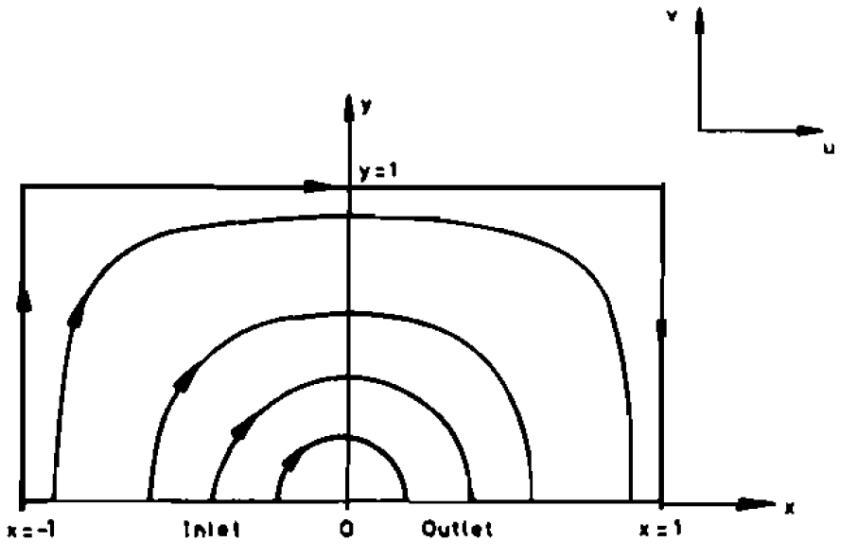

Figure 17. Smith-Hutton problem geometry and velocity streamlines. [23]

The aim of this problem is the same as for the case of the diagonal flow in the previous section, for observing the general variable behaviour as a function of the Péclet number.

Additionally, a comparison to benchmark solutions provided by [23] will be done.

The boundary conditions set for this problem are summarized on the table below, with $\alpha = 10$.

BOUNDARY	BC TYPE	BC DESCRIPTION
BOTTOM INLET ($-1 < x < 0$)	Dirichlet	General property value $\phi = 1 + \tanh[(2x + 1)\alpha]$
BOTTOM OUTLET ($0 < x < 1$)	Neumann	$\frac{\partial \phi}{\partial n} = 0$
TOP	Dirichlet	Uniform general property value $\phi = 1 - \tanh[\alpha]$
LEFT	Dirichlet	Uniform general property value $\phi = 1 - \tanh[\alpha]$
RIGHT	Dirichlet	Uniform general property value $\phi = 1 - \tanh[\alpha]$

Table 7. Smith-Hutton problem boundary conditions. [22]

3.6. Verification

As mentioned in the previous section, for the case of solenoidal flow, benchmark solutions for the three Péclet numbers analysed are available at [22]. A comparison between both literature and numerical results is depicted on the following figure.

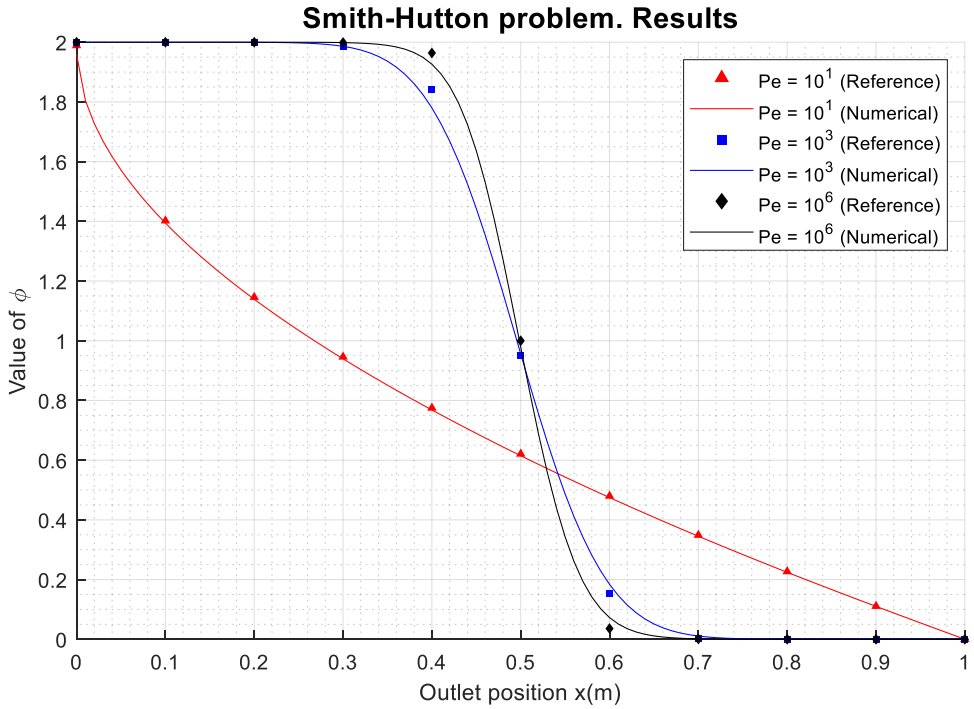

Figure 18. Smith-Hutton problem results comparison with benchmark solution.

As shown, computed results displayed as lines fit with the benchmark points. The coincidence is higher when diffusion dominates, and this is attributed to the phenomenon of false diffusion, mentioned in section *3.3. Discretization of the equations*, caused by the discretization of the convective term. Note that the numerical solution in all cases shows a slightly higher diffusion rate than the reference.

Phenomenon of false diffusion can be avoided by two ways: firstly, by increasing the mesh density, but this option may increase substantially the computational time; and secondly, by using higher order schemes, which is strongly preferable and more efficient than the use of finer meshes. Nevertheless, it is important to bear in mind that false diffusion is always present, even if high order evaluation schemes are used, due to the intrinsic nature of the discretization of the convection-diffusion equation.

One way to avoid the numerical diffusion is by means of symmetry-preserving schemes [24], yet some accuracy might be lost with high convection dominates. The implementation of this type of evaluation schemes has not been considered in this project, as high order schemes are enough according to the objectives.

3.7. Discussion of results

For the convection-diffusion problems of diagonal flow and solenoidal flow, a first qualitative analysis can be done in order to discuss the implications of the convective and diffusive terms in the resultant steady property field. In order to do this, computations of both problems have been run for three different Péclet numbers: 10, 1000 and 10^6.

Recall that Péclet number is defined as $Pe = \frac{\rho v L}{\Gamma}$, which is no more than the ratio between the transport due to convection and the transport due to diffusion. Hence, a low Péclet number implies diffusion dominance, whereas high Péclet numbers imply that the convection is much more important respect to the diffusion rate.

The mesh used to present the solutions to this problem is a uniform mesh of 100x100 elements. In Figure 19 on the following page are presented the property fields obtained for both diagonal and solenoidal flows under the aforementioned test conditions.

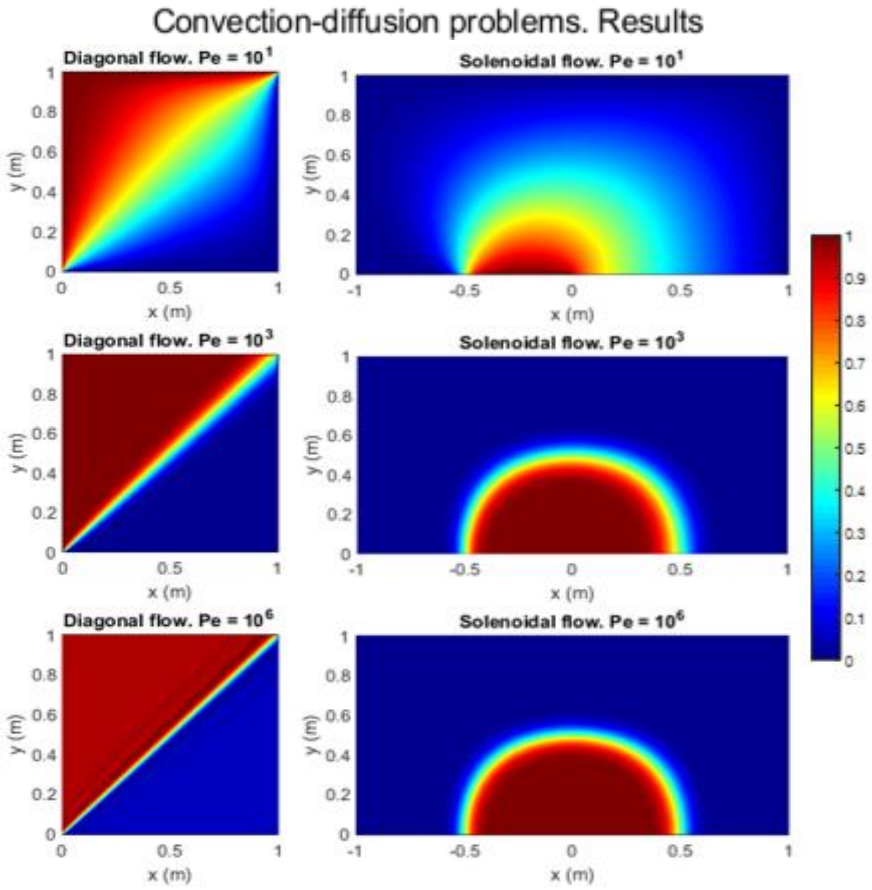

Figure 19. Convection-diffusion problems property fields.

The above figure allows to see very clearly the effect of convection and diffusion in the property field: for lower Péclet numbers, where convection is small, the value of the variable tends to change "as smoothly as possible" along the domain. On the other hand, when convection gains importance, it can be appreciated that the variable tends to be transported changing as little as possible following the direction of the flow and according to its inlet value.

3.8. Conclusions

Up to this point, the role of both convective and diffusive terms has been analysed and discussed, and the intrinsic difficulties of advection have been tackled.

It has been constated, however, that the complexity of the convective term is way higher than the diffusive term, especially in terms of numerical methods for its computation. This was indeed the main problem encountered during this phase, and on certain occasions, the convergence of the algorithm could not be achieved or some numerical oscillations were observed. It is for this reason that it is important to choose wisely the evaluation scheme of the convective term, not only to obtain converged results but also to reach the correct solution.

Understanding the convection-diffusion equation is of special relevance since, as it has been observed at the beginning of section *3.2. Mathematical formulation*, at the end the Navier-Stokes equations have all the same shape and can be derived from this equation, which is the next step of this project.

4. Navier-Stokes equations

4.1. Introduction

So far, all the types of terms present in the conservation laws have been reviewed and understood. However, as mentioned in the previous chapter, the velocity field was given, while normally the flow field is not known and it is part of the solution to be found. This chapter extends the convection-diffusion equation to those cases where the flow field is what has to be solved and found, and it is verified with several cases of different natures.

4.2. Mathematical formulation

Taking a look at the Navier-Stokes equations displayed on Table 5 from the previous chapter, it is possible to conclude that the equation that provides the solution of the velocity field is the momentum equation, whilst energy equation does not provide useful information for the moment (it will be tackled later on).

Therefore, $\phi = \vec{v}$, $\Gamma_\phi = \mu$ and $S_\phi = -\nabla p + \rho\vec{g}$ (assuming constant viscosity), and for an incompressible flow the Navier-Stokes mass and momentum equations have respectively the form

$$\nabla \cdot \vec{v} = 0 \tag{4.1}$$

$$\rho\frac{\partial \vec{v}}{\partial t} + (\rho\vec{v}\cdot\nabla)\vec{v} = -\nabla p + \mu\Delta\vec{v} + \rho\vec{g} \tag{4.2}$$

One of the main remarkable facts of the momentum equation is that the variable transported by the flow field is the flow field itself. This introduces a non-linearity in the convective term, due to the fact that the velocity is multiplied by its derivative. The main implication of this fact is the turbulence phenomenon, which will not be treated in this study as such high convection rates are not going to be achieved, but there is information available in the literature [25].

Besides, there is an additional complexity underlying the momentum equation, which is the fact that the pressure field is also unknown. For this reason, it will be also required to make use of the mass conservation equation in order to solve this coupling between pressure and velocity fields [15].

To the previous set of equations, it is also possible to introduce a coupling with the energy equation, i.e. in buoyancy problems, which implies that the temperature field of the fluid has also an influence on the final solution. This coupling is on the volume force term of equation (4.2), as temperature generates density variations that can be relevant depending on the flow conditions. This is explained on the following chapter.

4.3. Discretization of the equations: Fractional Step Method

In order to solve the Navier-Stokes equations of mass and momentum (and energy, if necessary) and find pressure and velocity fields, a methodology named Fractional Step Method (FSM from now on) was developed.

The starting point of the FSM are the incompressible Navier-Stokes equations shown in the previous chapter, which can be written in a more compact notation

$$\nabla \cdot \vec{v} = 0 \tag{4.3}$$

$$\rho \frac{\partial \vec{v}}{\partial t} = R(\vec{v}) - \nabla p \tag{4.4}$$

where $R(\vec{v}) = \mu \Delta \vec{v} - (\rho \vec{v} \cdot \nabla)\vec{v} + \rho \vec{g}$, which is a term only dependent on the velocity. Note that $\vec{v}$ is a vector, meaning that there is one velocity field per cartesian component.

The time integration used in FSM is slightly more complex than the simple implicit-explicit approach, and in this case two previous timesteps will be involved in the time-discretized Navier-Stokes momentum equation:

$$\nabla \cdot \vec{v}^{n+1} = 0 \tag{4.5}$$

$$\rho \frac{\vec{v}^{n+1} - \vec{v}^{n}}{\Delta t} = \frac{3}{2} R(\vec{v}^{n}) - \frac{1}{2} R(\vec{v}^{n-1}) - \nabla p^{n+1} \tag{4.6}$$

From the previous equations, $\vec{v}^{n}$ and $\vec{v}^{n-1}$ are assumed known, since the calculations at different timesteps advance in the direction of time, whilst the unknown fields are $\vec{v}^{n+1}$ and p^{n+1}. Thus, the evaluation of $R(\vec{v}^{n})$ and $R(\vec{v}^{n-1})$ can be done using the spatial discretizations shown above in the report for convective and diffusive terms.

The FSM is a resolution methodology based on the application of the Helmholtz-Hodge decomposition theorem to the Navier-Stokes equations. Through this theorem it is possible to define the so-called predictor velocity as the sum of a divergence-free vector (which is the real velocity, recall the mass conservation equation) and a pure gradient field (which is the pressure field conveniently arranged), as displayed below [26].

$$\vec{v}^{p} = \vec{v}^{n+1} + \frac{\Delta t}{\rho} \nabla p^{n+1} \tag{4.7}$$

Thus, by replacing the previous expression discretized in time in equation (4.6), it is possible to obtain an expression from which the predictor velocity can be found

$$\rho \frac{\vec{v}^p - \vec{v}^n}{\Delta t} = \frac{3}{2} R(\vec{v}^n) - \frac{1}{2} R(\vec{v}^{n-1}) \tag{4.8}$$

Then, from (4.8) the value of $\vec{v}^p$ can be found, from applying the divergence operator at (4.7), an expression to find the pressure field is obtained

$$\Delta p^{n+1} = \frac{\rho}{\Delta t} \nabla \cdot \vec{v}^p \tag{4.9}$$

At this point, an iterative solver has to be implemented in order to solve the linear system of equations of the pressure field discretized in space and time, that will have the form

$$a_P p_P^{n+1} = a_W p_W^{n+1} + a_E p_E^{n+1} + a_S p_S^{n+1} + a_N p_N^{n+1} + b_P \tag{4.10}$$

where the numerical coefficients have the following expressions:

$$a_W = \frac{S_w}{d_{PW}} \tag{4.11}$$

$$a_E = \frac{S_e}{d_{PE}} \tag{4.12}$$

$$a_S = \frac{S_s}{d_{PS}} \tag{4.13}$$

$$a_N = \frac{S_n}{d_{PN}} \tag{4.14}$$

$$a_P = a_W + a_E + a_S + a_N \tag{4.15}$$

$$b_P = -\frac{1}{\Delta t} [(\rho v_x^P)_e S_e - (\rho v_x^P)_w S_w + (\rho v_x^P)_n S_n + (\rho v_x^P)_s S_s] \tag{4.16}$$

Once found the pressure field, the calculation of $\vec{v}^{n+1}$ from equation (4.7) is straightforward

$$\vec{v}^{n+1} = \vec{v}^p - \frac{\Delta t}{\rho} \nabla p^{n+1} \tag{4.17}$$

and it is possible to advance to the following timestep and repeat the FSM procedure. However, there are certain numerical considerations that must be taken into account when applying the FSM, regarding space and time discretization, which are going to be discussed on the two following sections.

The above explained methodology has been explained for the case of the velocity fields and the momentum equation, but the formulation is analogous for the energy equation, that would have the discretized form

$$\rho c_p \frac{T^{n+1} - T^n}{\Delta t} = \frac{3}{2} R_T(T^n) - \frac{1}{2} R_T(T^{n-1}) \tag{4.18}$$

with $R_T(T) = -\rho c_p \vec{v} \cdot \nabla T + \nabla \cdot (\lambda \nabla T)$. In fact, for the case of the temperature, no iterative solver would be required since it is directly evaluated from the previous timestep, like the velocity field.

The only issue that should be taken into account when including the energy equation in the formulation is that it exists a coupling between both momentum and energy, which is responsible for the natural convection (or buoyancy) phenomena. This coupling is present in the volume force term of the momentum equation, where density changes are introduced as a function of temperature according to the Boussinesq approximation:

$$\rho = \rho_0 - \rho_0 \beta \Delta T_0 \tag{4.19}$$

with $\Delta T_0 = T - T_{ref}$. This allows to rewrite the term $R(\vec{v})$ as $R(\vec{v}) = \mu \Delta \vec{v} - (\rho \vec{v} \cdot \nabla)\vec{v} + \rho_0 \beta \Delta T \vec{g}$, thus introducing the temperature in the momentum equation. Note that temperature will only have an influence on the direction of $\vec{g}$. This is the underlying principle for the Differentially Heated Cavity problem that will be explained later on.

4.3.1. Checkerboard problem: staggered meshes

Once the Navier-Stokes equation has been discretized, when the real velocity is calculated from equation (4.7) at a particular node P, the following expression is obtained (simplified to a 1D case):

$$u^{n+1} = u_P^p - \frac{\Delta t}{\rho} \frac{p_E^{n+1} - p_W^{n1+}}{2\Delta x} \tag{4.20}$$

Hence, from the previous expression it may be concluded that the velocity of the main node does not depend on the pressure at that main node, but only on the pressure at the neighbour nodes. This generates solutions of pressure fields that are mathematically possible, since they satisfy the equation (4.20), but physically impossible, as they correspond to alternate values of pressure in consecutive nodes, as depicted in Figure 20.

This effect is known as the checkerboard problem, due to the shape on the pressure field obtained.

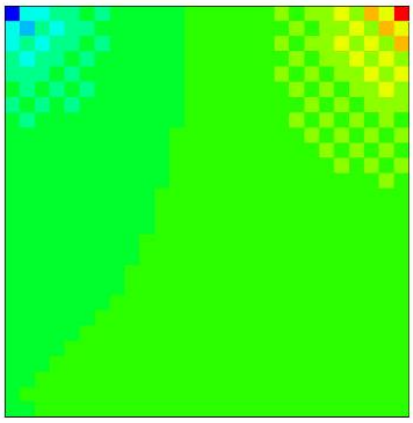

Figure 20. Checkerboard effect close to upper vertices in the Driven Cavity problem. [27]

There are strategies for dealing with this issue, and the one used in this project is the implementation of staggered meshes. These consist of different overlapped meshes, in which velocity and pressure is differently evaluated. The staggered mesh, which is used for the evaluation of velocity, is shifted with respect to the so-called collocated mesh, where pressure is evaluated (see Figure 21).

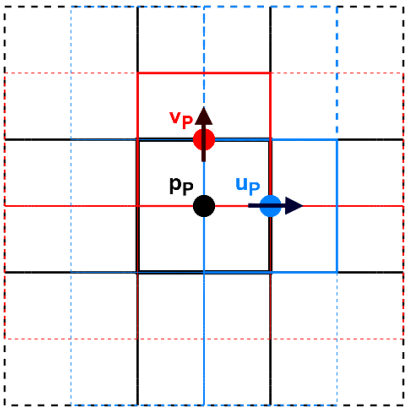

Figure 21. Pressure collocated mesh and staggered in x and y velocity meshes.

Thus, as shown, a total of 3 meshes are required with this methodology:

- The collocated mesh, for the evaluation of the pressure.
- A mesh staggered in the x-direction and collocated in the y-direction, for the evaluation of the horizontal velocity.
- A mesh collocated in the x-direction and staggered in the x-direction, for the evaluation of the vertical velocity.

This treatment allows the velocity of the main node depend on the pressure of the same main node, avoiding this way the checkerboard problem. There are alternative approaches that allow to evaluate both pressure and velocity in the main collocated mesh, without the use of the staggered meshes [20]. These alternatives are more efficient, since only information of a single mesh is required, and they also permit easily the use of unstructured meshes. However, for the geometries tested in this study, the FSM with staggered meshes is used.

4.3.2. Choosing the appropriate timestep: the CFL condition

Apart of space discretization concerns, it is also important to consider the timestep size. Since the FSM evaluates explicitly convective and diffusive term, the resultant algorithm is more unstable rather than with the implicit approach, as mentioned in section *1.5.3. Time discretization*. Thus, not small enough timesteps would result in the divergence of the calculations.

It is for the previous reason that the timestep size is calculated at each time instant to compute in order to optimally find the value of the next time instant. This is the so-called Courant-Friedrich-Levy (CFL) condition, and is based on the following criteria:

$$\Delta t_c = \min\left(0.35\frac{\Delta x}{|\vec{v}|}\right) \tag{4.21}$$

$$\Delta t_d = \min\left(0.20\frac{\rho \Delta x^2}{\mu}\right) \tag{4.22}$$

$$\Delta t_t = \min\left(0.20\frac{\Delta x^2}{\frac{\lambda}{\rho c_p}}\right) \tag{4.23}$$

$$\Delta t = \min(\Delta t_c, \Delta t_d, \Delta t_t) \tag{4.24}$$

where Δt_c is the maximum timestep for the velocity convective term, Δt_d the maximum timestep for the velocity diffusive term, Δt_t the maximum timestep for temperature diffusive term, and Δt the maximum timestep size for the whole algorithm. Note that Δt corresponds to the most critical case of the three cases. This approach implies that the timestep size can vary for different timesteps in the resolution process.

Although there are more sophisticated ways to find the optimal timestep size, the CFL condition is far enough according to the objectives of this project.

4.4. Global resolution algorithm

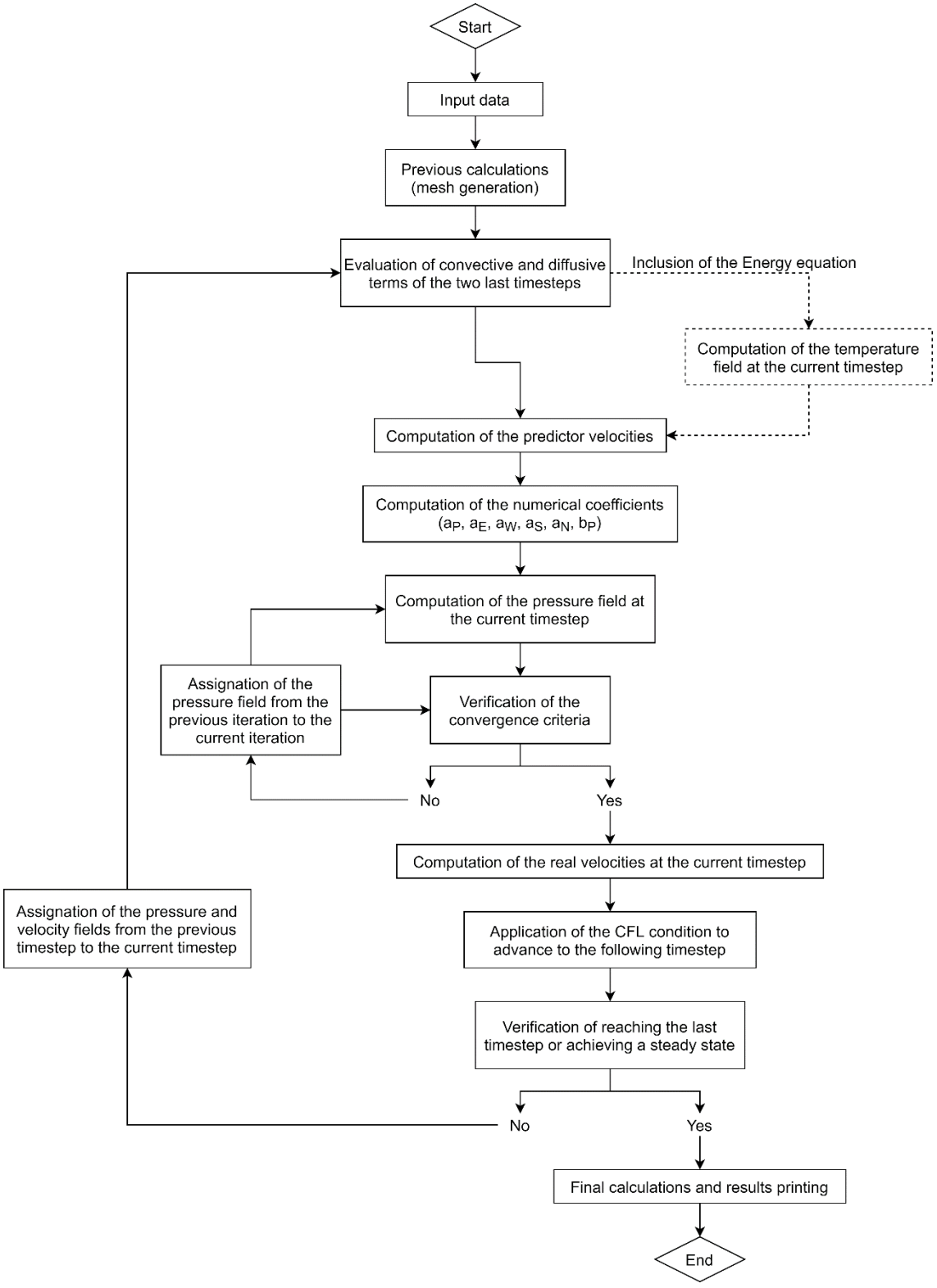

Figure 22. Navier-Stokes Equations global resolution algorithm.

4.5. Test cases description

This section provides the explanation of the three problems used as verification for the FSM algorithm implemented. The results and numerical studies developed for the three cases are displayed also all together on the next section. The reason of this arrangement is due to the fact that several and varied problems have been used for the verification of this part of the study.

4.5.1. Test case 1: Driven Cavity

Consider a two-dimensional squared domain of size L, where a fluid is enclosed by left, right and bottom edges, as seen in Figure 23. On the upper edge, the squared cavity is in contact with a fluid moving at a particular velocity u_{ref}. Also depicted in Figure 23, velocity BC's consists of the non-slip conditions in the cavity walls and a Dirichlet BC with u_{ref} at the top boundary, whilst for pressure BC's, pressure gradients are assumed to be null at all boundaries (Neumann BC).

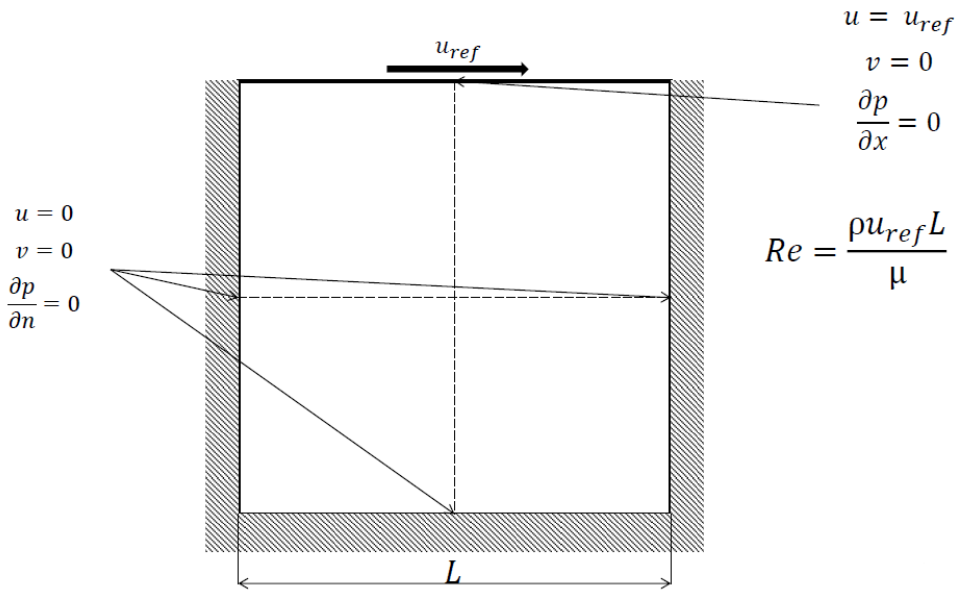

Figure 23. Driven cavity problem geometry and boundary conditions. [20]

The objective of the problem is to find the velocity field once reached the steady state for different Reynolds numbers, being the definition of this non-dimensional group the one displayed in the previous figure.

This is the very first problem to be treated when solving numerically the momentum Navier-Stokes equations for its simplicity, added to the fact that benchmark solutions are available for a wide range of Reynolds numbers, and it allows to clearly see the effect (not only physical but also computationally speaking) of the dominance of convection or diffusion on the solution velocity field.

The main difference with the convection-diffusion problem explained in the previous section is the fact that the velocity field is no longer imposed, but calculated.

4.5.2. Test case 2: Channel Flow

Consider a two-dimensional domain consisting of a channel of height H and length L, with an inlet at the left side and an outlet at the right side, as depicted in Figure 24. A fluid enters parallel to the channel at the inlet (with null vertical velocity).

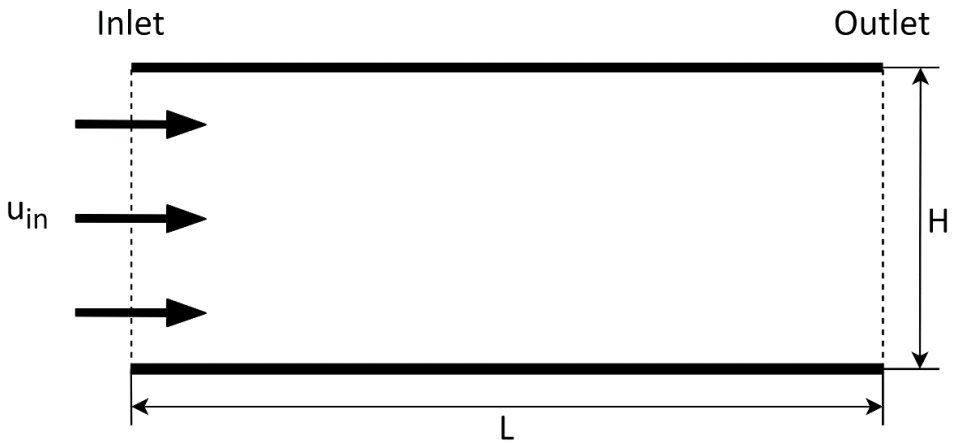

Figure 24. Channel flow problem geometry.

The aim is to find the velocity profile versus the horizontal position according to the following boundary conditions:

BOUNDARY	VARIABLE	BC TYPE	BC DESCRIPTION
BOTTOM $(y = 0)$	Velocity	Dirichlet	Non-slip condition $\vec{v} = 0$
	Pressure	Neumann	Null pressure gradient $\frac{\partial p}{\partial n} = 0$
TOP $(y = H)$	Velocity	Dirichlet	Non-slip condition $\vec{v} = 0$
	Pressure	Neumann	Null pressure gradient $\frac{\partial p}{\partial n} = 0$
INLET $(x = 0)$	Velocity	Dirichlet	Uniform velocity in x $v_x = u_{ref}$ Null velocity in y $v_y = 0$
	Pressure	Neumann	Null pressure gradient $\frac{\partial p}{\partial n} = 0$
OUTLET $(x = L)$	Velocity	Neumann	Null velocity gradient $\frac{\partial \vec{v}}{\partial n} = 0$
	Pressure	Dirichlet	Constant discharge pressure $p = p_{ref}$

Table 8. Channel flow problem boundary conditions.

Further details about the treatment of BC's in this particular case is detailed in section *4.6. Verification and discussion of the results* for the Channel Flow problem.

This problem is of interest for two main reasons: firstly, the velocity profile for a fully-developed flow in a channel is known and has a parabolic distribution, so the verification of the code is possible, and on the other hand this problem allows to study the flow development until reaching the steady state under laminar conditions for different Reynolds numbers. Moreover, it is the first step before tackling the problem displayed on the following section.

4.5.3. Test case 3: Differentially Heated Cavity

Consider a two-dimensional squared domain of size D, where a fluid is enclosed the four edges, as seen in Figure 25. The fluid is considered to be under the effect of the gravity volume force, and temperatures in left and right boundaries of the domain differ in temperature by ΔT, whilst top and bottom boundaries assumed to be adiabatic.

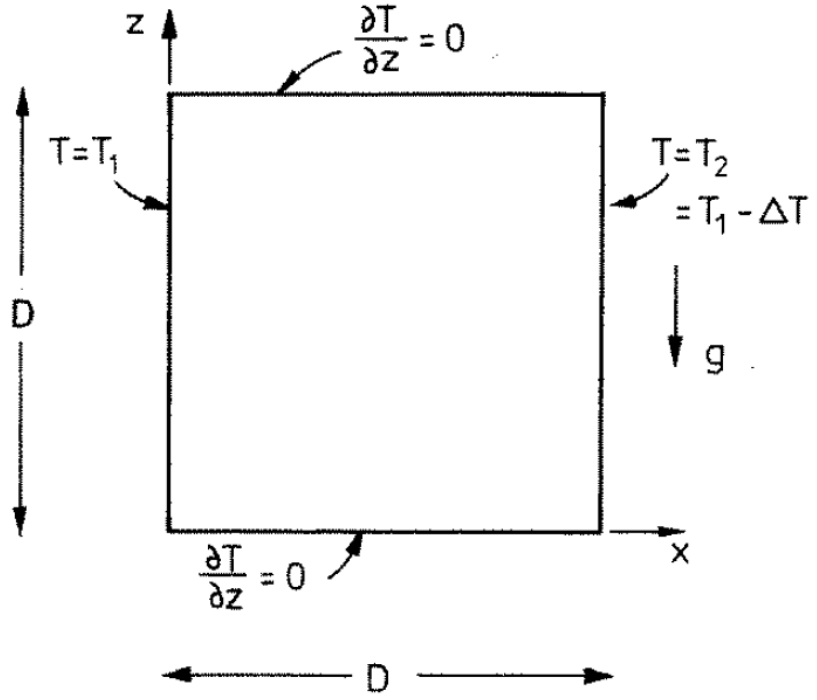

Figure 25. Differentially heated cavity problem geometry. [28]

The objective is therefore to find the velocity field as well as the rest of the fluid properties at each point of the domain, considering the temperature BC's displayed above in Figure 25 and the following BC's for pressure and velocity:

BOUNDARY	VARIABLE	BC TYPE	BC DESCRIPTION
ALL BOUNDARIES	Velocity	Dirichlet	Non-slip condition $\vec{v} = 0$
	Pressure	Neumann	Null pressure gradient $\frac{\partial p}{\partial n} = 0$

Table 9. Differentially heated cavity problem boundary conditions.

The interest of this problem remains on the coupling of momentum Navier-Stokes equation with energy Navier-Stokes equation due to the effect of gravity, which generates a buoyancy effect and thus a natural convection inside the cavity.

In this case, the obtained velocity and temperature fields will be analysed for different Rayleigh numbers, which is the main non-dimensional parameter that conditions this problem.

4.6. Verification and discussion of the results

As benchmark or analytical solutions are possible for the test cases, a comparison against reference solutions is done. Parallel to the verification of results, additional analyses are also detailed here, for the three problems studied.

4.6.1. Test case 1: Driven Cavity

For the Driven Cavity problem, both reference and computed results are depicted below for three Reynolds numbers of analysis: 100, 1000 and 5000. Tests have also been conducted using different convective evaluation schemes.

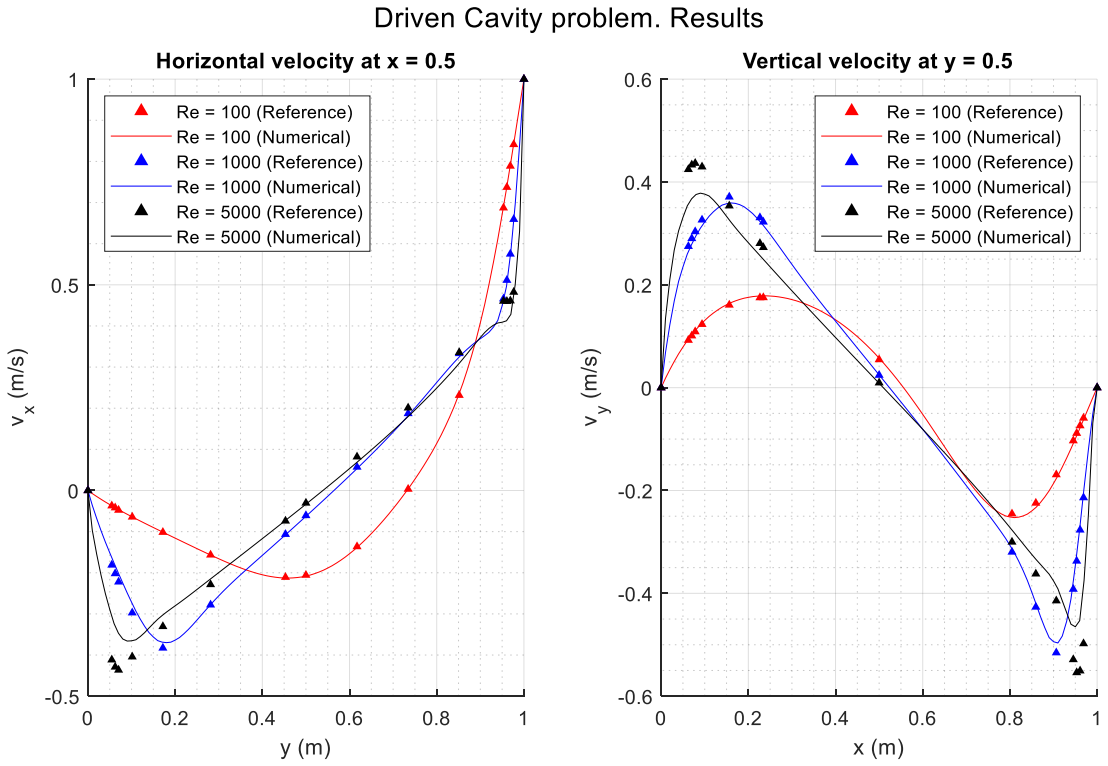

Figure 26. Driven Cavity problem results comparison with benchmark solution.

It can be appreciated that, for the tested mesh resolution, numerical results fit reference solutions in a higher or lower degree depending on the Reynolds number: while the results for the lowest number match perfectly, for the highest value a discrepancy is observed. This can be attributed to the effect of false diffusion.

Nevertheless, leaving aside this expected behaviour, accuracy obtained allows to ensure that, at least for this case, the algorithm is verified. On the other hand, such high Reynolds numbers will not be achieved in later stages of the project.

It is also of special relevance to analyse the convergence of the solution respect to the number of elements used in the simulation. On the figure below is displayed this issue, for three different mesh sizes at a Reynolds number of 1000.

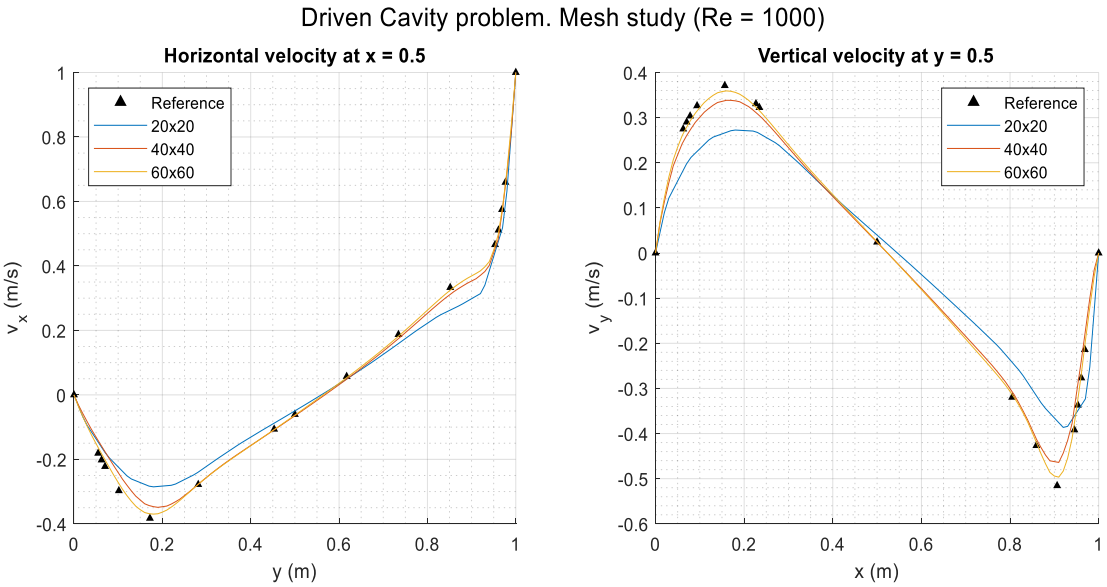

Figure 27. Driven Cavity problem mesh analysis.

As expected, increasing the mesh resolution allows to obtain a more precise solution compared to the reference one. However, finer meshes also imply higher computational times. For example, for the case of the three meshes displayed in Figure 27 the running time of the simulation is summarized in Table 10.

MESH SIZE	COMPUTATIONAL TIME
20X20	21.9 s
40X40	169.8 s
60X60	565.3 s

Table 10. Computational time required for different meshes.

As it is observed, the time required for a simulation increases exponentially. Added to this, the Reynolds number was also observed to have an effect on the computational time, since the 60x60 simulation of Reynolds 5000 lasted around one hour to be completed, which is almost 60 times more than the same mesh resolution for Reynolds 1000.

All those concerns must be taken into consideration when running further simulations in this project, in order to achieve accurate results in feasible amounts of time.

Finally, the accuracy of the results for each scheme used is also studied. This will allow to utilize the most suitable scheme in later simulations. On the following figure, this study is shown for a Reynolds number of 1000 and a mesh size of 40x40.

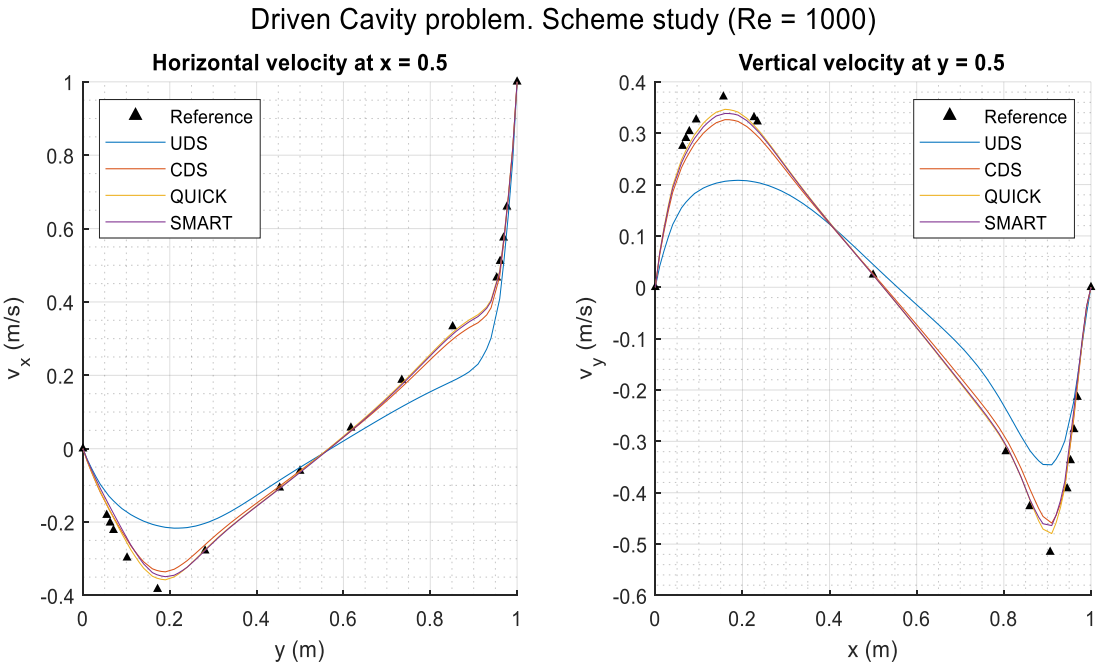

Figure 28. Driven Cavity problem results scheme analysis.

Despite similar, there are slight differences among the different schemes implemented. The Upwind scheme is clearly less accurate than the others, since it is the scheme of the lowest order, and thus it enhances the phenomenon of numerical or false diffusion. Obviously, as the mesh resolution increases, differences among the schemes vanish since false diffusion is compensated by a higher number of nodes that provides a more exact solution.

Central Difference Scheme provides a more accurate solution, but it has the problem that in some cases is more unstable in terms of convergence since it only considers the immediate neighbour nodes on the basic discretization molecule. This was especially observed for really dense meshes at high Reynolds numbers. However, its results are comparable to the ones provided by QUICK and SMART out of the mentioned conditions.

Higher order schemes, QUICK and SMART, allow a more accurate solution for the same mesh resolution, with a comparable degree of precision. Additionally, since SMART is also a bounded scheme, it ensures a higher degree of robustness concerning the convergence of the solutions, which is an advantage respect to the other schemes.

As mentioned before, all these issues will be taken into account when selecting a convective scheme for the future simulations to develop.

Additionally, the streamlines of the three cases tested are as well presented.

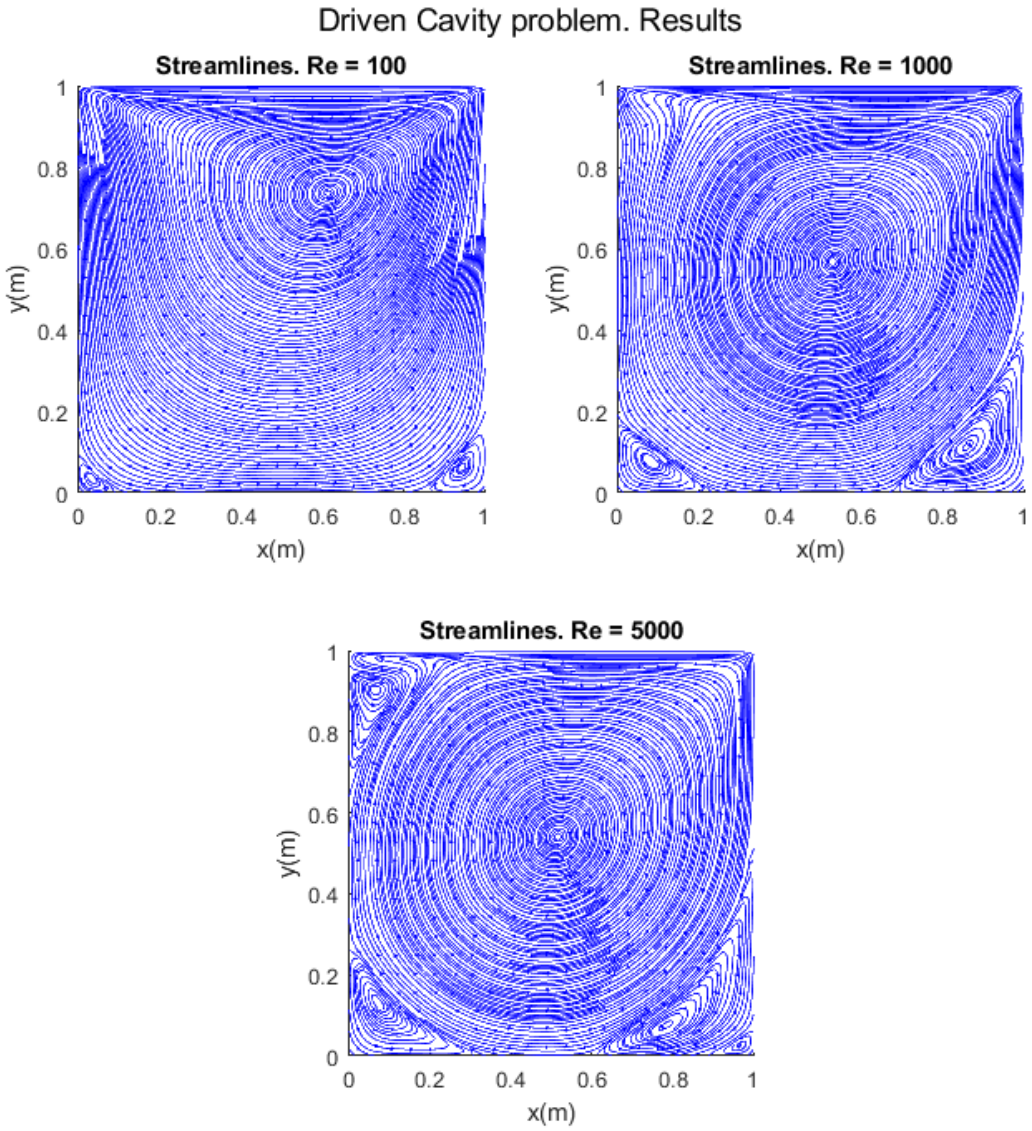

Figure 29. Driven Cavity problem velocity fields streamlines.

The effect of convection generates recirculation in the sharp edges of the geometry, as can be appreciated in the figure above. For low Reynolds numbers, the high viscosity tends to minimize this effect and this is the reason why the size of the eddies at the bottom are smaller. As Reynolds number is increased, size of the vortexes also increases, and even a new vortex in the upper left vertex is generated. Additionally, in the bottom right vertex an additional small vortex is also created. Thus, this problem allows to observe the effect of the balance between convection and diffusion of momentum.

On the other hand, it should be noted that, for this problem in particular, mesh refinements close to the boundaries would be effective, since the smallest scales in the domain are located there. This would allow to decrease the computational time while maintaining the mesh resolution.

4.6.2. Test case 2: Channel Flow

The solution of velocity profile for a fully developed flow in a channel is the well-known parabolic distribution with a linear pressure decrease along the channel. If the starting profile is set as uniform inlet velocity, the point where the flow becomes fully developed depends essentially on the Reynolds number and the length of the channel. Thus, this case is of special interest since it allows to verify the algorithm with the aforementioned analytical solution.

For this particular verification case, the boundary conditions treatment must be pointed out. For the case of velocity, at the inlet the Dirichlet condition together with the non-slip condition of the walls are obvious, and the Neumann condition allows to model the outlet of the channel. For the case of pressure, the following explanation is given: at the end, the movement of the flow along a channel is driven by a pressure difference between the inlet and the outlet, it is required to somehow model this pressure drop as a function of the channel length and the Reynolds number. The alternative used in this project consists of imposing the outlet pressure, and the algorithm computes the inlet pressure to generate the fluid motion.

Below are presented the results of velocity distribution for a channel of aspect ratio 2 at the left and 5 at the right for a Reynolds of 100.

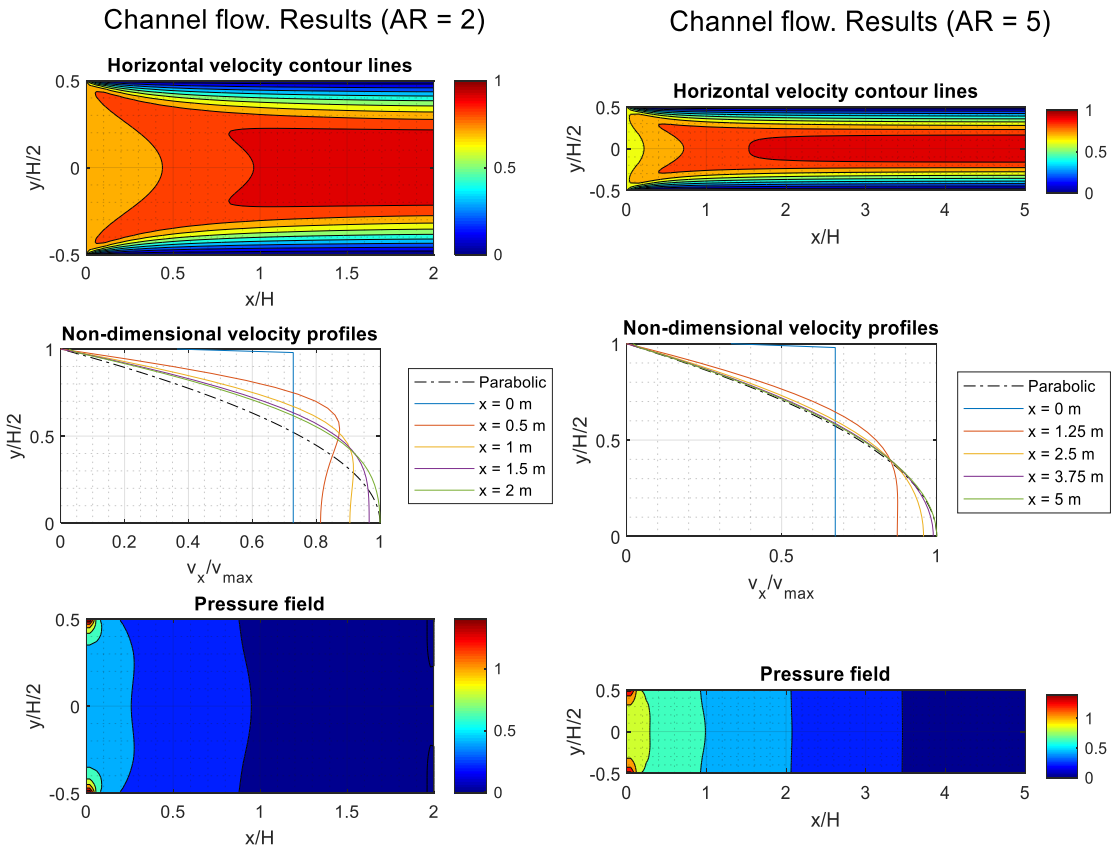

Figure 30. Channel Flow problem velocity profile (Re=100, AR=2 (left) and AR=5 (right)).

On the central plots from the previous figure, the development of the flow versus the position in the channel is clearly seen: the solution is stabilized at a parabolic profile with the maximum velocity at the centre of the channel. The further from the inlet, the more developed the flow is, and the closer is the profile to the parabolic one.

An additional conclusion that can be extracted is that the conservation of mass is satisfied, since the product of the velocity multiplied by the section at the inlet and at the outlet of the channel is maintained.

For the case of the pressure, it can be appreciated that, as the tube length increases, the pressure tends to be equal for the same horizontal position (this is only dependent on x), and the distribution becomes more linear. Pressure peaks observed in the inlet corners are due to the evaluation of the BC's at the vertex nodes.

If the longitude of the tube is increased to an aspect ratio of 10, it is observed in Figure 31 below that the parabolic profile is maintained once reached. Additionally, the pressure distribution behaves as expected, with a linear distribution once the flow is fully developed.

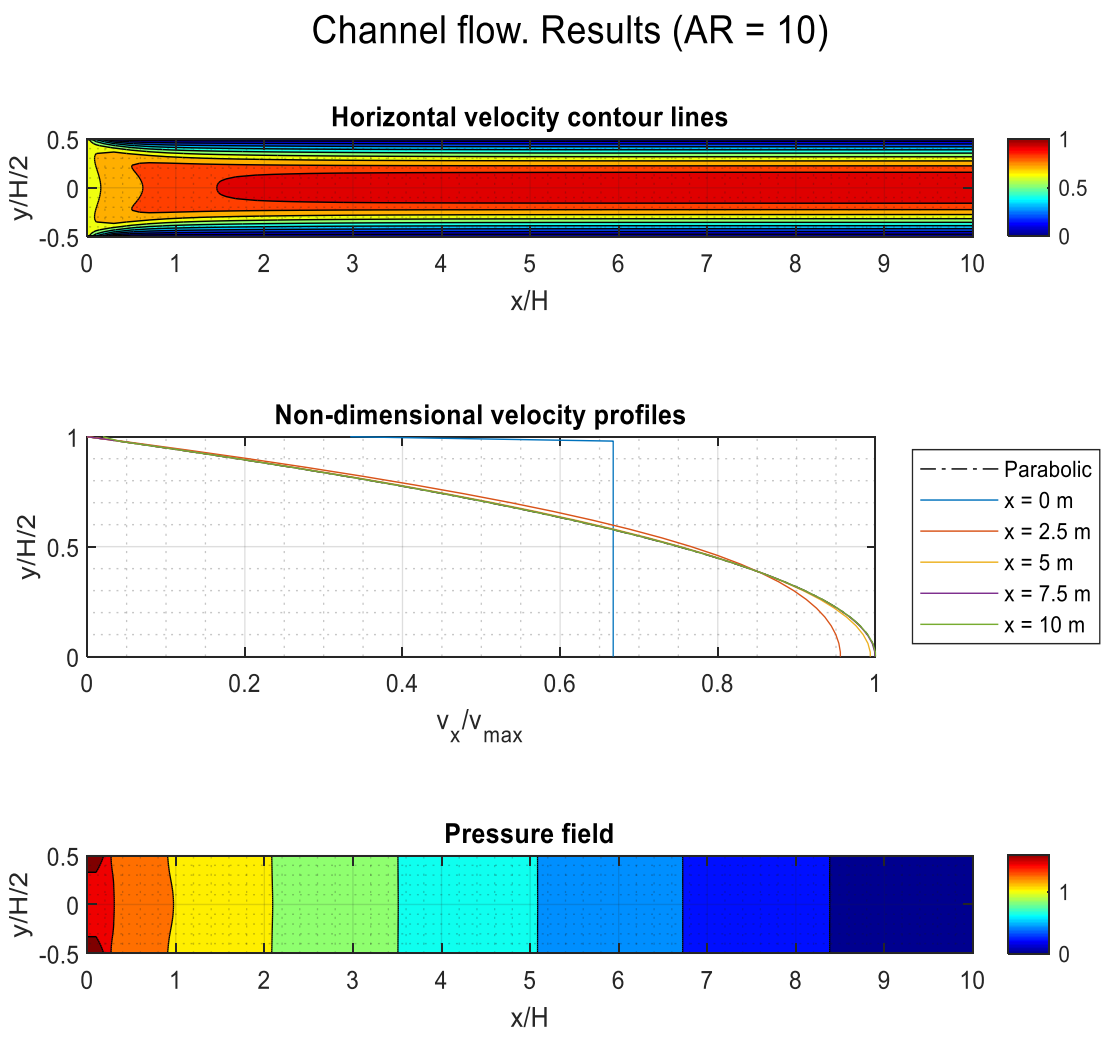

Figure 31. Channel Flow problem velocity distribution (Re=100 and AR=10).

Yet, if the Reynolds number is increased to 1000 while maintaining the aspect ratio, the development of the flow is slower and it is observed that the parabolic profile is found further from the inlet, as depicted in the following page. It is observed that 10 m is not enough for this higher Reynolds to achieve the parabolic profile solution. The same happens with the linear distribution of pressures.

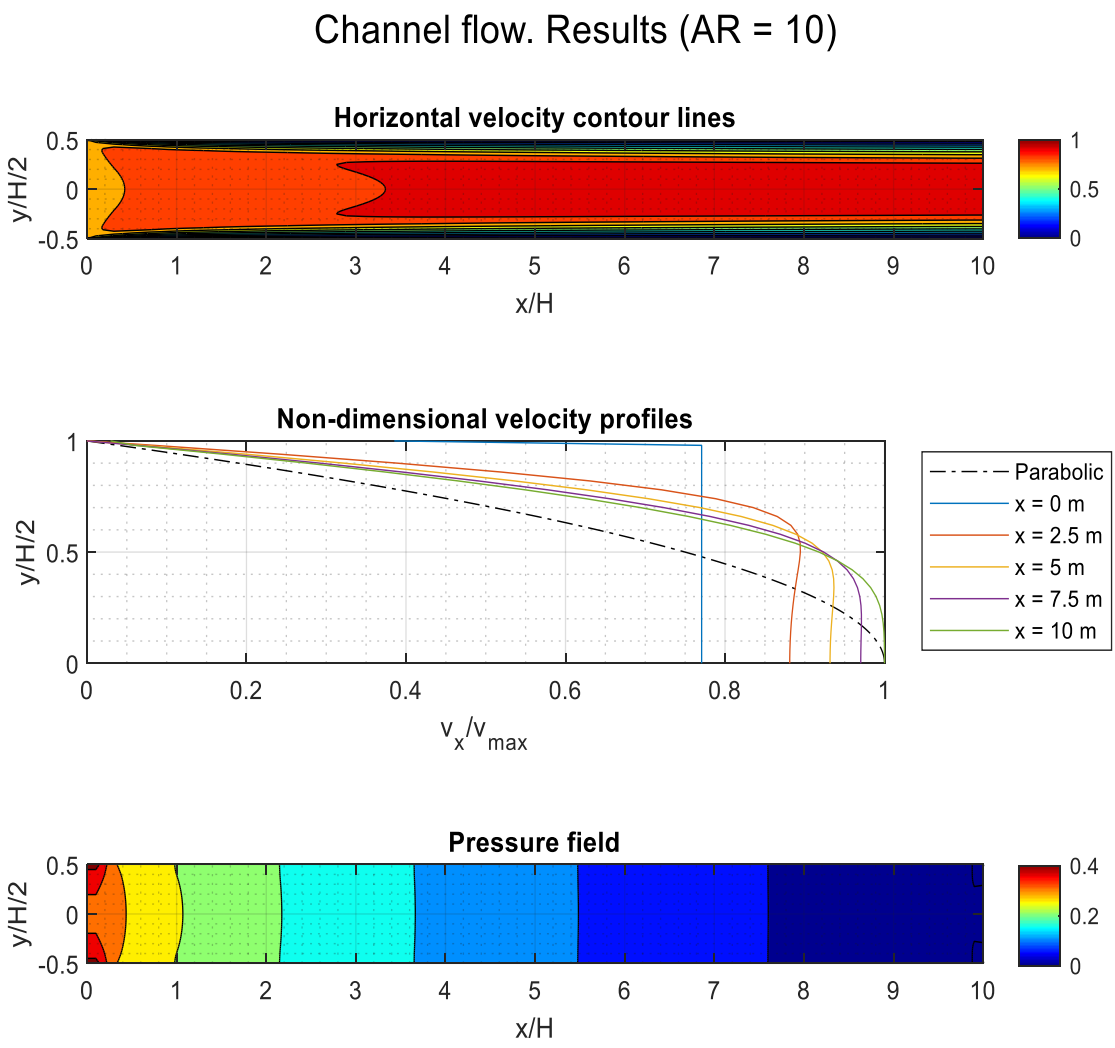

Figure 32. Channel Flow problem velocity distribution (Re=1000 and AR=10).

All the results above presented have been developed for a uniform mesh of 50x50 elements. Higher Reynolds numbers have not been tested since the transition to turbulent flow may be too close, and the developed flow behaviour is no longer a parabolic profile in turbulent regimes.

4.6.3. Test case 3: Differentially Heated Cavity

For the case of the Differentially Heated Cavity, the reference solutions provided by [28] consist of several non-dimensional parameters, such as maximum horizontal and vertical velocities and certain Nusselt numbers (both local and global), calculated as $Nu = \int_0^y \left(\frac{dT}{dx}\right)_{x=0} dy$ and its correspondent position on the grid. On the following table, a comparison between both benchmark and computed solutions is presented.

Rayleigh number	*10^3*			*10^4*			*10^5*			*10^6*		
Mesh 50x50	Reference	Simulation	Error (%)	Reference	Simulation	Error (%)	Reference	Simulation	Error (%)	Reference	Simulation	Error (%)
u_{max}	3.649	3.649	0.011	16.178	16.119	0.367	34.730	34.368	1.044	64.630	66.031	2.168
$y(u_{max})$	0.813	0.810	0.369	0.855	0.830	2.924	0.855	0.850	0.585	0.850	0.830	2.353
v_{max}	3.697	3.703	0.173	19.617	19.661	0.225	68.590	68.707	0.171	219.360	222.069	1.235
$x(v_{max})$	0.178	0.170	4.494	0.119	0.110	7.563	0.066	0.070	6.061	0.038	0.030	21.053
Nu_{av}	1.118	1.113	0.423	2.243	2.245	0.069	4.519	4.565	1.024	8.800	9.181	4.334
Nu_{max}	1.505	1.511	0.367	3.528	3.564	1.030	7.717	7.999	3.654	17.925	20.176	12.558
$y(Nu_{max})$	0.092	0.070	23.913	0.143	0.130	9.091	0.081	0.050	38.272	0.038	0.010	73.684
Nu_{min}	0.692	0.687	0.724	0.586	0.556	5.182	0.729	0.718	1.509	0.989	0.947	4.247
$y(Nu_{min})$	1.000	0.970	3.000	1.000	0.970	3.000	1.000	0.970	3.000	1.000	0.970	3.000

Table 11. Differentially Heated Cavity problem results comparison with benchmark solution (50x50 uniform mesh).

As it is shown, the correspondence of the results for the different cases tested in the different parameters is confirmed. The main discrepancies are in the location of the maximum and minimum local Nusselt numbers, which is attributed to the mesh size used. The values present on the previous table are directly the values at the grid points calculated, without using any interpolation to find the exact point.

Another important issue to remark is that, in general, the error tends to increase with the Rayleigh number, which could be explained by the fact that higher Rayleigh numbers imply a more relevant effect of the buoyancy (this is also why the velocity is increased). Thus, for high Rayleigh numbers, the transported heat by convection dominates in front of transported heat by diffusion, which is analogous to the transport of momentum with the Reynolds number. Thus, more refined meshes are more suitable for higher Rayleigh numbers.

The same study has been conducted for an optimized mesh of 30x30 with a full-cosine distribution of the nodes, whose results are detailed below.

Rayleigh number	10^3			10^4			10^5			10^6		
Mesh 30x30	Reference	Simulation	Error (%)	Reference	Simulation	Error (%)	Reference	Simulation	Error (%)	Reference	Simulation	Error (%)
u_{max}	3.649	3.622	0.735	16.178	15.928	1.548	34.730	33.856	2.515	64.630	64.374	0.396
$y(u_{max})$	0.813	0.806	0.854	0.855	0.806	5.725	0.855	0.844	1.230	0.850	0.844	0.649
v_{max}	3.697	3.673	0.657	19.617	19.735	0.599	68.590	69.251	0.964	219.360	222.034	1.219
$x(v_{max})$	0.178	0.194	8.959	0.119	0.121	1.362	0.066	0.063	4.808	0.038	0.041	6.634
Nu_{av}	1.118	1.116	0.147	2.243	2.241	0.072	4.519	4.518	0.014	8.800	8.845	0.510
Nu_{max}	1.505	1.508	0.184	3.528	3.541	0.375	7.717	7.734	0.221	17.925	17.837	0.492
$y(Nu_{max})$	0.092	0.063	31.710	0.143	0.121	15.650	0.081	0.063	22.436	0.038	0.023	39.657
Nu_{min}	0.692	0.690	0.286	0.586	0.577	1.606	0.729	0.705	3.344	0.989	0.812	17.944
$y(Nu_{min})$	1.000	0.990	1.024	1.000	0.990	1.024	1.000	0.990	1.024	1.000	0.990	1.024

Table 12. Differentially Heated Cavity problem results comparison with benchmark solution (30x30 full-cosine mesh).

Note that, even with a coarser mesh, the effect of concentrating the nodes at the domain boundaries allows to reduce the error at the same time that decreases the computational cost of the simulation, especially at high Rayleigh numbers, since the distance between two consecutive nodes at the boundaries is inferior with this type of discretization.

Having validated the results with the literature, the solutions of temperature and velocity field are presented in the following pages, from Figure 33 to Figure 36. The conclusions that can be drawn from the observation of the fields are the following:

- From Figure 33, it is observed is that, as Rayleigh number increases, the effect of buoyancy becomes more evident and isotherms experiment a twist with respect to the centre of the domain. This is caused by the movement of the fluid, which is higher and thus convection is more relevant and energy is transported by both means. The most extreme tested case is for a Rayleigh number of 10^6, where isotherms only remain parallel to the vertical walls in their immediate surroundings, but far from the walls they are perpendicular to the vertical walls. On the contrary, the solution for the lowest Rayleigh number is close to the one-dimensional heat conduction problem, with a linear distribution of temperatures perpendicular to the differentially heated walls. This would be the expected solution if the buoyancy effect was neglected.
- From Figure 34, it is appreciated how, as happened in the Driven Cavity problem, when convection dominates, recirculation vortexes are generated.
- From Figure 35 and Figure 36, it is observed that the increase in the buoyancy effect increases the velocity of the flow, reaching the peak values of velocities closer to the vertical walls of the domain.

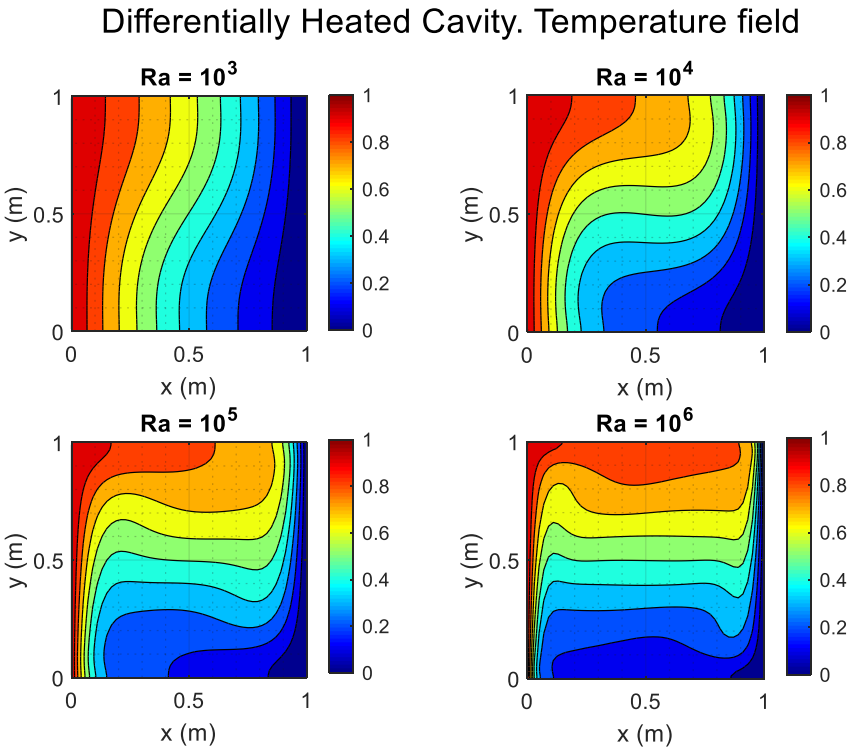

Figure 33. Differentially Heated Cavity problem temperature field.

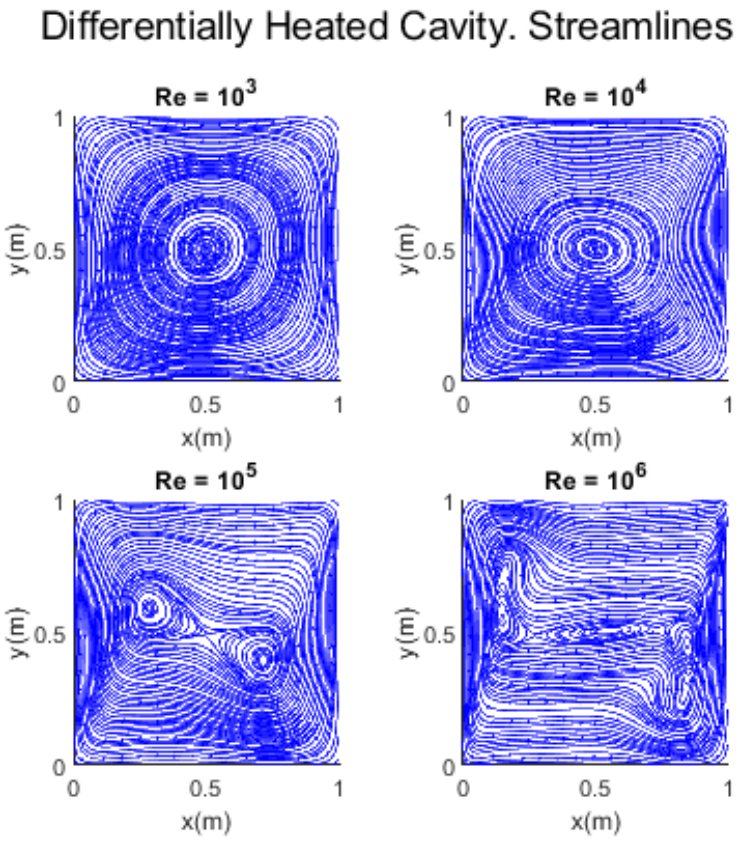

Figure 34. Differentially Heated Cavity problem streamlines.

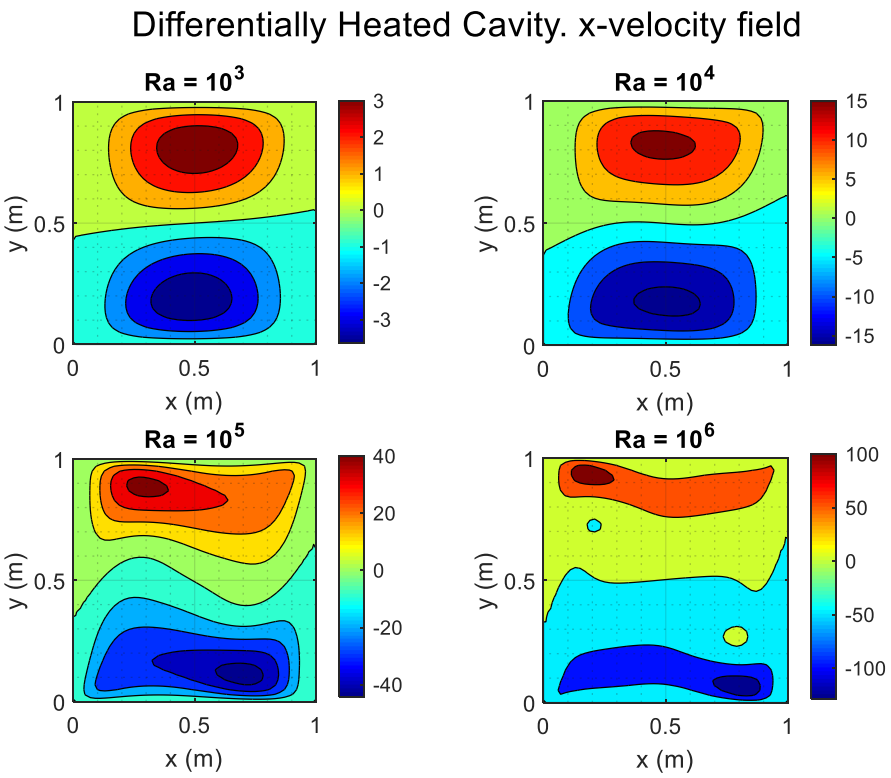

Figure 35. Differentially Heated Cavity problem x-velocity field.

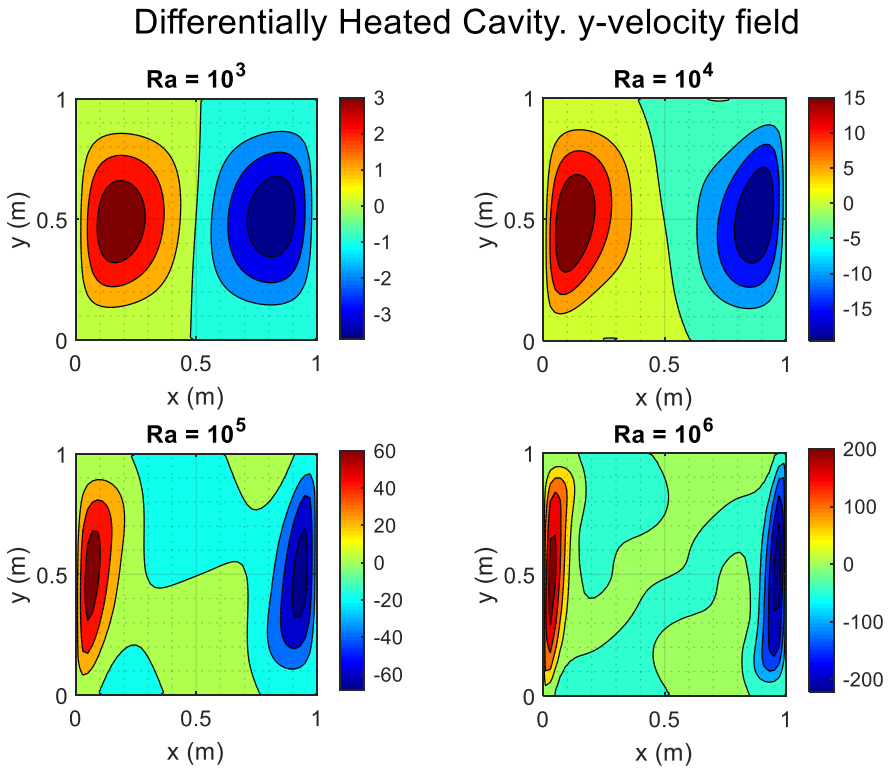

Figure 36. Differentially Heated Cavity problem y-velocity field.

4.7. Conclusions

Until now, the most important underlying principles of incompressible Fluid Dynamics and Heat Transfer have been reviewed, numerically tested and discussed. The development of algorithms capable of solving correctly the Navier-Stokes equations (both momentum and energy) and provide results contrasted to benchmark cases culminates the first part of this study.

It has been seen that Navier-Stokes equations provide a coupling between pressure, velocity and, for some cases, density and temperature, despite working with incompressible flows, thanks to the Boussinesq approximation. Yet, the physics of the problem is what determines if some assumptions can be done (i.e. weak or null effect of temperature in quasi-isothermal flows) and simplify the resolution of the problem.

Another issue that has been observed and commented along the report is how the computational cost of solving the problems has substantially increased, from being able to compute thousands of timesteps in less than a minute to spend hours until reaching the steady state of the problem. Additionally, the computational effort is increased at higher Reynolds numbers and Rayleigh numbers (in general, for convection dominance), since the transient state is much longer due to the presence of smaller scales in the velocity field. It is for this reason that new strategies had to be used at this stage, being the three more highlightable the following:

- Special treatment for the numerical coefficients of the boundary nodes, allowing to include the imposition of BC's inside the resolution of the system of equations and avoiding this way the re-imposition of the BC's after each iteration.
- Implementation of the Conjugate Gradient solver, allowing to substantially reduce the time spent per iteration due to its fast convergence properties [16], especially in the Differentially Heated Cavity problem.
- Implementation of full-cosine distributed grids, allowing to obtain more accurate results with a lower computational cost, since coarser meshes can be used.

All these improvements have allowed enhancing the performance of the developed algorithm.

5. Mass transfer

5.1. Introduction

Until now, all the problems and formulation reviewed only considered momentum and energy transfer, with pressure, velocity and temperature variations, whether or not coupled, in the Navier-Stokes equations. From now on, the additional phenomenon of Mass Transfer, also present in many engineering applications, will be tackled and incorporated to Fluid Dynamics and Heat Transfer problems. This chapter is aimed to fulfil this objective, and also presents a verification case at the end.

5.2. Mathematical formulation

Recovering what was explained in chapter *3. Convection-diffusion equation*, the transport of a property along a domain with a fluid in motion can be summarized through the convection-diffusion equation, that has the form

$$\frac{\partial(\rho\phi)}{\partial t} + \nabla \cdot (\rho\vec{v}\phi) = \nabla \cdot \left(\Gamma_\phi \nabla\phi\right) + S_\phi \tag{5.1}$$

Recall that ϕ accounts for a generic variable of the fluid. However, the fact that heat transfer and mass transfer are analogous phenomena [29] allows to apply equation (5.1) also for the transport of species along a fluid. For these cases, the variable transported is $\phi = Y_k$, which accounts for the mass fraction of Y of the species k in the fluid [5], defined as

$$Y_k = \frac{m_k}{m} = \frac{\rho_k}{\rho} \tag{5.2}$$

It is important to remark that it is immediately verified that $\sum_{k=1}^{N_e} Y_k = 1$, being N_{sp} the number of species present in the mixture. Despite that, for the introduction of this issue, only one species will be considered for simplicity in this chapter.

Unsteady and convective terms (right-hand side of equation (5.1)) do not experiment any difference compared to how they have been studied so far.

For the case of the diffusive term, its evaluation is, in general, quite complex. Nevertheless, the so-called First Fick's Law provides a good approximation of mass diffusion. First Fick's Law establishes a relation between the mass flux $\vec{j}$ (mass transfer by diffusion per unit time and per unit area normal to the direction of mass transfer [29]) and the concentration of a species k in a particular region of the space as follows

$$\vec{j_k} = -\rho D_{km} \nabla Y_k \tag{5.3}$$

where D_{km} is the mass diffusivity coefficient of k in the mixture. Note that, at the end, Fick's Law has the same form as thermal conduction Fourier's Law.

In this case, this diffusion law establishes that mass motion goes from regions of high concentration of particles to regions where concentration is lower, and this diffusion is more important if the difference in concentrations is higher.

However, it is important to mention that this law is non-conservative in terms of mass, and this is why, if several species are involved, mass conservation has to be somehow imposed. The methodology proposed consists of evaluating the mass transport equation for all species except one. Further comments on this issue are detailed in the following section *5.3. Discretization of the equations*.

If in heat conduction the source term S_ϕ accounted for heat generation inside a domain, its meaning in Mass Transfer is $S_\phi = \dot{\omega}_k$, which is related to the generation or destruction of species k. On a first approximation, this term will be assumed as null, but its contribution becomes important in problems involving chemical reactions, such as combustion phenomena, where there is a transformation of some species (destruction of reactants) to others (generation of products). The treatment of this term will be tackled in the next chapter.

In summary, the equation that will be solved in the problem of this chapter according to the aforementioned simplifications is

$$\frac{\partial(\rho Y_k)}{\partial t} + \nabla \cdot (\rho \vec{v} Y_k) = -\nabla \cdot \vec{j}_k \tag{5.4}$$

It is also important to remark that mass transport also has an effect on the energy equation due to the energy transported by each species. This creates a new term in the energy equation, which remains as

$$c_p \left[\frac{\partial(\rho T)}{\partial t} + \nabla \cdot (\rho \vec{v} T) \right] = \nabla \cdot (\lambda \nabla T) - \nabla T \cdot c_{pk} \vec{j}_k \tag{5.5}$$

As a final comment, all the previous formulation, which has been established in terms of mass fractions of species, can alternatively be written in terms of molar fractions or molar concentrations of species. This last approach is also useful when dealing with chemical reactions, so it will be used later on.

5.3. Discretization of the equations

The procedure used to discretize the species equation will be analogous to the one used for momentum and energy in the FSM. This means that a fully explicit resolution will be applied to find the mass fraction of species Y_k^{n+1} at each node from the mass fraction at the previous instant Y_k^n, leading to the following discretized equation

$$\rho c_p \frac{Y_k^{n+1} - Y_k^n}{\Delta t} = \frac{3}{2} R_{Y_k}(Y_k^n) - \frac{1}{2} R_{Y_k}(Y_k^{n-1}) \tag{5.6}$$

with $R_{Y_k}(Y_k) = -\rho \vec{v} \cdot \nabla Y_k + \nabla \cdot (\rho D_{km} \nabla Y_k)$. The discretization of $R_{Y_k}(Y_k)$ is of the same form as for the case of the velocity explained in the previous chapter. The particularity in this case is that, as mentioned before, this equation will have to be solved for each species k from 1 to $N_{sp} - 1$, and mass fraction of species N_{sp} will be computed as follows:

$$Y_{N_{sp}} = 1 - \sum_{k=1}^{N_{sp}-1} Y_k \tag{5.7}$$

This procedure allows to ensure the mass conservation among the whole system, and it will be the most abundant species the one that will be evaluated this way. As a matter of example, for the first verification case presented in section *5.5. Test case: Heat and Mass Transfer on Moist Air*, only two species are involved, which are dry air and water, and only the mass fraction of water will be computed.

Additionally, similar to what was done with thermal buoyancy, a coupling between momentum and mass transfer is also present, and it can be approximated through the Boussinesq approximation as well. Hence, the density will vary both due to temperature and concentration differences according to the expression

$$\rho = \rho_0 - \rho_0 \beta_T \Delta T_0 - \sum_{k=1}^{N} \rho_0 \beta_{Y_k} \Delta Y_{0_k} \tag{5.8}$$

with $\Delta Y_{0_k} = Y_k - Y_{k_{ref}}$. This allows to rewrite the term $R(\vec{v})$ as

$$R(\vec{v}) = \mu \Delta \vec{v} - (\rho \vec{v} \cdot \nabla)\vec{v} + \rho_0 \beta_T \Delta T \vec{g} + \sum_{k=1}^{N} \rho_0 \beta_{Y_k} \Delta Y_k \vec{g} \tag{5.9}$$

Note that the whole buoyancy effect will only have an influence on the direction of $\vec{g}$, due to both mass and heat.

5.4. Global resolution algorithm

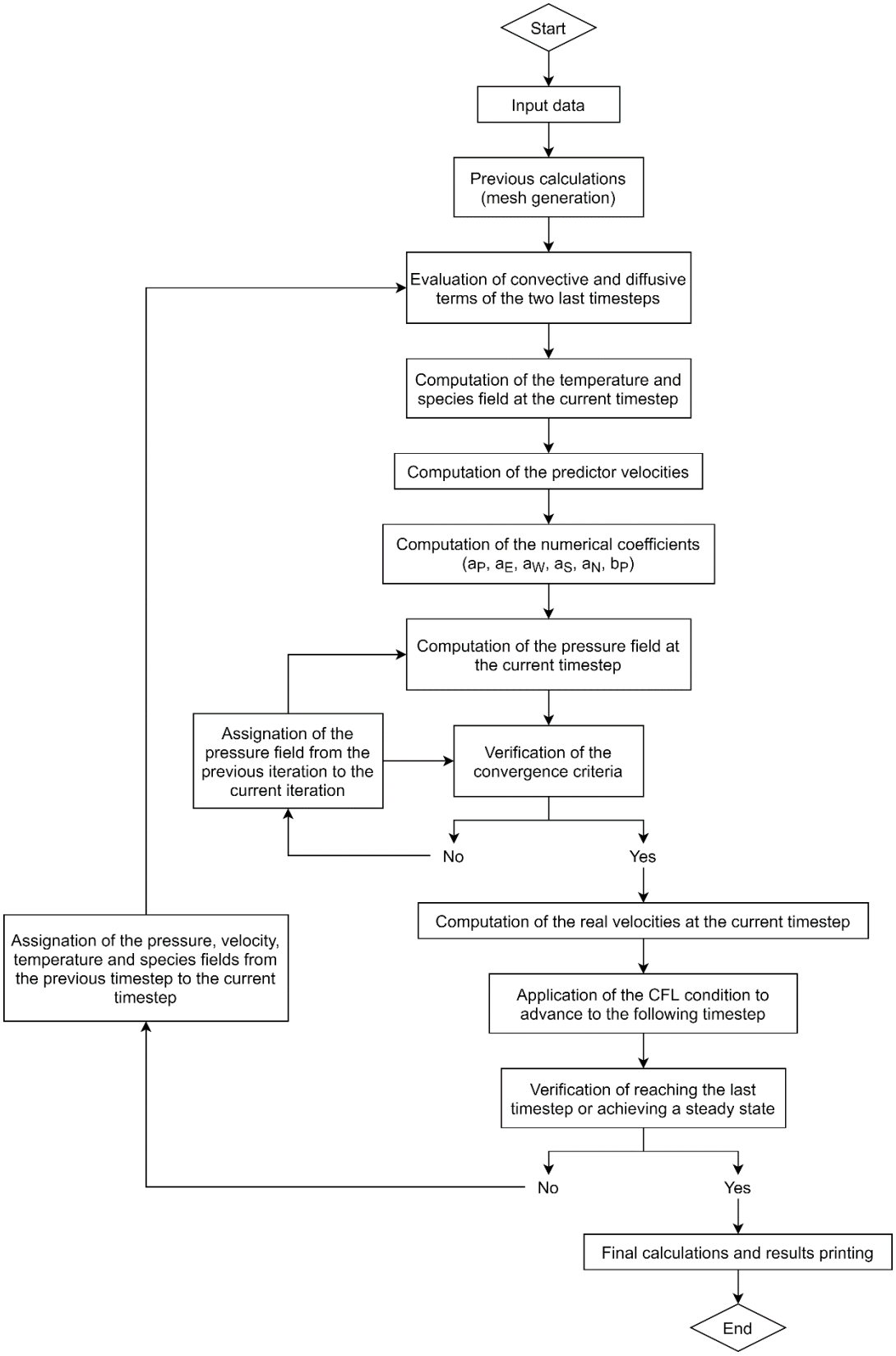

Figure 37. Momentum, heat and mass transport resolution algorithm.

5.5. Test case: Heat and Mass Transfer on Moist Air

Consider a two-dimensional domain consisting of the central plane in x-direction ($x = \frac{b}{2}$) of the 3D geometry displayed in Figure 38. The domain has a length L and a height H, with an inlet at the left and an outlet at the right. A fluid enters parallel to the channel at the inlet with a fully developed velocity profile (with null vertical velocity), and it is in contact with water at saturation conditions at the bottom boundary of the domain [30].

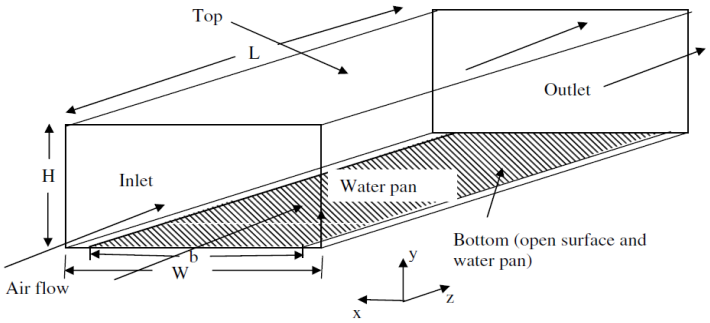

Figure 38. Heat and Mass Transfer on Moist Air problem 3D geometry. [30]

This problem aims to analyse the heat and mass transfer present due to the evaporation of water, diffusion and convection effects, according to the following boundary conditions:

BOUNDARY	VARIABLE	BC TYPE	BC DESCRIPTION
BOTTOM $(y = 0)$	Velocity	Dirichlet	Non-slip condition $\vec{v} = 0$
	Pressure	Neumann	Null pressure gradient $\frac{\partial p}{\partial n} = 0$
	Temperature	Dirichlet	Fixed temperature $T = T_{ref}$
	Species	Dirichlet	Fixed concentration $Y = Y_{ref}$
TOP $(y = H)$	Velocity	Dirichlet	Non-slip condition $\vec{v} = 0$
	Pressure	Neumann	Null pressure gradient $\frac{\partial p}{\partial n} = 0$
	Temperature	Neumann	Null temperature gradient $\frac{\partial T}{\partial n} = 0$
	Species	Neumann	Null concentration gradient $\frac{\partial Y}{\partial n} = 0$
INLET $(x = 0)$	Velocity	Dirichlet	Uniform velocity in x $v_x = u_{ref}$ Null velocity in y $v_y = 0$
	Pressure	Neumann	Null pressure gradient $\frac{\partial p}{\partial n} = 0$
	Temperature	-	Heat flux equal to vaporization enthalpy $-k\frac{\partial T}{\partial n} = h_{fg} D_{AB} \frac{\partial Y}{\partial n}$
	Species	Dirichlet	Saturation concentration $Y = Y_{sat}(T)$
OUTLET $(x = L)$	Velocity	Neumann	Null velocity gradient $\frac{\partial \vec{v}}{\partial n} = 0$
	Pressure	Dirichlet	Constant discharge pressure $p = p_{ref}$
	Temperature	Neumann	Null temperature gradient $\frac{\partial T}{\partial n} = 0$
	Species	Neumann	Null concentration gradient $\frac{\partial Y}{\partial n} = 0$

Table 13. Heat and Mass Transfer of Moist Air problem boundary conditions.

This problem is of special interest since it introduces the diffusion of species as a function of temperature. Here, the concept of saturation properties of a fluid is incorporated, and connection and analogy between mass transfer and heat transfer is put on relevance.

5.6. Verification

In [30] the local Nusselt and Sherwood numbers as a function of the position in water surface along the channel are provided. Those are calculated as follows:

$$Nu_x = \frac{-\left(\frac{\partial T}{\partial y}\right)_{y=0}}{T_w - T_m} D_h \tag{5.10}$$

$$Sh_x = \frac{-\left(\frac{\partial C}{\partial y}\right)_{y=0}}{C_w - C_m} D_h \tag{5.11}$$

where the subindex "w" refers to the water and "m" stands for the bulk mean property, and $D_h = 0.0384\ m$ is the hydraulic diameter of the geometry. Nusselt and Sherwood numbers account for the convection-to-diffusion ratio for heat and mass, respectively.

The previous two non-dimensional groups have been calculated for a simulation using a mesh of 50x50 elements with a full-cosine distribution, in order to increase the number of elements in the inlet and outlet regions as well as the water surface.

The comparison with the reference data is displayed on the following figure.

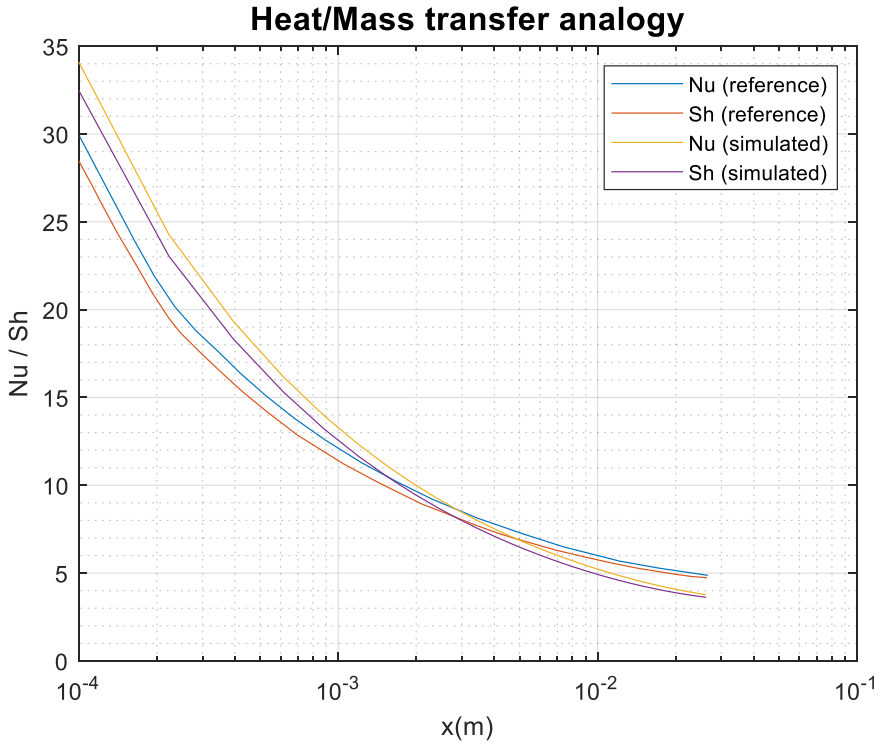

Figure 39. Heat and Mass Transfer on Moist Air problem verification.

As it is shown, there is a similarity between the behaviour of the Sherwood and Nusselt numbers, with a vertical asymptote at the inlet and a horizontal asymptotic tendency at the outlet. This is explained since, at the inlet, water finds a flow with uniform properties all along the y-axis, which means that, initially, the temperature gradient is high and heat transport by convection dominates in front of diffusion.

As the fluid advances on the channel, the effect of diffusion tends to smooth this gradient and the convective effect becomes less important. At the end, an equilibrium is found around a value of 4 for both Nusselt and Sherwood numbers, once the thermal boundary layer is fully-developed.

An analogous explanation can be done for the mass transfer. In fact, Nusselt and Sherwood numbers are found to be related by the factor $\frac{D_{AB}h_{fg}\Delta C}{k\Delta T}$, according to the boundary condition imposed at the water surface. This value resulted to be of 1.05 for the simulation developed, compared to a value of 1.06 for the reference solution in [30]. This means that the mass diffusion is slightly higher than the thermal diffusion. The equilibrium Nusselt and Sherwood numbers depend on the thermal and diffusivity properties of the fluids involved, being lower at higher conduction (for temperature) and diffusivity (for species).

It is of special relevance to remark that reference solution shows a greater rate of both mass and energy diffusion with respect to convection especially close to the inlet. These observed discrepancies between reference and simulation results are attributed to differences in the computation of air and water properties as well as the difference in mesh density. For the case of the simulations, those properties were calculated according to [31], since not all of them were detailed on the reference literature.

5.7. Discussion of results

In this section are presented the results of both temperature and concentration fields for a Reynolds number of 844, and inlet conditions of air at 22.4ºC and a relative humidity of 53.1%.

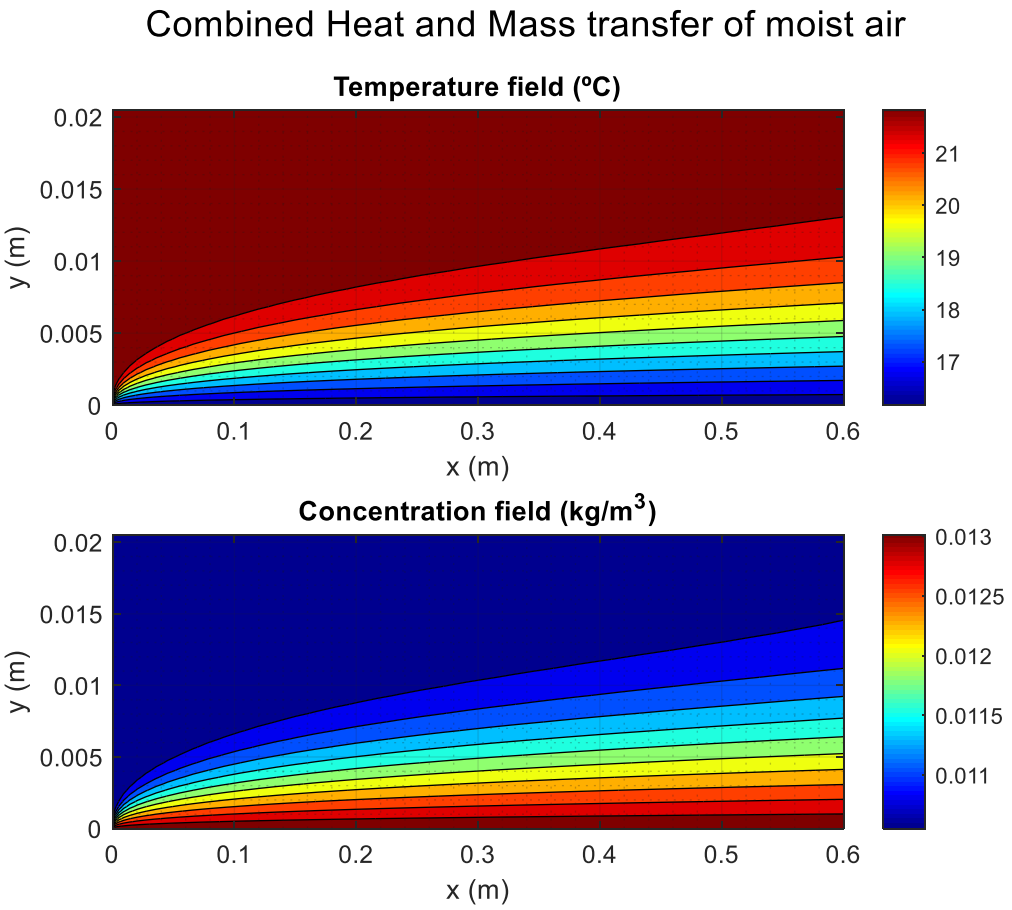

Figure 40. Heat and Mass Transfer on Moist Air problem temperature and species fields.

Again, in these results, the analogy between Heat and Mass Transfer is observed, as the distribution of both temperature and species have the same shape.

The first remarkable fact from the previous figure is the temperature drop in the water surface. This is due to the fact that heat is inverted to produce the phase change on liquid water, and then this temperature difference is transported by diffusion to upper layers of the fluid, leading to the resulting profile.

Regarding the concentration of water vapour, it is observed that higher values are found logically where the evaporation takes place, which is close to the liquid water surface. Then, similar to the temperature, the mass is transferred from higher-concentration regions to lower concentration ones, as expected according to Fick's first law of diffusion.

It is important to remark, however, that in this problem the source term was set as null, and the generation of vapour water is only due to the imposition of the evaporation condition at the bottom boundary of the domain.

5.8. Conclusions

In this chapter, a review on Mass Transfer has been done and its link with Heat Transfer has been studied, both theoretically and in the simulations. Regarding the improvements of the algorithm, the incorporation of the reviewed Mass Transfer model equations has been successfully done.

Since an explicit scheme has been used in the inclusion of the Mass Transfer equation for species in the code, the computational cost is not substantially increased, as no iterative solvers are used for the evaluation of the species distribution. However, it is important to bear in mind that this approach implies the use of smaller timesteps to achieve convergence, which is done in the imposition of the CFL condition for the timestep. Nevertheless, this approach is enough according to the aims of this project, at least up to this point.

On the other hand, this stage of the project was carefully implemented to ease the next objectives: although the presented problem of Heat and Mass Transfer of Moist Air only considers the transport of a single species, which is the water vapour in air, other species may be present. In fact, in combustion problems, this will be for sure the case. Hence, the algorithm was implemented generalizing the code for multiple species, having the particularity that the number of species was of 1 for this case, with a null source term. Those will be the next steps to follow.

6. Combustion

6.1. Introduction

Having reached this point, the momentum, energy and mass transport phenomena have been completely reviewed and brought together in the developed algorithms. However, only non-reactive mixtures of gases have been tackled, without any generation or destruction of species. This chapter culminates the study with the addition of thermochemistry to the already reviewed problems, and a final analysis with a simple reaction mechanism is developed at the end.

6.2. Mathematical formulation

6.2.1. Implications of the species source term

Equation (5.6) in the previous chapter presented the convection-diffusion equation applied to the transport of species, but for the last problem studied, the source term S_ϕ was considered null. From now on, this term on the convection-diffusion equation will no longer be zero, leading to the following equation of species

$$\frac{\partial(\rho Y_k)}{\partial t} + \nabla \cdot (\rho \vec{v} Y_k) = -\nabla \cdot \vec{j}_k + \dot{\omega}_k \tag{6.1}$$

where $\dot{\omega}_k$ accounts for the production or destruction of the species k in the domain.

The presence of this term increases reasonably the complexity of the problem to be solved, since the amount of mass of species generated or destroyed depends on the chemical reactions that may happen according to the present species. Not only this, but one must also bear in mind that the presence of $\dot{\omega}_k$ makes a new term appear in the energy equation, which will have the form

$$c_p \left[\frac{\partial(\rho T)}{\partial t} + \nabla \cdot (\rho \vec{v} T) \right] = \nabla \cdot (\lambda \nabla T) - \nabla T \cdot \sum_{k=1}^{N_{sp}} c_{pk} \vec{j}_k - \sum_{k=1}^{N_{sp}} h_k \dot{\omega}_k \tag{6.2}$$

thus meaning that chemistry has obviously an effect on the energy balance of the mixture [5], since there is an additional transport of energy due to the diffusion of species.

The complexity of the problem depends therefore in the number of reactions and number of species involved, which is known as the reaction mechanism. The more species considered, the more accurate the model will be, but the computational cost will be also higher.

6.2.2. Chemical kinetics

For a generic case, let's assume a mechanism with N_r reactions where N_{sp} species are involved, expressed as

$$\sum_{k=1}^{N_{sp}} \nu'_{kl} N_k \rightleftarrows \sum_{k=1}^{N_{sp}} \nu''_{kl} N_k \quad (l = 1,2,\dots,N_r) \tag{6.3}$$

where N_k refers to the chemical formulation of a particular species k, ν'_{kl} is the coefficient of the species k as a reactant and ν''_{kl} the coefficient of the species k as a product, for the reaction l. With this, the evaluation of the source term for a particular species reads as follows

$$\dot{\omega}_k = W_k \sum_{l=1}^{N_r} (\nu''_{kl} - \nu'_{kl}) \left[k_l^f \prod_{q=1}^{N_{sp}} [X_q]^{\nu'_{ql}} - k_l^b \prod_{q=1}^{N_{sp}} [X_q]^{\nu''_{ql}} \right] \tag{6.4}$$

with W_k being the molecular weight of the species k, $[X_q]$ the molar concentration of the species q and k_l^f and k_l^b the forward and backward kinetic constants of the reaction l. Since the mechanism of reaction is given, the remaining unknowns from equation (6.4) are k_l^f and k_l^b, and depend on the chemical kinetics and chemical equilibrium of the reaction [5].

The forward kinetic constant can be calculated according to the Arrhenius modified law

$$k_l^f = A_l T^{\beta_l} \exp\left(\frac{-\hat{E}_{a_l}}{\hat{R}T}\right) \tag{6.5}$$

where A_l, β_l and $\hat{E}_{a_l}$ are empirical coefficients of the reaction l and $\hat{R}$ is the universal gas constant.

For the backward kinetic constant, it is related to k_l^f through the concentration equilibrium constant of the reaction K_{c_l}:

$$k_l^b = \frac{k_l^f}{K_{c_l}} \tag{6.6}$$

with $K_{c_l} = K_{p_l} \left(\frac{p}{\hat{R}T}\right)^{\sum_{k=1}^{N_{sp}} (\nu''_{kl} - \nu'_{kl})}$ and $K_{p_l} = \exp\left(\frac{-\Delta G_l^0}{\hat{R}T}\right)$ is the pressure equilibrium constant, which is only dependent on the temperature. The evaluation of the Gibbs free energy ΔG_l^0 is done in the following manner:

$$\Delta G_l^0 = \sum_{k=1}^{N_{sp}} (\nu'_{kl} - \nu''_{kl}) \hat{g}_k^0 = \sum_{k=1}^{N_{sp}} (\nu'_{kl} - \nu''_{kl}) \left[\hat{h}_k^0(T) - T\hat{s}_k^0(T) \right] \tag{6.7}$$

where $\hat{h}_k^0$ and $\hat{s}_k^0$ are the standard molar enthalpy and entropy, whose function of temperature is known. These thermophysical properties are function of the temperature and can be calculated as follows

$$\hat{h}_k(T) = \hat{h}_k^0(T^0) + \int_{T^0}^{T} \hat{c}_{p_k} dT \tag{6.8}$$

$$\hat{s}_k(T) = \hat{s}_k^0(T^0) + \int_{T^0}^{T} \hat{c}_{p_k} \frac{dT}{T} \tag{6.9}$$

yet there are empirical correlations that allow to find directly the values of enthalpy and entropy versus temperature [32].

As the reader may appreciate, the procedure is neither straightforward nor linear, and can become highly demanding in terms of computations if complex mechanisms are studied. Deeper details on chemical kinetics and chemical equilibrium can be found in the literature, i.e. [5], [33] and [34].

Due to computational resources and scheduling reasons, this study has been limited to the analysis of a chemical mechanism made of a single reaction.

6.2.3. Concept of equivalence ratio

A generic combustion process involves the participation of two essential elements: the fuel and the oxidizer. It is the selection of the fuel and the proportion of these two compounds as reactants what will determine the resultant combustion process. It is for this reason that the concept of equivalence ratio ϕ needs to be introduced. It is defined as

$$\phi = \frac{\left(\frac{m_{air}}{m_{fuel}}\right)_{stoich}}{\left(\frac{m_{air}}{m_{fuel}}\right)} \tag{6.10}$$

where $\left(\frac{m_{air}}{m_{fuel}}\right)$ is the real proportion of air and fuel (either in terms of mass or molar quantity) and $\left(\frac{m_{air}}{m_{fuel}}\right)_{stoich}$ is the proportion that would be in a stoichiometric combustion. This parameter is especially important, since it conditions the maximum temperature reached in the combustion, and also the formation of minor species according to the reaction mechanism.

6.3. Discretization of the equations

The evaluation of the equations making use of numerical methods in a discrete domain is exactly the same as stated in sections *4.3. Discretization of the equations: Fractional Step Method* and *5.3. Discretization of the equations*, since the equations to solve are the same of momentum, energy and mass transfer. The difference is that the source term is added, and it has to be evaluated at each grid point and for each species.

Yet, the introduction of the net species production rate modifies substantially the nature of the numerical resolution of the problem. This obeys to the strong non-linearity behind the Arrhenius law and the additional dependence of the chemical kinetics not only on the temperature, but also on the concentration of the species.

The mentioned non-linearity converts the mass transport equation in a so-called stiff equation, which means that the equation is likely to be numerically unstable. This can be avoided by a high decrease on the timestep used for the computation, allowing the algorithm to capture the smooth variations on the chemical mechanism and compute the mixture ignition. This is the approach that was used in this study, through the modification of the CFL condition by decreasing the timestep several orders of magnitude below the calculated value.

The reason of this relies on the timescales present on the reaction mechanisms, since the initiation of a combustion process, called ignition, can be extremely fast. Additionally, the reactants conditions must be suitable for this phenomenon to be produced, as the mixture must have a temperature high enough to acquire the required amount of heat to overcome the activation energy and start the chemical reaction.

6.4. Global resolution algorithm

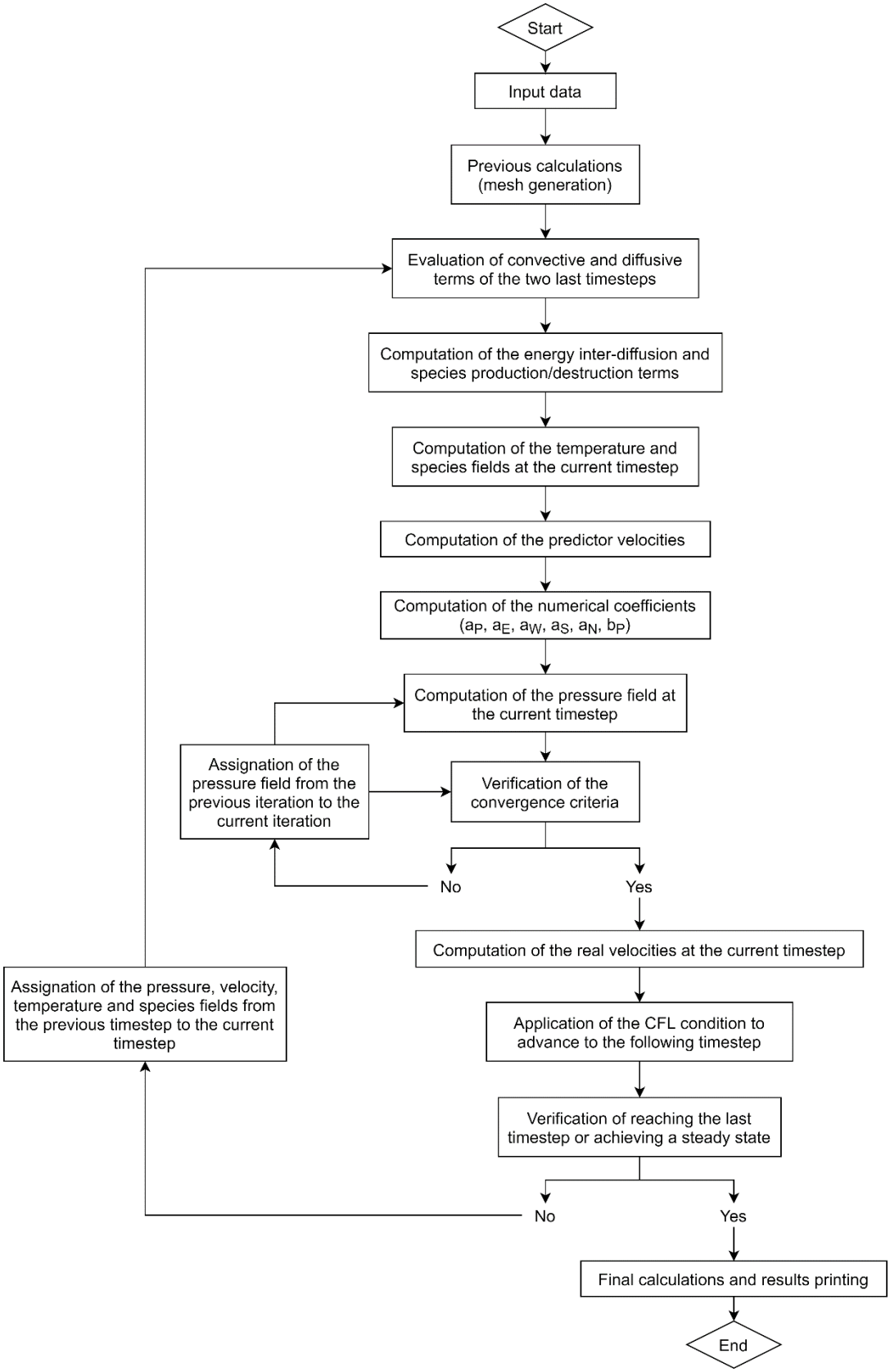

Figure 41. Combustion resolution algorithm.

6.5. Test case: simulation of laminar flames

Consider a vertical domain with symmetry of revolution, of a total length $L = 20\ cm$ and radius $r_o = 4.76\ cm$ and $r_i = 0.555\ cm$ with to differentiated inlets at the bottom and one outlet at the top (similar to the domain tested in *4.5.2. Test case 2: Channel Flow* but in the vertical direction), as depicted below.

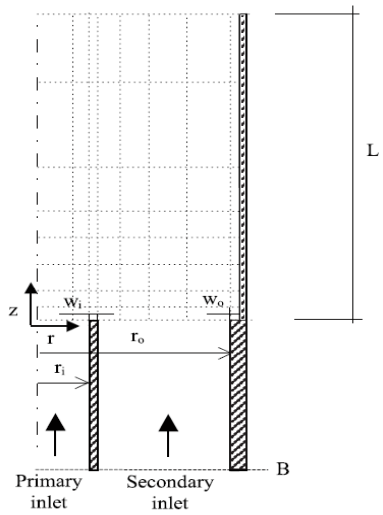

Figure 42. Co-flow laminar flame problem geometry. [35]

Through the primary inlet flows pure methane with a parabolic velocity profile and a mass flow of 0.2165 g/min, and through the secondary inlet flows air (assumed as 79% nitrogen and 21% oxygen) with a uniform velocity profile and a mass flow of 51.88 g/min. Both inlets are at 298 K.

This problem allows to test the algorithm when adding the chemical kinetics for computing combustion processes, according to the following boundary conditions:

BOUNDARY	VARIABLE	BC TYPE	BC DESCRIPTION
INLET $(y = 0)$	Velocity	Dirichlet	Prescribed velocity profile
	Pressure	Neumann	Null pressure gradient $\frac{\partial p}{\partial n} = 0$
	Temperature	Dirichlet	Fixed temperature $T = T_{ref}$
	Species	Dirichlet	Fixed concentration $Y = Y_{ref}$
OUTLET $(y = L)$	Velocity	Dirichlet	Null velocity gradient $\frac{\partial \vec{v}}{\partial n} = 0$
	Pressure	Neumann	Constant discharge pressure $p = p_{ref}$
	Temperature	Neumann	Null temperature gradient $\frac{\partial T}{\partial n} = 0$
	Species	Neumann	Null concentration gradient $\frac{\partial Y}{\partial n} = 0$
LEFT $(x = 0)$	Velocity	Neumann	Symmetry conditions $\frac{\partial T}{\partial n} = 0$ and $v_y = 0$
	Pressure		
	Temperature		
	Species		
RIGHT $(x = L)$	Velocity	Neumann	Non-slip condition $\vec{v} = 0$
	Pressure	Dirichlet	Null pressure gradient $\frac{\partial p}{\partial n} = 0$
	Temperature	Neumann	Null temperature gradient $\frac{\partial T}{\partial n} = 0$
	Species	Neumann	Null concentration gradient $\frac{\partial Y}{\partial n} = 0$

Table 14. Co-flow laminar flame problem boundary conditions.

6.6. Verification

Due to the quantity of changes to be implemented, it is required to carefully develop this verification stage step by step, since sources of error can be numerous.

The first step was to obtain a map of the inlet components once reached the steady state before introducing the combustion. The map obtained is depicted below, for a 50x50 mesh hyperbolically concentrated towards the inlet, and for an equivalence ratio of $\phi = \infty$.

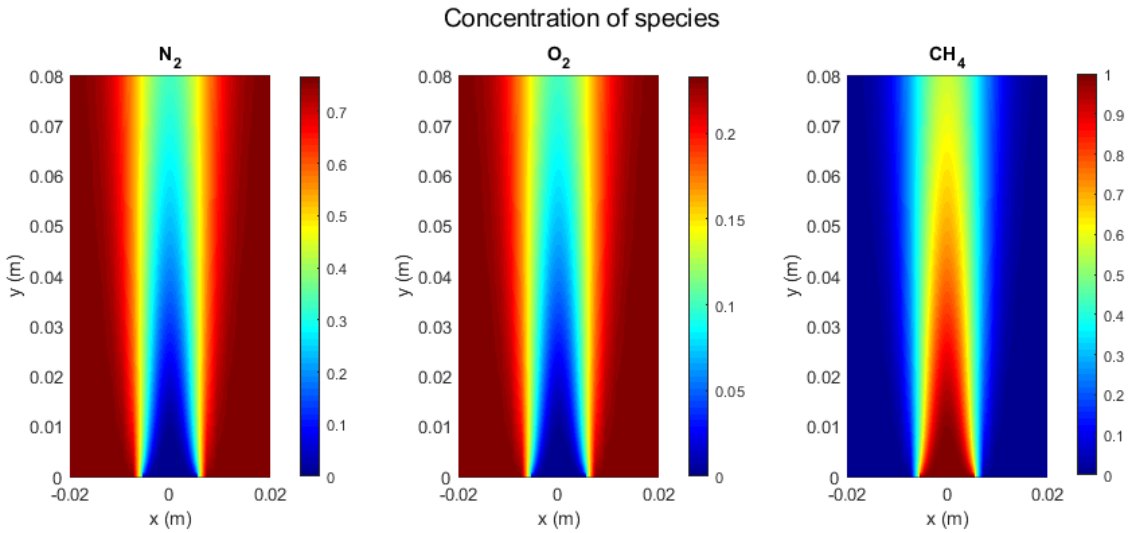

Figure 43. Steady diffusion of reactants in the domain.

From the previous figure it is clearly appreciated the difference between the two inlets, being the internal the one who provides the fuel and the external the one who provide the oxidizer in form of air. Diffusion phenomenon is observed, and enhanced when getting further from the inlets. It is this diffusion what will provoke the mixture between fuel and oxidizer to start the combustion.

It is additionally seen that boundary conditions are as well satisfied, since mass fraction of methane is unity at the internal inlet and null at the external one, and mass fractions of nitrogen and oxygen at the outlet correspond to air composition of 79-21% in volume fraction.

Afterwards, the calculation of enthalpy (and entropy) as a function of temperature is involved in the combustion approach used, as seen in equations (6.2) and (6.7). For this, a function implementing the CHEMKIN coefficients database [32] was created and verified with reference data of tabulated values of enthalpy and entropy [34] of the species involved in the methane combustion. According to the expected range of temperatures to reach, values are comparted for 298, 1000 and 2000 K, with the results shown in the table on the following page.

	ABSOLUTE ENTHALPY (KJ/KMOL)								
	298 K			1000 K			2000 K		
	Tabulated	CHEMKIN	Error (%)	Tabulated	CHEMKIN	Error (%)	Tabulated	CHEMKIN	Error (%)
N2	0	-2.93073	-	21460	21469.9	0.00046	56141	56132.3	0.00015
O2	0	-4.40666	-	22707	22706.8	0.00001	59199	59205.1	0.00010
CO2	-393520	-393514	0.00002	-360115	-360111	0.00001	-302080	-302064	0.00005
H2O	-241820	-241830	0.00004	-215842	-215822	0.00009	-169131	-168788	0.00203

	ABSOLUTE ENTROPY (KJ/KMOL)								
	298 K			1000 K			2000 K		
	Tabulated	CHEMKIN	Error (%)	Tabulated	CHEMKIN	Error (%)	Tabulated	CHEMKIN	Error (%)
N2	191.502	191.498	0.00002	228.057	228.089	0.00014	251.969	251.986	0.00007
O2	205.033	205.134	0.00049	243.471	243.587	0.000476	268.655	268.77	0.00043
CO2	213.685	213.768	0.00039	269.215	269.287	0.000267	309.21	309.282	0.00023
H2O	188.72	188.811	0.00048	232.597	232.735	0.000593	264.059	264.916	0.00325

Table 15. Comparison of the implemented CHEMKIN database with reference values.

The results show relative errors below 10^{-3} % in all cases, meaning that the computation of the thermodynamic properties for the species involved is verified.

The chemical kinetics mechanism was implemented using a fully explicit approach, being the reaction introduced the single-step irreversible combustion of methane, given by

$$CH_4 + 2O_2 \rightarrow CO_2 + 2H_2O \tag{6.11}$$

with a free Gibbs energy of -801 kJ/kmol at 25ºC. This gives an equilibrium constant greater than 10^{100}, which is expected since the reaction is spontaneous and irreversible. Several values of Arrhenius equation parameters for reaction (6.11) were found in the literature [7] [8] [9], and the final values used were the ones from the Westbrook and Dryer (WD) mechanism, with $A = 2.119 \cdot 10^{11}\ (mol, cm^3, s)$, $\beta = 0$ and $E_a = 35000\ cal/mol$.

However, when the simulation was run it, was found that the amount of products formed was several orders of magnitude below what was expected. Additionally, the temperature field remained unperturbed at a temperature equal to the inlet temperature in the steady state.

Since the temperature equation had been verified with test cases explained on sections *4.5.3. Test case 3: Differentially Heated Cavity* and *5.5. Test case: Heat and Mass Transfer on Moist Air*, this discrepancy was initially attributed to a bug in the computation of the source term. Several revisions were made in this line.

Additionally, further simulations were run making use of the different values of Arrhenius parameters found in the literature as well as different inlet temperatures, obtaining the same result. An alternative approach, proposed by [36] and used by [35] was also implemented and tested, using the values of $A = 4{,}2 \cdot 10^{15}\ (kg, m^3, s)$, $\beta = 0$ and $\frac{E_a}{\hat{R}} = 16900\ K$.

After a deep research in the bibliography, the root of the discrepancy found was attributed to the explicit evaluation of the source term. As it was mentioned above, the underlying equation of chemical kinetics is the modified Arrhenius law (see equation (6.5)), which is a strongly non-linear equation that depends exponentially on the temperature and on the molar concentrations of reactants and products. This leads to a high sensitivity especially on the temperature, and it is also for this reason why there are different values of Arrhenius parameters in the literature.

The approach followed in this project to solve the problem consisted of decreasing the timestep size. Nevertheless, there are alternative ways to tackle the stiffness of the equations. As a matter of example, there is the possibility to solve the species equation in two steps, initially calculating an intermediate mass fraction by evaluating explicitly the diffusive and convective terms, and afterwards solving implicitly the source term by using a direct resolution method for the nonlinear system of equations (i.e. modified damped Newton's method) [5] [37].

On the other hand, there is another parameter that affects the simulation time, which is the moment of auto-ignition of the mixture. As explained, the chemical reaction (6.11) is spontaneous, but it is required that the reactants accumulate the required amount of energy to overcome the activation energy and start the combustion. This obviously depends on the initial temperature of the mixture: the lower the inlet temperature of the reactants, the more time it will take the mixture to ignite and start the combustion. This is well-shown for different mechanisms in the following figure.

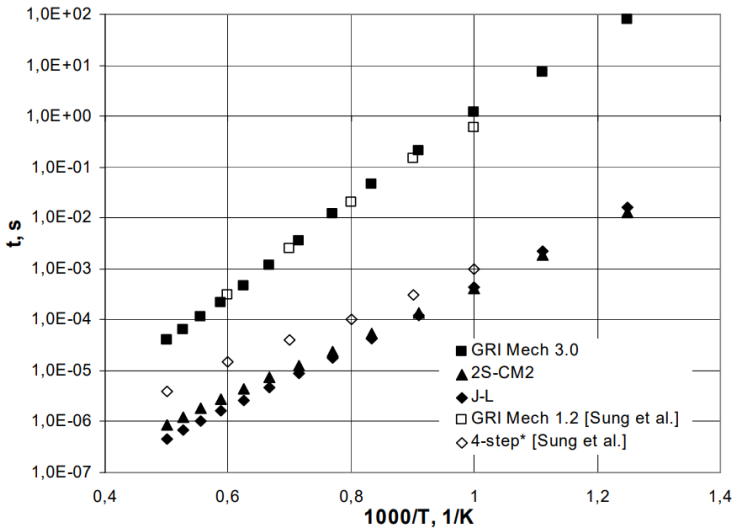

Figure 44. Auto-ignition delay times for stoichiometric air-methane combustion. [10]

According to the computational power of the computer used, an initial temperature of 1000 K has been used to produce the results displayed on the next section, since it allows a substantial decrease in time compared to the temperature used in [35]. On the other hand, the used temperature is above methane auto-ignition temperature, which is of 870 K [38], which should ensure the spontaneous ignition of the mixture.

6.7. Discussion of the results

In this section results of the simulations run for the single-step combustion mechanism are presented. The mesh used is of 50x50 elements, hyperbolically concentrated towards the inlet of the geometry, at the bottom of the domain. A Lewis number of 1 was used for the computations, considering that the main thermophysical properties of the mixture (i.e. viscosity, thermal conductivity and diffusivity) are constant and equal to the ones of air (the most abundant species).

Results of the steady state temperature field for an equivalence ratio $\phi = \infty$ and $\phi = 1$ at the internal inlet are displayed on the following figure.

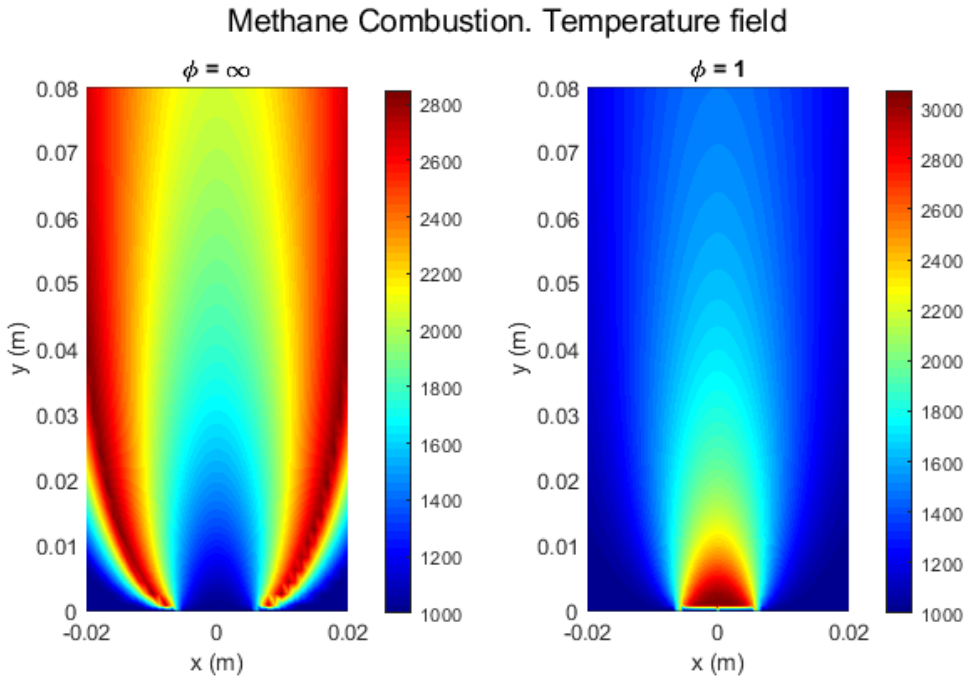

Figure 45. Laminar flames temperature field for $\phi = \infty$ (left) and $\phi = 1$ (right).

For the case of $\phi = \infty$ (see Figure 45 left), it is clearly appreciated how the maximum temperature takes place in the regions where there is sufficient mixture between air and methane, which does not coincide with the axis of symmetry. This does not happen close to the inlets, since pure methane is supplied by one channel and only air is supplied by the other, meaning that both components must be mixed through diffusion for reaching the optimal concentrations for the combustion. Differences between the result obtained and the temperature field displayed in [35] are attributed to the different inlet temperature tested.

For the case of $\phi = 1$ (see Figure 45 right), the maximum temperature is observed to occur right above the internal inlet, on the axis of symmetry of the geometry. Since a stoichiometric mixture is fed at the internal inlet, optimal concentrations to ignite are found there. Away from this point, temperature decreases due to the diffusion effect of species, since further from the inlet the concentration of air increases.

The presence of air flowing outside the flame also allows to control its propagation in the radial direction, and this is why the flame front is not completely normal to the bottom of the domain.

Additionally, it was observed that the maximum temperature reached was higher for $\phi = 1$ than for $\phi = \infty$. However, it is important to remark that results of temperature do not match with experimental results for a very reduced chemical mechanism such as the single-step tested here. For these cases, simulations tend to give higher values of temperature as there is no heat inverted in the formation of additional products apart of carbon dioxide and water.

Ignition processes have been also analysed for both equivalence ratios tested, with the aim of studying the start of the combustion and the flame front propagation along the domain until reaching the stabilized steady state. This is shown in Figure 46, right below.

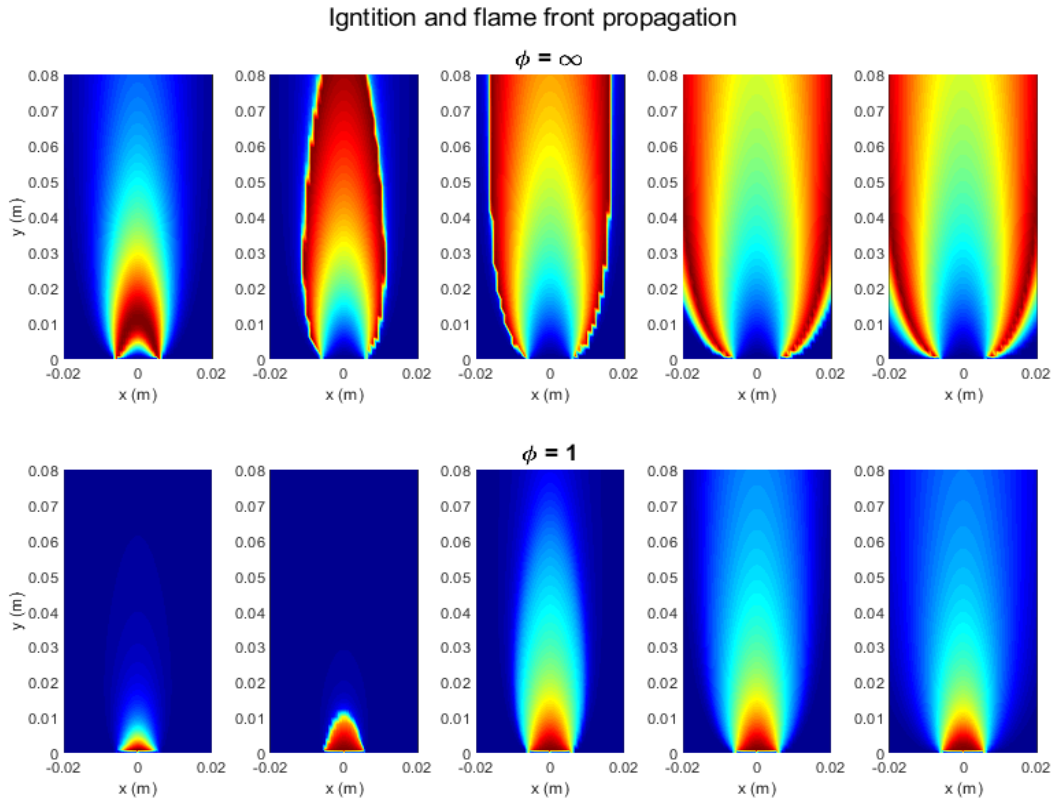

Figure 46. Ignition and flame front propagation for $\phi = \infty$ (top) and $\phi = 1$ (bottom).

For the case of $\phi = \infty$ (see Figure 46 top), the ignition of the mixture is observed to happen 1 cm away from the inlet, and the flame front propagates rapidly upwards and then to the sides. The flame reaches a steady state with a maximum generation of products at the points where the proportion of methane and oxygen is optimal. The combustion process was observed to be very fast once the ignition was produced, consuming all the oxygen in the regions where its concentration was high enough.

For the case of $\phi = 1$ (see Figure 46 bottom), the flame front propagated slower than in the previous case, since methane is initially less diffused (less quantity enters the domain as it is premixed with air). On the other hand, it can be highlighted that, whereas with $\phi = \infty$ the location of the maximum temperature region varies from the ignition to the steady state, for $\phi = 1$ it remains at the same position.

Concerning the mass fraction of species, results are shown below in Figure 47 and Figure 48 (case of $\phi = \infty$) and on the following page in Figure 49 and Figure 50 (case of $\phi = 1$), followed by a brief discussion of the results obtained.

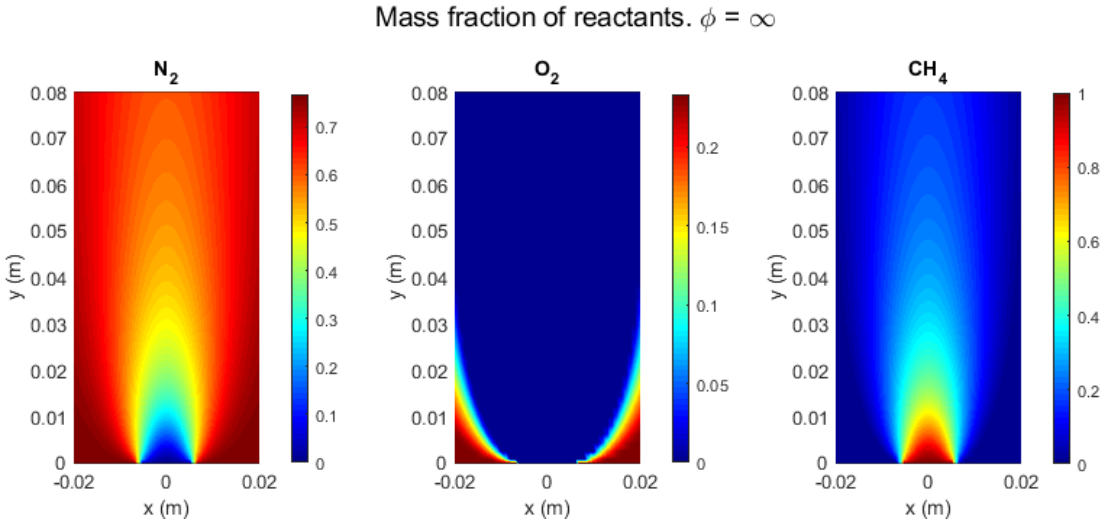

Figure 47. Laminar flames result of reactants mass fraction field for $\phi = \infty$.

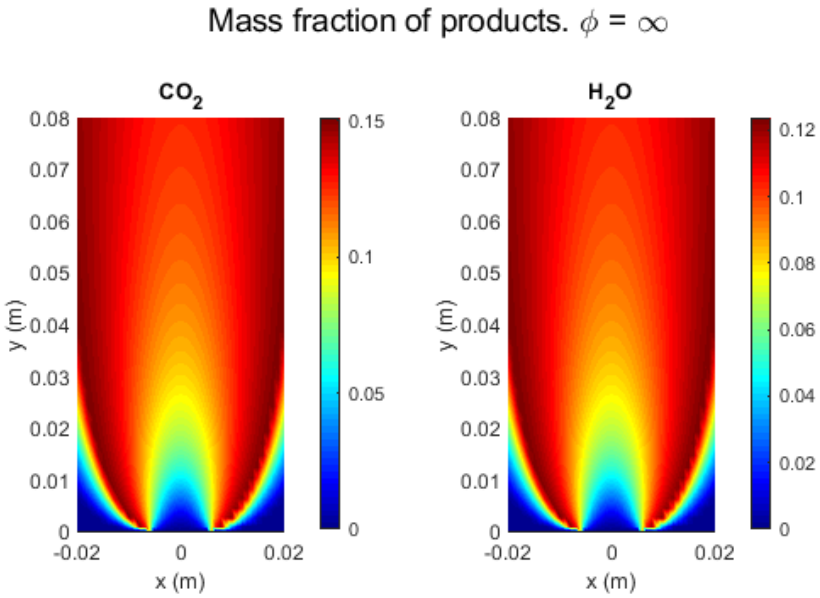

Figure 48. Laminar flames result of products mass fraction field for $\phi = \infty$.

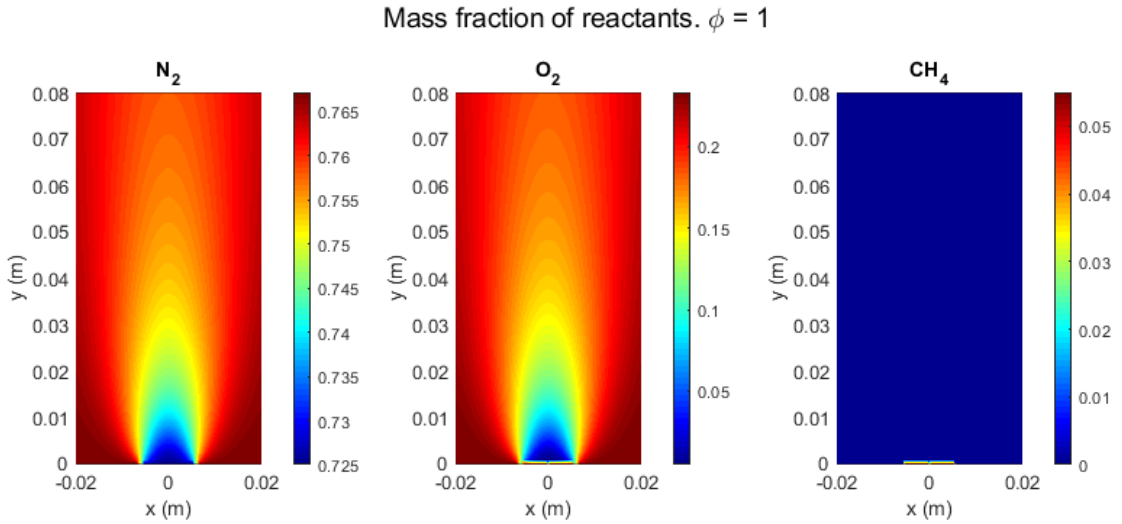

Figure 49. Laminar flames result of reactants mass fraction field for $\phi = 1$.

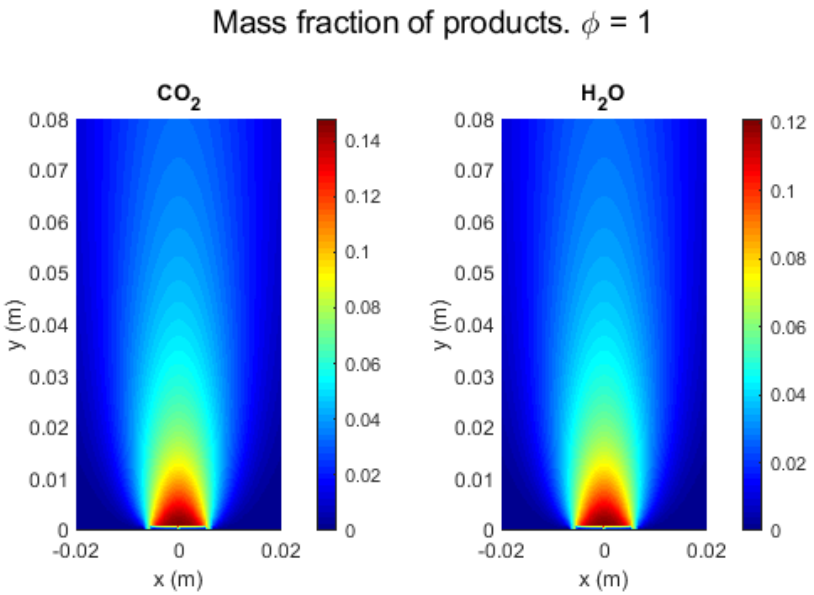

Figure 50. Laminar flames result of products mass fraction field for $\phi = 1$.

The first remarkable fact is that, as expected according to the single-step mechanism used, nitrogen remains unaltered (see Figure 47 and Figure 49), since this species is non-participant in the chemical reaction (6.11).

Additionally, a direct correlation can be established between regions of lower concentrations of oxygen and methane and high-temperature regions. This is attributed to the fact that, as it was detailed in section *6.2.2. Chemical kinetics*, the speed of the reaction strongly depends on the temperature, which also explains where the highest concentration of products is found.

Finally, note that close the high-temperature regions the summation of mass fractions of products and nitrogen is unity, meaning that both oxygen and methane are completely burnt. This is logical since, as mentioned, an irreversible chemical reaction has been tested.

7. Environmental impact

This chapter provides an analysis of the possible environmental and safety implications regarding the development of this study that must be taken into account.

For this study, the only resource that has been required to use is a computer. Hence, the single effect on the environment to consider is in terms of the carbon footprint generated by the energy consumption during the whole project.

The average power consumption of a laptop is of 50 Watts, but running simulations is expected to increase this amount of energy, since it makes use of higher space on RAM and, for cooling reasons, the refrigeration fan works at full power. Due to this, the amount of energy consumed for the study will be fixed on an average of 70 W. However, the characteristics of voltage and current supplied increase the power consumption in more than 6 times, thus meaning that the energy supplied is way higher than the energy used.

On the other hand, the PC has been used for a total of 350 hours on this study (added to the working hours, some simulations required to maintain the computer functioning during the night). This gives a total of 151.2 kWh of energy consumed (considering a supply of 240 V and 1.8 A). As the 90% of the hours dedicated the location has been France, the carbon footprint of carbon dioxide for electricity production is of 60 g/kWh, leading to a total amount of 9 kg of CO_2.

Nevertheless, the above calculated carbon footprint is likely to be way below the one caused by the development of an experiment, since all the machinery required would consume a much higher amount of energy.

8. Planning and scheduling

In order to develop the whole study, it was required to define a certain number of tasks and to fix deadlines for performing all the work within the specified time interval. Thus, the project was split into smaller activities easily definable and manageable in a time interval and in quantity of work. The breakdown of all the tasks is depicted on Table 16 on the following pages, as well as the Gantt diagram displaying the layout of the study schedule in Figure 51.

On the whole, the study can be divided into 6 major stages, excluding the preparation of all the documentation. The first stage (phase A) is the preliminary research of information on the field of the project. This phase is reflected in section *1.4. State of the art* (for task A1) and *1.5. Background: Introduction to Numerical Methods* (for task A2).

From this point on, the different stages are divided according to the blocks in which algorithm development and simulations can be grouped, according to the problems to be solved. These 5 remaining stages (phases B to F) coincide with the ones stated in section *1.1. Aim and scope*, and are explained from chapters *2. Diffusion phenomena* to *6. Combustion*. All of them are divided into their corresponding subphases, that are:

1. Review on equations behind the physics to be solved and its correspondent numerical approach.
2. Preliminary design of the algorithm to be developed in terms of structure.
3. Implementation of the algorithm
4. Debugging and correction of errors during the implementation process.
5. Verification of the results with the correspondent reference case or cases.
6. Run of the required simulations to obtain the demanded results.
7. Data processing of the results to develop the necessary plots and statistics to present the results.

These sub-tasks are repeated for each major phase, with their correspondent particularities.

If future implementations with the aim of enhancing, optimizing or completing the CFD code developed, such as extensions to compressible flow, computational performance improvements or extensions to unstructured meshes, the phases needed to follow are approximately the same of the ones followed by this study: documentation, implementation and verification, with probably a similar duration in time and quantity of hours to be dedicated, always depending on the degree of complexity of the improvement to develop.

Phase	*Task*	*Description*	*Precedence*	*Start date*	*Finish date*	*Hours*
A		***Research and information gathering***		***27 Jan***	***2 Feb***	***10***
	A1	General research on Computational Fluid Dynamics		27 Jan	29 Jan	3
	A2	Preliminary review and research on numerical methods applied to CFD	A1	30 Jan	2 Feb	7
B		***Study of diffusion phenomena***	***A***	***3 Feb***	***1 Mar***	***100***
	B1	Study of Heat Conduction		3 Feb	14 Feb	45
	B1.1	Review on mathematical formulation and discretization of the equations		3 Feb	4 Feb	5
	B1.2	Preliminary design of the algorithm to be developed	B1.1	5 Feb	5 Feb	2
	B1.3	Implementation of the algorithm	B1.2	6 Feb	10 Feb	10
	B1.4	Debugging of the algorithm		9 Feb	10 Feb	3
	B1.5	Verification with the Four-Material problem		9 Feb	10 Feb	5
	B1.6	Run of the required simulations	B1.4, B1.5	11 Feb	12 Feb	15
	B1.7	Result treatment an analysis	B1.6	13 Feb	14 Feb	5
	B2	Study of Potential Flows		15 Feb	27 Feb	50
	B2.1	Review on mathematical formulation and discretization of the equations		15 Feb	16 Feb	5
	B2.2	Preliminary design of the algorithm to be developed	B2.1	17 Feb	17 Feb	2
	B2.3	Implementation of the algorithm	B2.2	18 Feb	21 Feb	10
	B2.4	Debugging of the algorithm		22 Feb	23 Feb	3
	B2.5	Verification with the Flow along a Cylinder problem		22 Feb	23 Feb	10
	B2.6	Run of the required simulations	B2.4, B2.5	24 Feb	25 Feb	15
	B2.7	Result treatment an analysis	B2.6	26 Feb	27 Feb	5
	B3	Final debugging, optimization and commenting of the code	B1, B2	28 Feb	1 Mar	5
C		***Study of convection-diffusion phenomena***	***B***	***2 Mar***	***22 Mar***	***70***
	C1	Review on mathematical formulation and discretization of the equations		2 Mar	4 Mar	5
	C2	Preliminary design of the algorithm to be developed	C1	5 Mar	5 Mar	2
	C3	Implementation of the algorithm	C2	6 Mar	10 Mar	15
	C4	Debugging of the algorithm		11 Mar	13 Mar	5
	C5	Verification with the Diagonal Flow problem		12 Mar	13 Mar	5
	C6	Verification with the Smith-Hutton problem		13 Mar	14 Mar	5
	C7	Run of the required simulations	C4, C5, C6	15 Mar	18 Mar	20
	C8	Result treatment an analysis	C7	19 Mar	20 Mar	10
	C9	Final debugging, optimization and commenting of the code	C8	21 Mar	22 Mar	3
D		***Study of the Navier-Stokes equations***	***C***	***23 Mar***	***3 May***	***100***
	D1	Review on mathematical formulation and discretization of the equations		23 Mar	25 Mar	7
	D2	Preliminary design of the algorithm to be developed	D1	26 Mar	27 Mar	3
	D3	Implementation of the algorithm with the NS momentum equation	D2	28 Mar	3 Apr	20
	D4	Debugging of the algorithm		4 Apr	9 Apr	10
	D5	Verification with the Driven Cavity problem		10 Apr	11 Apr	6
	D6	Verification with the Channel Flow problem		12 Apr	14 Apr	6
	D7	Addition of the NS energy equation to the algorithm	D5, D6	15 Apr	17 Apr	10
	D8	Verification with the Differentially Heated Cavity problem	D7	18 Apr	20 Apr	6
	D9	Run of the required simulations	D5, D6, D8	21 Apr	26 Apr	20
	D10	Result treatment an analysis	D9	27 Apr	30 Apr	10

Phase	Task		Description	Precedence	Start date	Finish date	Hours
	D11		Final debugging, optimization and commenting of the code	D10	1 May	3 May	3
E			***Study of Mass Transfer phenomena***	***D***	***4 May***	***24 May***	***60***
	E1		Review on mathematical formulation and discretization of the equations		4 May	5 May	5
	E2		Preliminary design of the algorithm to be developed	E1	6 May	7 May	2
	E3		Addition of the species equation to the algorithm	E2	8 May	11 May	10
	E4		Debugging of the algorithm		10 May	12 May	5
	E5		Verification with the Moist Air problem		12 May	14 May	5
	E6		Run of the required simulations	E4, E5	15 May	19 May	20
	E7		Result treatment an analysis	E6	20 May	22 May	10
	E8		Final debugging, optimization and commenting of the code	E7	23 May	24 May	3
F			***Study of Combustion phenomena***	***E***	***25 May***	***17 Jun***	***80***
	F1		Review on mathematical formulation and discretization of the equations		25 May	27 May	7
	F2		Preliminary design of the algorithm to be developed	F1	28 May	29 May	3
	F3		Addition of the chemical kinetics to the algorithm	F2	30 May	3 Jun	20
	F4		Debugging of the algorithm		3 Jun	5 Jun	5
	F5		Verification with the premixed laminar flame problem		4 Jun	6 Jun	5
	F6		Run of the required simulations	F4, F5	7 Jun	12 Jun	25
	F7		Result treatment an analysis	F6	13 Jun	15 Jun	10
	F8		Final debugging, optimization and commenting of the code	F7	16 Jun	17 Jun	5
G			***Document writing and preparation***	***A***	***4 Feb***	***24 Jun***	***40***
	G1		Report		4 Feb	24 Jun	25
		G1.1	Writing		4 Feb	22 Jun	20
		G1.2	Revision	G1.1	23 Jun	24 Jun	5
	G2		Budget		15 Jun	19 Jun	10
		G2.1	Documentation		15 Jun	16 Jun	2
		G2.2	Writing	F, G2.1	18 Jun	20 Jun	5
		G2.3	Revision	G2.2	21 Jun	22 Jun	3
	G3		Final revision and correction of errors	F, G1, G2	25 Jun	28 Jun	5
H			***Presentation preparation***	***F, G***	***29 Jun***	***12 Jul***	***20***
	H1		Support material elaboration		29 Jun	5 Jul	10
	H2		Oral presentation preparation	H1	6 Jul	12 Jul	10

Table 16. Tasks to develop for the study.

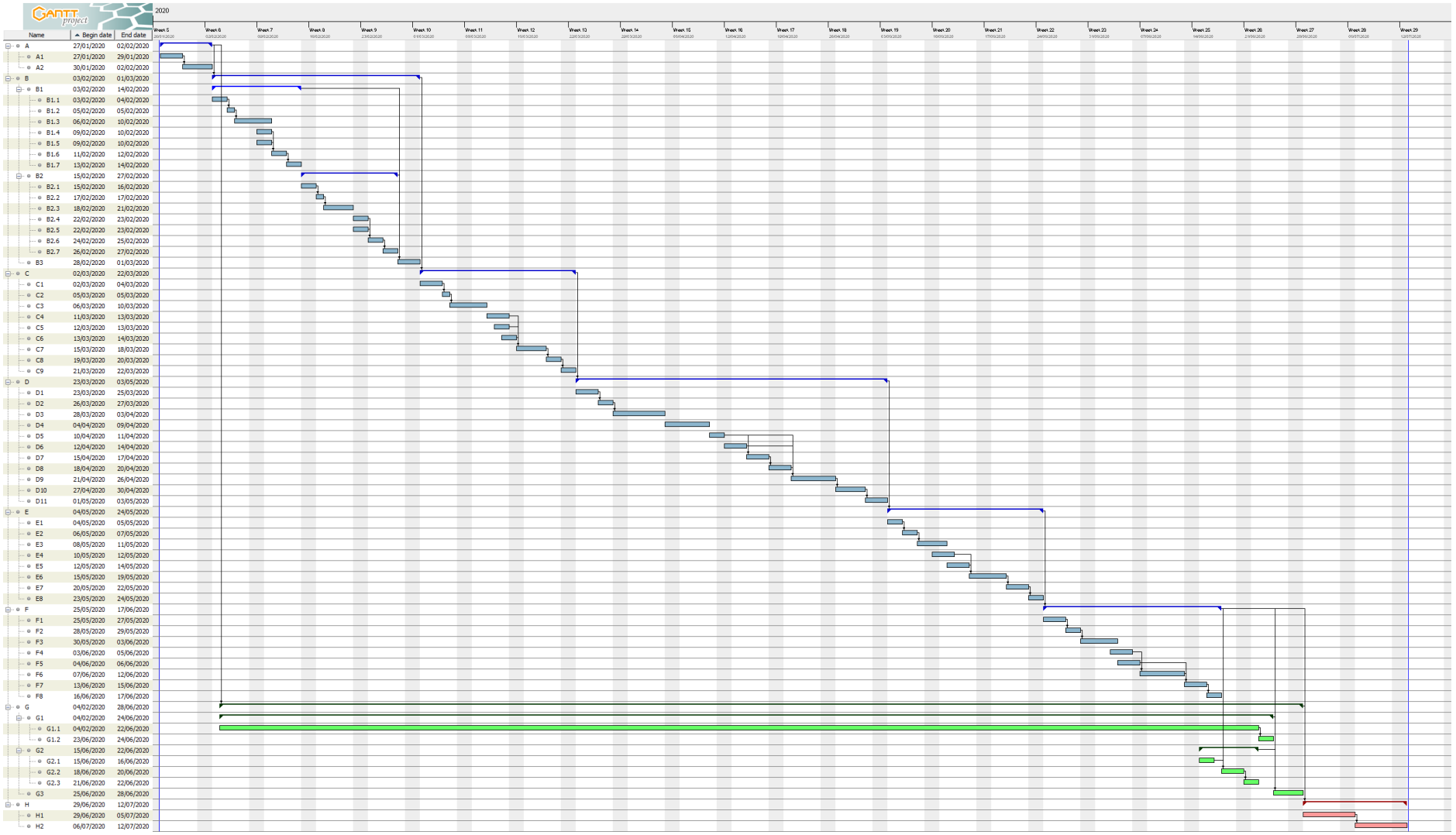

Figure 51. Gantt diagram of the study planning and scheduling.

9. General conclusions and recommendations

As defined at the beginning of the report, this study was intended to implement an algorithm capable of solving Fluid Dynamics Navier-Stokes equations of mass, momentum and energy coupled with Chemical Kinetics mechanisms, following CFD techniques. The development of this code was intended to solve basic combustion problems. At this point, the established objective has been fulfilled and some conclusions can be drawn.

The first general issue to be discussed is the effectiveness of Computational Fluid Dynamics in the field of Industrial and Aerospace Engineering. Thanks to the increasing power of modern computers, this tool is no longer restricted to supercomputing centers but accessible to anybody with an average laptop. Thus, CFD has been proven to be a powerful and cheaper alternative to the development of complex experiments and is capable to provide accurate enough results in feasible amounts of time for realistic simulations.

Focusing on more technical aspects, the methodology followed along the whole study has allowed to successfully comprehend the physics behind Fluid Dynamics, Head and Mass Transfer and Combustion phenomena, as well as the numerical methods used in the resolution of their underlying equations. The project was started with two simple diffusion problems, followed by the addition of the treatment of the convective term in steady flows with a known velocity field. Afterwards, the FSM was implemented to shift to the transient domain for the resolution of NS equations, initially for the transport of momentum and energy as well. Finally, the mass transfer phenomenon was incorporated, initially with non-reactive species and at the end adding the modelization of chemical kinetics to simulate chemical reaction mechanism.

All this has led to the resultant code of this project, which has proven to be complete enough to the extent of which the study has been developed. Relevant and enhanced features have been included, such as:

- Implementation of several types of structured meshes (i.e. uniform, hyperbolically concentrated and full-cosine)
- Implementation of different solvers (i.e. Gauss-Seidel or point-by-point, line-by-line and conjugate gradient)
- Implementation of several convective evaluation schemes (i.e. UDS, CDS, QUICK and SMART)
- Loading and saving options for avoiding the loss of simulations in progress, together with several monitoring output information during the computation

Studies concerning those different possibilities implemented have been also developed, allowing to always select the best numerical parameters for each simulation with the aim of saving computational time without losing accuracy on the solutions. The explicit method has resulted to be enough at the first stages of the study, as it allowed to obtain converged results in reasonable time and with the demanded accuracy.

Yet, it has been proven that this approach is not suitable for the calculation of the net species production term, despite being used for scheduling reasons. Although it has been possible to develop simulations with it, the timestep scale required for achieving convergence was excessively small, making prohibitive the computational cost of this type of simulations until reaching a steady state with this approach. It would be thus imperative, for further and more complex studies, to implement an implicit resolution of the source term i.e. making use of the modified damped Newton's method.

On the other hand, not only knowledge in the fields of expertise tackled in this project has been gained, but also programming skills have widely been improved. The development of the practical part of this study has required to follow certain strategies in order to optimize at maximum the tasks to implement, in terms of reusability of the code among the different stages. This also has allowed to optimize the time spent in debugging and correction of errors, but to succeed in this aspect it is necessary to anticipate and structure the algorithm before putting hands on. Thus, it has been experienced that, as it is often said, "programming is thinking, not typing".

The programming approach followed has allowed to obtain a modular, well-structured code, which has been as much documented as possible to be easily comprehensible for a third person. The different sections of the algorithm are clearly differentiated, and its implementation has also intended to be generalized, to facilitate changes on the physics of the problem (i.e. boundary conditions, number of species, etc.) without excessively affecting to the main core of the CFD resolution. This also may simplify the implementation of further extensions on the code. Some possibilities of extensions are provided on the next chapter.

Some problems were encountered in this final stage, since information of test conditions for the reference problems was difficult to find or even in some cases parameters were different depending on the literature source. This, together with the complexity found in the coupling between chemical kinetics and energy transport, increased the length of the last stage more than it was expected. Other complications were also found in the treatment of solids inside the domain due to the particular difficulty of the treatment of the wall nodes of the internal solid. All this prevented from developing further analysis using more complex approaches of the combustion processes or more elaborated geometries.

In summary, it can be said that the outputs of this study are useful, detailed and complete, having dealt with a wide range of types of problems strongly linked to multiple Industrial and Aerospace Engineering fields.

10. Future lines of work

This project has been developed to a particular extent in which the algorithm developed is capable of solving the NS equations of momentum and energy, together with the mass transport for multiple species, and also considering chemical mechanisms for domains with structured meshes. Yet, there are several possibilities in order to both enhance the performance of the current developed code or the addition of new features to it. Some ideas are detailed below:

- **Algorithm optimization:** as it was mentioned in section *1.1. Aim and scope*, the main objective of the study was to develop a clear algorithm rather than an extremely efficient one. Thus, a future improvement of the code would consist of a full revision of its execution with the aim of decreasing the computational time.
- **Algorithm parallelization:** all the simulations run in this study have used a single processor, and it was far enough according to the purpose of the project. However, for running more demanding simulations with much finer meshes or higher Reynolds numbers (turbulent regime), the possibility of running the simulation in several processors is a must.
- **Implementation of more stable resolution methods for stiff equations:** as mentioned, the explicit approach with a small timestep size has been used for the computation of the chemical kinetics. However, if further analyses regarding combustion processes were done, it would be a high priority to continue the work in this line before running simulations.
- **Implementation of more stable or accurate convective schemes:** for this study it has been enough with the implementation of the four above-presented evaluation schemes of the convective term, since it has allowed to see the difference among them. There are many other schemes existent [21] that could also be included in the code.
- **Development of tests with further reference cases:** in this study, the program implemented has been successfully tested with a total of 8 reference problems of different sources and scopes. Nevertheless, even further verifications could be performed, especially for the last stage of combustion, in order to continue ensuring the correctness of the results provided by the simulations.
- **Extension to unstructured meshes:** the current code is limited to the resolution of simple domains (i.e. rectangular or with symmetry characteristics). If more complex geometries wanted to be solved, it would be required to implement a different approach to the above-presented. There is an alternative to the FSM for collocated meshes which would allow to solve problems with unstructured grids [20]. Likewise, other resolution algorithms, i.e. the SIMPLE algorithm, offer a different approach that may also be considered [39].

- **Addition of turbulence models:** the presented methodology has been used to develop a DNS-like approach for the CFD code implemented, and the problems studied were part of the laminar regime. For solving problems with higher Reynolds numbers, it would be required to tackle the turbulence phenomenon, this is the Kolmogorov energy cascade, in order to deal with the transport of energy to the smallest scales and its later dissipation. There are several turbulence models in the literature that could be used as a complement for solving problems beyond the laminar regime.
- **Extension to compressible flow:** in this study only incompressible Navier-Stokes equations have been treated. Improvements in the line of compressible regime would allow to study a wide range of additional problems, i.e. flows in rocket nozzles.
- **Implementation of a complete species database:** to the extent of this study, only the few species used in the reaction mechanism have been given as an input. Alternatively, the program could contain thermophysical and transport properties of different species, selecting only the ones that are involved in the particular problem to solve.

All of the previously described items or any other improvement proposed shall be developed following the same steps used at each stage of the project, consisting of documentation and study of mathematical formulation, implementation and debugging of the algorithm and verification with reference solutions available in the literature. The length in time of each of the proposed further stages would be approximately the same as the phases used in the project, always depending on the degree of accuracy desired.

11. Bibliography

[1] V. Giovangigli and M. D. Smooke, "Application of Continuation Methods to Plane Premixed Laminar Flames," *Combust. Sci. Technol.*, pp. 241–256, 1993.

[2] V. Vilag, J. Vilag, R. Carlanescu, A. Mangra, and F. Florean, "CFD Application for Gas Turbine Combustion Simulations," in *Computational Fluid Dynamics Simulations*, 2019.

[3] C. K. Westerbrook and F. L. Dryer, "Simplified Reaction Mechanisms for the Oxidation of Hydrocarbon Fuel in Flames," *Combust. Sci. Technol.*, 1981.

[4] J. Yue and L. Luo, "A review on catalytic methane combustion at low temperatures : Catalysts , mechanisms , reaction conditions and reactor designs," *Renew. Sustain. Energy Rev.*, vol. 119, 2020.

[5] CTTC, "Introducción de la Formulación Matemática de la Combustión de Gases Reactivos." Universitat Politècnica de Catalunya, pp. 1–22.

[6] J. Andersen, C. L. Rasmussen, T. Giselsson, and P. Glarborg, "Global Combustion Mechanisms for Use in CFD Modeling under Oxy-Fuel Conditions," *Energy & Fuels*, pp. 1379–1389, 2009.

[7] L. Acampora and F. S. Marra, "Investigation by Thermodynamic Properties of Methane Combustion Mechanisms under Harmonic Oscillations in Perfectly Stirred Reactor," *Chem. Eng. Trans.*, vol. 57, pp. 1459–1464, 2017.

[8] R. Ennetta and R. Said, "Comparison of different chemical kinetic mechanisms of methane combustion in an internal combustion engine configuration," *Therm. Sci.*, pp. 43–51, 2008.

[9] D. C. Toncu and S. Soleimani, "On methane pyrolysis special applications," *IOP Conf. Ser. Mater. Sci. Eng.*, vol. 95, pp. 17–20, 2015.

[10] J. Bibrzycki and T. Poinsot, "Reduced chemical kinetic mechanisms for methane combustion in O2 / N2 and O2 / CO2 atmosphere," 2010.

[11] B. Fiorina, R. Baron, O. Gicquel, D. Thevenin, S. Carpentier, and N. Darabiha, "Modelling non-adiabatic partially premixed flames using flame-prolongation of ILDM," *Combust. Theroy Model.*, pp. 449–470, 2003.

[12] L. Eder, M. Ban, and A. Wimmer, "Development and Validation of 3D-CFD Injection and Combustion Models for Dual Fuel Combustion in Diesel Ignited Large Gas Engines," *Energies*, 2018.

[13] E. Dick, "Introduction to Finite Element Methods in Computational Fluid Dynamics," in *Computational Fluid Dynamics: an Introduction*, 2009, pp. 235–236.

[14] R. J. LeVeque, *Finite Volume Methods for Hyperbolic Problems*. New York, 2002.

[15] S. V. Patankar, *Numerical Heat Transfer and Fluid Flow*. New York, 1980.

[16] J. R. Shewchuk, "An Introduction to the Conjugate Gradient Method Without the Agonizing Pain," 1994.

[17] CTTC, "A Two-dimensional Transient Conduction Problem." Universitat Politècnica de Catalunya, pp. 3–5.

[18] CTTC, "Non-viscous flows. Potential Flows." Universitat Politècnica de Catalunya, pp. 1–21.

[19] I. H. Shames, *Mechanics of Fluids*, 3rd ed. New York, 1982.

[20] CTTC, "Course on Numerical Methods in Heat Transfer and Fluid Dynamics." Universitat

Politècnica de Catalunya, pp. 1–8.

[21] M. S. Darwish and F. H. Moukalled, "Normalized variable and space formulation methodology for high-resolution schemes," *Numer. Heat Transf. Part B Fundam.*, vol. 26, no. 1, pp. 79–96, 1994.

[22] CTTC, "Verification strategies for the convection-diffusion equation." Universitat Politècnica de Catalunya, pp. 1–5.

[23] R. M. Smith and A. G. Hutton, "The numerical treatment of advection: A performance comparison of current methods," *Numer. Heat Transf.*, vol. 5, pp. 439–461, 1982.

[24] A. E. P. Veldman, "High-order symmetry-preserving discretization of convection-diffusion equations on strongly stretched grids," *EPRINTS-BOOK-TITLE*, pp. 1–8, 2006.

[25] CTTC, "Chaos, nonlinearity and turbulence." Universitat Politècnica de Catalunya, pp. 1–14.

[26] CTTC, "Introduction to the Fractional Step Method." Universitat Politècnica de Catalunya, pp. 1–10.

[27] T. Neckel, M. Mehl, and C. Zenger, "Enhanced Divergence-Free Elements for Efficient Incompressible Flow Simulations in the PDE Framework Peano," *Prooceedings Fifth Eur. Conf. Comput. Fluid Dyn.*, 2010.

[28] G. De Vahl Davis, "Natural convection in a square cavity: a comparison exercise," *Int. J. Numer. Methods Fluids*, vol. 3, pp. 227–248, 1983.

[29] Y. A. Çengel and A. J. Ghajar, *Heat and Mass Transfer. Fundamentals & Applications*, 5th ed. New York, 2015.

[30] P. Talukdar, C. R. Iskra, and C. J. Simonson, "Combined heat and mass transfer for laminar flow of moist air in a 3D rectangular duct : CFD simulation and validation with experimental data," *Int. J. Heat Mass Transf.*, vol. 51, pp. 3091–3102, 2008.

[31] CTTC, "Formulae for the Resolution of Fluid Dynamics and Heat and Mass Transfer Problems." Universitat Politècnica de Catalunya, pp. 1–33.

[32] CTTC, "Thermodynamic and transport properties of gases." Universitat Politècnica de Catalunya, pp. 1–12.

[33] M. J. Moran and H. N. Shapiro, *Fundamentals of Engineering Thermodynamics*. West Sussex, 2006.

[34] Y. A. Çengel and M. A. Boles, *Thermodynamics: An Engineering Approach*, 8th ed. New York, 2015.

[35] K. Claramunt, J. Cadafalch, and A. Oliva, "Detailed numerical simulation of laminar flames by a parallel multiblock algorithm using loosely coupled computers," *Combust. Theroy Model.*, vol. 7, pp. 525–544, 2003.

[36] H. C. De Lange and L. P. H. De Goey, "Two-dimensional Methane / Air Flame," *Combust. Sci. Technol.*, vol. 92, pp. 423–427, 1993.

[37] L. M. T. Somers, "The simulation of flat flames with detailed and reduced chemical models," Tehnical University of Eindhoven, 1994.

[38] C. Robinson and D. B. Smith, "The auto-ignition temperature of methane," *J. Hazard. Mater.*, pp. 199–203, 1984.

[39] Z. Virag, "Comparison of the SIMPLER and the SIMPLE Algorithm for Solving Navier-Stokes Equations on Collocated Grid," *Trans. FAMENA*, pp. 27–36, 2006.